

**The Role of Myofilament Modifications in Regulation of
Cardiac Function under Acute and Chronic Stress**

BY

JILLIAN NOELLE SIMON
B.S., Alma College, 2006

THESIS

Submitted as partial fulfillment of the requirements
for the degree of Doctor of Philosophy in Physiology and Biophysics
in the Graduate College of the
University of the Illinois at Chicago, 2013

Chicago, Illinois

Defense Committee:

Brenda Russell, Chair
Beata M. Wolska, Cardiology, Advisor
R. John Solaro
Mark Brodie
Papasani Subbaiah, Endocrinology Diabetes and Metabolism

This thesis is dedicated to my Lord and God, for He is in all that I do and all that I am.

ACKNOWLEDGMENTS

I would like to express a great deal of gratitude to the many people that played a role in my training and successes while here at the University of Illinois at Chicago:

To my UIC Family –

I would like to first and foremost thank my thesis committee; my advisor Dr. Beata Wolska, my thesis chair, Dr. Brenda Russell and my committee members Dr. R. John Solaro, Dr. Mark Brodie and Dr. Papasani Subbaiah for your constant support, scientific insights and commitment to the completion of my thesis work. Also, to the faculty, staff and fellow students in this department who have made this process a little easier and a lot more enjoyable.

I would also like to especially thank my advisor, Dr. Beata Wolska for constantly putting my priorities above her own, for supporting me in every imaginable way and, above all, for making this journey an amazing experience. Special thanks is also owed to my co-advisor and mentor Dr. R. John Solaro, for teaching me how to think critically, design each experiment with a purpose and for helping me to achieve my goals and realize my place in the scientific community.

To my colleague and friend Tangy Wilder for her kind heart, critical insights, generosity, good humor and never-ending support. I would also like to thank Shamim Chowdhury for her encouragement, help and for her kind spirit, which makes every day brighter. To all the Wolska and Solaro lab members, especially Chad Warren, who have freely shared their knowledge and skills and have offered countless conversations about science (and sometimes not about science).

To my Family –

I would like to thank my parents, Rod and Kathy Gettel and Fred and Mo Simon for their unrelenting love and support which carried me through all the failures and successes; for making all of this possible and for encouraging me along the way. To my children, Madeline and Logan, for gracing me with love, hugs, smiles and sometimes even a lab mate, which got me through some of the most trying times. Above all, I wish to thank my husband, Bob. You gave of yourself every day, you never lost faith in me, and you remain my constant source of love and compassion – I can never thank you enough.

JNS

TABLE OF CONTENTS

<u>CHAPTER</u>	<u>PAGE</u>
I. INTRODUCTION	1
A. Energy Supply of Cardiac Muscle.....	3
1. Fatty Acid β -Oxidation	3
2. Sphingolipid Metabolism	4
B. The Sarcomere and Energy Utilization	7
1. Excitation-Contraction Coupling.....	7
2. Sarcomeric Structure	9
3. The Cross-bridge Cycle	13
C. Heart Disease.....	15
1. Hypertrophic Cardiomyopathy	17
2. Cardiac Lipotoxicity.....	21
II. ACUTE EXPOSURE OF CARDIOMYOCYTES TO CERAMIDE CAUSES NEGATIVE INOTROPY MEDIATED BY PKC ϵ	24
A. Introduction.....	24
B. Materials and Methods	25
1. Isolation of Adult Rat Cardiomyocytes	25
2. Perfusion Solutions.....	26
3. Simultaneous Cell Shortening and Ca ²⁺ Transient Measurements	27
4. Treatment of Isolated Cardiomyocytes	28
5. Cell Shortening and Ca ²⁺ Transient Analysis.....	28
6. Cell Culturing and Treatment.....	29
7. Subcellular Fractionation of Adult Rat Cardiomyocytes	29
8. Statistical Analysis	31
C. Results	33
1. Acute Ceramide Treatment of Isolated Cardiomyocytes Depresses Contractility without Altering Ca ²⁺ Transients.....	33
2. Ceramide-mediated Effects are Specific to Ceramide's Known Bioactivity.....	34
3. PKC ϵ Mediates Ceramide's Negative Inotropic Response	35
D. Discussion	45
III. IDENTIFICATION OF POST-TRANSLATIONAL MODIFICATIONS TO MYOFILAMENT PROTEINS FOLLOWING CERAMIDE TREATMENT.....	49
A. Introduction.....	49
B. Materials and Methods	50
1. Isolation of Adult Rat Cardiomyocytes	50

TABLE OF CONTENT (continued)

<u>CHAPTER</u>	<u>PAGE</u>
2. Cell Culturing and Treatment.....	51
3. Western Blot Analysis.....	52
4. 2-Dimensional Difference In-gel Electrophoresis.....	54
5. Statistical Analysis.....	55
C. Results.....	55
D. Discussion.....	62
IV. CHRONIC MODIFICATION TO THE MYOFILAMENT BY A HYPERTROPHIC CARDIOMYOPATHY-LINKED MUTATION IN TROPOMYOSIN (TM K70T) CAUSES MALADAPTIVE REMODELING OF EXCITATION-CONTRACTION COUPLING.....	68
A. Introduction.....	68
B. Materials and Methods.....	72
1. Generation of α Tm K70T Transgenic Mice.....	72
2. Immunohistochemical Analysis.....	72
3. Hydroxyproline Content Assay.....	73
4. Transthoracic Echocardiography.....	74
5. Skinned Fiber Preparations.....	75
6. Programmed Electrical Stimulation.....	75
7. Isolation of Mouse Cardiomyocytes.....	76
8. Simultaneous Cell Shortening and Ca^{2+} Transient Measurements.....	78
9. Western Blot Analysis.....	79
10. Statistical Analysis.....	80
C. Results.....	80
1. Generation of Tm70 Transgenic Mice.....	80
2. Age-dependent Alterations in Morphology and Hemodynamics in Hearts from Tm70 Mice.....	81
3. Modifications in Excitation-Contraction Coupling with Persistent Increases in the Myofilament Calcium- Sensitivity.....	89
4. Arrhythmogenic Susceptibility in Tm70 Mice.....	91
D. Discussion.....	101
1. Alterations in Ca^{2+} Homeostasis Induce Contractile Dysfunction in Aging Tm70 Mice.....	101
2. Elevations in Intracellular Ca^{2+} Provide a Substrate for Reentrant Arrhythmias.....	103
3. The Onset and Severity of the Arrhythmias is Gender- dependent.....	105
V. GENERAL DISCUSSION.....	107
A. Conclusions of the Thesis.....	107

TABLE OF CONTENTS (continued)

<u>CHAPTER</u>	<u>PAGE</u>
B. Speculations.....	108
1. Communication <i>to</i> the Sarcomere	108
2. Communication <i>from</i> the Sarcomere	111
VI. CITED LITERATURE.....	114
VII. APPENDICES.....	137
VIII. CIRRICULUM VITAE.....	142

LIST OF TABLES

<u>TABLE</u>		<u>PAGE</u>
I.	PARAMETERS OF CELLULAR MECHANICS AND INTRACELLULAR Ca^{2+} TRANSIENTS	43
II.	KNOWN HYPERTROPHIC CARDIOMYOPATHY MUTATIONS IN α TM	71
III.	ECHOCARDIOGRAPHY OF NTG AND TM-70 MICE AT 4 MONTHS AND 10 MONTHS OF AGE	85
IV.	FORCE- pCa^{2+} RELATION IN NTG AND TM-70 SKINNED FIBER PREPARATIONS.....	95
V.	VENTRICULAR TACHYCARDIA DURING PROGRAMMED ELECTRICAL STIMULATION	100

LIST OF FIGURES

<u>FIGURE</u>		<u>PAGE</u>
1.	Fatty acid metabolism in the heart	5
2.	<i>De novo</i> biosynthesis and metabolism of ceramide	6
3.	Schematic of cardiac myofilament proteins	11
4.	Schematic diagram of crossbridge cycling	16
5.	Regulatory Mechanisms of Cardiac Function by Extrinsic and Intrinsic Stressors.....	19
6.	Tropomyosin structure and mutations linked to hypertrophic cardiomyopathies	20
7.	Preparation of subcellular fractions from isolated rat cardiomyocytes	32
8.	Concentration-dependent effects of exogenous C ₆ -ceramide treatment on contractile mechanics and [Ca ²⁺] _i in ventricular cardiomyocytes	37
9.	Time-dependent effects of exogenous C ₆ -ceramide treatment on contractile mechanics in ventricular cardiomyocytes.....	38
10.	Effects of acute C ₆ -ceramide treatment on contractile mechanics and [Ca ²⁺] _i in ventricular cardiomyocytes	39
11.	Assessment of functional specificity using the non-bioactive sphingolipid C ₆ -dihydroceramide.....	40
12.	Attenuation of the functional effects of acute C ₆ -ceramide treatment by inhibition of PKCs.....	41
13.	Inhibition of Ca ²⁺ -dependent PKCs in the presence of C ₆ -ceramide has no effect on cardiomyocyte shortening or [Ca ²⁺] _i	42

LIST OF FIGURES (continued)

<u>FIGURE</u>	<u>PAGE</u>
14. Translocation of the Ca ²⁺ -independent PKC isoforms.....	44
15. 2D-DIGE of myofilament protein phosphorylation for Tm, RLC, cTnT and cMyBP-C.....	58
16. Site-specific immunoblotting for cMyBP-C and Tm phosphorylation.....	59
17. 2D-DIGE and Western blotting of cTnI phosphorylation.....	60
18. The role of PKC in C ₆ -ceramide-mediated effects on cTnI phosphorylation.....	61
19. Protocol summary for programmed electrical stimulation.....	77
20. Endogenous transgene transcript and protein levels in α-Tm70 mice	83
21. Histological assessment of NTG and Tm70 hearts	84
22. Morphology of NTG and Tm70 hearts.....	86
23. Hypertrophic signaling through activation of Akt	87
24. Diastolic parameters from echocardiography in NTG and Tm70 mice	88
25. Force-Ca ²⁺ relation in skinned fiber preparations from young and old Tm70 mice.....	93
26. Measurement of [Ca ²⁺] _i transient and kinetics in isolated cardiomyocytes from NTG and Tm70 mice.....	95

LIST OF FIGURES (continued)

<u>FIGURE</u>		<u>PAGE</u>
27.	Expression level of SERCA2a protein.....	96
28.	Spontaneous Premature Contractions in Older Tm70 Mice	97
29.	Arrhythmogenicity of Tm70 mice undergoing programmed electrical stimulation	98

LIST OF ABBREVIATIONS

α MHC	Alpha Myosin Heavy Chain
α Tm	Alpha Tropomyosin
A	Peak Velocity of Flow After Left Atrial Contraction
A'	Peak Myocardial Velocity After Left Atrial Contraction
ADP	Adenosine Diphosphate
AMPK	AMP-activated Protein Kinase
AO	Ascending Aorta
APD	Action Potential Duration
ATP	Adenosine Triphosphate
ANOVA	Analysis of Variance
β MHC	beta Myosin Heavy Chain
BDM	2,3-butanedione Monoxime
BSA	Bovine Serum Albumin
BW	Body Weight
Ca ²⁺	Calcium
CaM	Calmodulin
CaMKII	Ca ²⁺ /Calmodulin Protein Kinase II
CCT	Creatine-Carnitine-Taurine Medium
cDNA	Complimentary Deoxyribnucleic Acid
CHAPS	3-[(3-Cholamidopropyl)dimethylammonio]-1-Propanesulfonate
CS	Control Solution
cMyBP-C	Cardiac Myosin Binding Protein-C

LIST OF ABBREVIATIONS (continued)

cTn	Cardiac Troponin Complex
cTnC	Cardiac Troponin C
cTnI	Cardiac Troponin I
cTnT	Cardiac Troponin T
Cy	Cyanine Dye
DCM	Dilated Cardiomyopathy
DIGE	Difference In-gel Electrophoresis
DMSO	Dimethyl-Sulfoxide
DTT	Dithiothreitol
E	Peak Velocity of Flow in the Early Phase of Diastole
E'	Peak Myocardial Velocity in the Early Phase of Diastole
ECL	Enhanced Chemiluminescence
EDTA	Ethylenediaminetetraacetic Acid
EGTA	Ethylene Glycol Tetraacetic Acid
EKG	Electrocardiogram
FB	Fractionation Buffer
GAPDH	Glyceraldehyde 3-phosphate dehydrogenase
GTP	Guanosine Triphosphate
H&E	Hematoxylin & Eosin
H ₂ O	Water
HCM	Hypertrophic Cardiomyopathy
HEPES	4-(2-Hydroxyethyl)-1-piperazineethanesulfonic Acid

LIST OF ABBREVIATIONS (continued)

HOP	Hydroxyproline
IEF	Isoelectric Focusing
EKG	Electrocardiogram
ERP	Effective Refractory Period
IPG	Immobilized pH Gradient
IVRT	Isovolumic Relaxation Time
IVS	Interventricular Septum
LA	Left Atria
LV	Left Ventricle
LVID	Left Ventricular Internal Dimension
LVOT	Left Ventricular Outflow Tract
MAP	Monophasic Action Potential
MgADP	Magnesium Adenosine Diphosphate
MgATP	Magnesium Adenosine Triphosphate
MHC	Myosin Heavy Chain
MLP	Muscle LIM Protein
MRM	Multiple Reaction Monitoring
MS/MS	Tandem Mass Spectrometry
NCX	$\text{N}^+/\text{Ca}^{2+}$ Exchanger
NTG	Non-transgenic
PAGE	Polyacrylamide Gel Electrophoresis
Pak-1	p21-activated Kinase 1

LIST OF ABBREVIATIONS (continued)

PBS	Phosphate Buffered Saline
PCL	Pulsing Cycle Length
PCR	Polymerase Chain Reaction
PES	Programmed Electrical Stimulation
P_i	Inorganic Phosphate
PKA	Protein Kinase A
PKC	Protein Kinase C
PKC α	Protein Kinase C alpha isoform
PKC β I	Protein Kinase C beta 1 isoform
PKC δ	Protein Kinase C delta isoform
PKC ϵ	Protein Kinase C epsilon isoform
PKC ζ	Protein Kinase C zeta isoform
PMA	Phorbol 12-myristate 13-acetate
PVC	Premature Ventricular Contraction
PVDF	Polyvinylidene Difluoride
PW	Posterior Wall
RLC	Regulatory Light Chain
ROS	Reactive Oxygen Species
RWT	Relative Wall Thickness
RyR	Ryanodine Receptor
S1	Myosin Subfragment 1
SCD	Sudden Cardiac Death

LIST OF ABBREVIATIONS (continued)

SDS	Sodium Dodecyl Sulfate
S.E.	Standard Error
Ser	Serine
SERCA2a	Sarcoplasmic Reticulum Ca ²⁺ ATPase, cardiac isoform
SMVT	Sustained Monomorphic Ventricular Tachycardia
SR	Sarcoplasmic Reticulum
TAG	Triacylglyceride
TBS-T	Tris-Buffered Saline with 0.1% Tween-20
TCA	Tricarboxylic Acid Cycle
TDI	Tissue Doppler Imaging
Thr	Threonine
Tm	Tropomyosin
VT	Ventricular Tachycardia

SUMMARY

This thesis is aimed at globally examining the regulation of cardiac contractility through charge modifications of the sarcomere. Specifically, our data address how acutely, ceramide accumulation associated with altered lipid uptake can directly regulate cardiomyocyte contractile function through post-translational modifications of the sarcomeric proteins and how long-term charge modifications of the sarcomere can trigger maladaptive remodeling leading to cardiac disease and increased risk for sudden cardiac death.

Metabolic perturbations associated with obesity and type 2 diabetes are emerging as a major contributor to heart disease, termed cardiac lipotoxicity, particularly in industrialized countries. Increases in circulating lipids promote greater uptake of fatty acids in excess of mitochondrial fatty acid oxidation. As a result, fatty acids are shuttled to non-oxidative pathways resulting in the accumulation of triglycerides and ceramide. These toxic lipid intermediates have been associated with reduced contractile function and disease pathogenesis, yet a direct link is lacking. The first part of this thesis tests the hypothesis that increased ceramide can directly alter cardiomyocyte contractility through transient modifications of the myofilament proteins. Studies performed herein demonstrate that ceramide treatment to isolated ventricular cardiomyocytes leads to a depression in both the peak and the rate of cell shortening without altering intracellular Ca^{2+} transients. These functional effects were associated with PKC ϵ -dependent phosphorylation of the myofilament proteins troponin I, troponin T and myosin binding protein-C. Our data provide the first evidence that ceramide can directly depress

SUMMARY (continued)

contractility and further suggest that ceramide be considered as a significant contributor to the contractile dysfunction ascribed to cardiac lipotoxicity.

The second part of this thesis sought to test the hypothesis that chronic increases in myofilament Ca^{2+} sensitivity due to the HCM-linked missense mutation in tropomyosin at position 70 (Tm70) is causal of arrhythmias and increased risk for sudden cardiac death apart from the development of hypertrophy and fibrosis. HCM is a genetically-linked form of cardiomyopathy linked to mutations primarily in sarcomeric proteins. It remains today the leading cause of sudden cardiac death in young individuals, yet the clinical phenotype is heterogeneous making understanding the pathogenesis of disease development uncertain. Our findings from Tm70 transgenic mice not only recapitulates the human disease phenotype but further demonstrate that persistence of a single charge change within the tropomyosin coiled-coil structure is sufficient to alter the inherent myofilament response to Ca^{2+} leading to age-dependent alterations in diastolic dysfunction, intracellular Ca^{2+} homeostasis and increased susceptibility to arrhythmia. Moreover our data show a gender-dependent difference in disease onset and severity.

On the whole, this collective work demonstrates the cross-talk that exists within the cardiomyocyte, such that changes in intracellular processes can signal to the sarcomere to alter cardiac function and show that the reciprocal occurs as well. Understanding the interdependence of these processes will provide us with critical

SUMMARY (continued)

information on which to design successful treatment modalities for cardiac disorders in the future.

CHAPTER I

INTRODUCTION

Regulation of cardiac pump function is an incredibly dynamic process in which the heart can adapt to various stressors to maintain overall cardiovascular homeostasis. The heart differs from other muscle types in that it is terminally differentiated and further lacks a significant pool of resident stem cells to permit repair and growth. For this reason, it employs distinct regulatory mechanisms to allow for continual adaptation to the ever-changing hemodynamic demands, both acutely and chronically. Under physiological stress, such as exercise, an increase in venous return is compensated for by an increase in the rate and force of contraction, along with an enhanced rate of relaxation, thereby increasing heart rate and permitting cardiac output to increase. This is all accomplished through various mechanical and neurohormonal strains on the heart that initiate signal transduction mechanisms which, acutely, lead to transient post-translational modifications of proteins critical to cardiac excitation-contraction coupling. If the stressor persists (i.e. endurance exercise training) these signaling cascades promote transcription, translation and assembly of new proteins leading to hypertrophic growth and remodeling. All of this is done as a compensatory response to the extrinsic stressor, allowing for the maintenance of normal cardiac function (177).

Central to the regulation of normal cardiac function is the sarcomere. Given the critical importance of the contractile machinery in maintaining adequate pump function and, therefore, systemic perfusion, one can easily argue that regulation of cardiac function is dominated by alterations in intrinsic myofilament properties. The kinetics of

both Ca^{2+} binding to troponin C (cTnC) to activate the thin filament and crossbridges interacting with actin are crucial for pressure development, ejection and ventricular filling. These kinetics can be influenced by several factors including, but by no means limited to, temperature, pH, the concentration of Ca^{2+} ($[\text{Ca}^{2+}]$) and the concentration of ATP ($[\text{ATP}]$), their maintenance, therefore, is imperative for continual mechanical force production by the sarcomere.

Concentrations of intracellular Ca^{2+} and pH are regulated by ion channels and pumps confined to membrane structures, while ATP concentrations are maintained by mitochondrial respiration. Perhaps less apparent is the fact that the sarcomeres themselves play a vital role in regulation of $[\text{Ca}^{2+}]$ and $[\text{ATP}]$. ATP utilization by the sarcomere accounts for 85% of the total ATP consumed by the myocyte (21) and therefore, any change in the actomyosin ATPase activity can affect the intracellular $[\text{ATP}]$. Likewise, since cTnC serves as a major buffer of intracellular $[\text{Ca}^{2+}]$ (176), changes in the inherent binding kinetics of Ca^{2+} to cTnC can alter intracellular $[\text{Ca}^{2+}]$. Despite this highly interdependent nature, how this cross-talk occurs and changes during disease development is not fully understood.

Collectively, this thesis provides new insight into the reciprocity between the sarcomere and the intracellular environment. It demonstrates how acute alterations of metabolism can directly regulate contractile function through post-translational modifications of the sarcomeric proteins and how long-term charge modifications within the sarcomere can provoke maladaptive remodeling leading to cardiac disease and increased risk for sudden cardiac death. In this introduction I wish to provide the reader

with a brief overview of cardiac physiology focused on processes fundamental to concepts discussed herein.

A. Energy Supply of Cardiac Muscle

The myocardium is an highly oxidative tissue with roughly 90% of its energy coming from mitochondrial respiration (211). Mitochondria are found woven throughout the myocyte in close proximity to the myofilament, and occupy nearly 40% of the cardiomyocyte's intracellular space (140). ATP is generated primarily through β -oxidation of fatty acids supplied to the heart, with a much smaller contribution (<5%) derived from glycolysis and GTP from the tricarboxylic acid (TCA) cycle (103). The extent of fatty acid breakdown through β -oxidation is dictated by many factors, including fatty acid uptake across the plasma membrane as well as into the mitochondria, oxygen supply, overall mitochondrial function, competing energy substrates (glucose, lactate, etc.), and transcriptional regulation of key enzymes involved in β -oxidation. Supply is also largely dependent on energy demand and energetic matching is critical for maintaining normal cardiac function.

1. Fatty Acid β -Oxidation

Fatty acids circulating in the form of free fatty acids bound to albumin or those released from triacylglycerol (TAG) of the lipoproteins are taken up either passively through the lipid bilayer or by two major fatty acid transporters, the fatty acid translocase, CD36, and the fatty acid transporter protein FATP1/6. Protein-facilitated transfer of fatty acids appears to be the predominant means of myocardial uptake (64). Prior to uptake, TAG from lipoproteins must first be hydrolyzed by endogenous lipoprotein lipases to generate free fatty acids. Once

inside the cell, fatty acids are converted to long-chain acyl CoAs which can then be transported more readily into the mitochondria and oxidized (See Figure 1). However, long-chain acyl CoAs represent a cross-road in fatty acid fate, inasmuch as these intramyocardial fatty acids can also be converted into TAG and shuttled into liable intracellular TAG pools, or they may be used to form lipid intermediates, such as the sphingolipid ceramide, through non-oxidative pathways.

2. **Sphingolipid Metabolism**

Sphingolipids are a class of polar, mostly membrane-restricted lipids that are defined by the presence of a sphingoid base, 18-carbons in length. They are one of the major components of cellular membranes (125) and can participate in bioactive signaling in response to stress. One such bioactive sphingolipid is ceramide. Ceramide is composed of a sphingoid base with an acyl chain of varying lengths (ranging from 14-28 carbons in length, with the most abundant species being C16-ceramide at 27% in left ventricle (137)) linked to the primary amine. Its *de novo* biosynthesis utilizes the 16-carbon long acyl CoA, palmitoyl CoA, generated from fatty acids taken up into the myocyte (as just described). Figure 2 shows a general schematic of sphingolipid biosynthesis. Condensation of palmitoyl CoA with serine within the endoplasmic reticulum generates 3-ketosphinganine, which then undergoes reduction to form sphinganine in the golgi (this reduction is coupled to NADPH oxidation to NADP⁺). This is followed by addition of an acyl chain to the amine of sphinganine to form dihydroceramide (also known as *N*-acylsphinganine). Finally, dihydroceramide is desaturated by dihydroceramide desaturase to form ceramide, which is present on the plasma

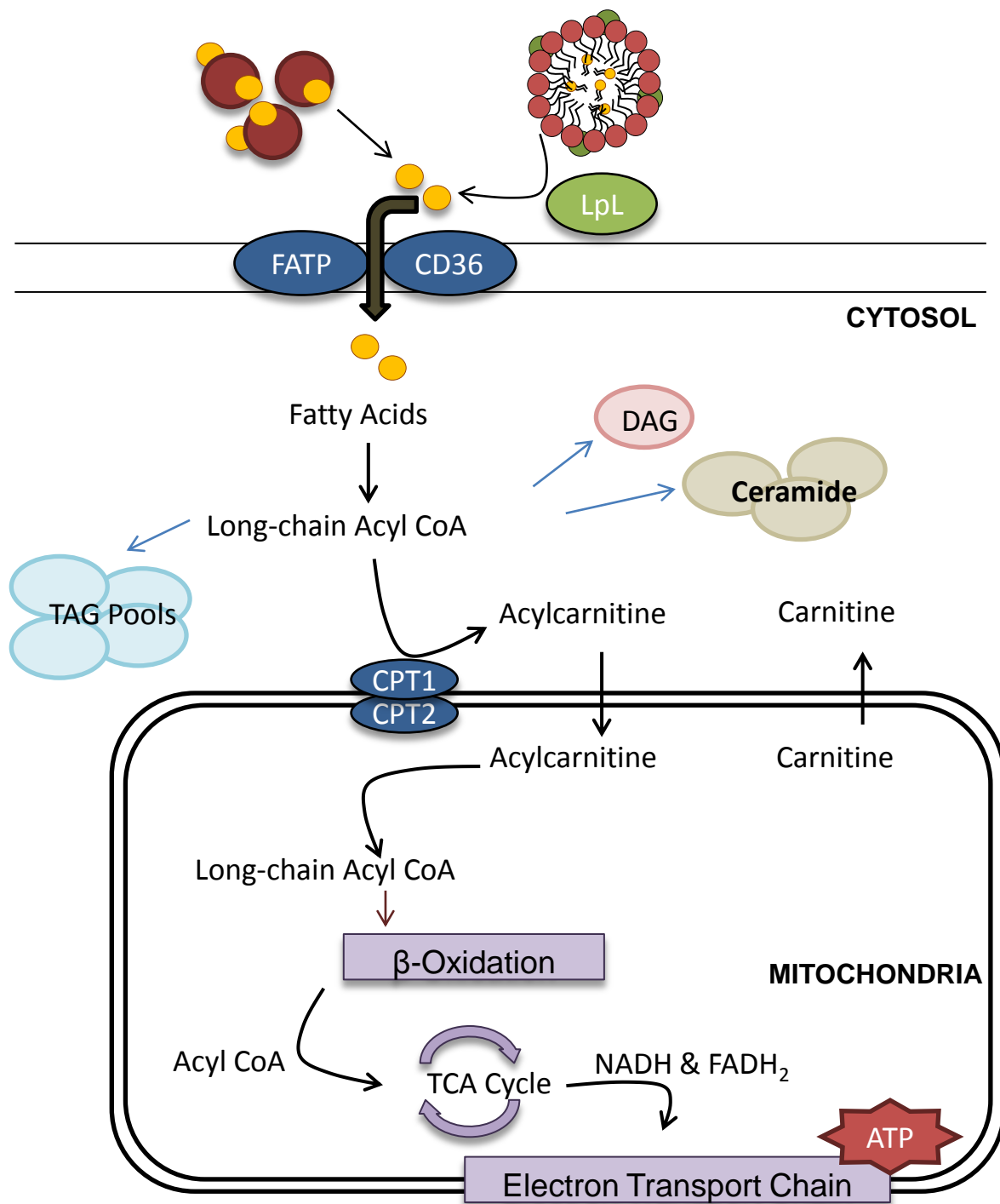


Figure 1: Fatty acid metabolism in the heart. The cartoon depicts the processes involved in fatty acid uptake and metabolism in the heart. See text for more detail. LpL, lipoprotein lipase; FATP, fatty acid transport protein 1/6; CD36, fatty acid translocase; DAG, diacylglycerol; TAG; triacylglycerol; CTP1 & 2, carnitine palmitoyl transferase; TCA, tricarboxylic acid cycle.

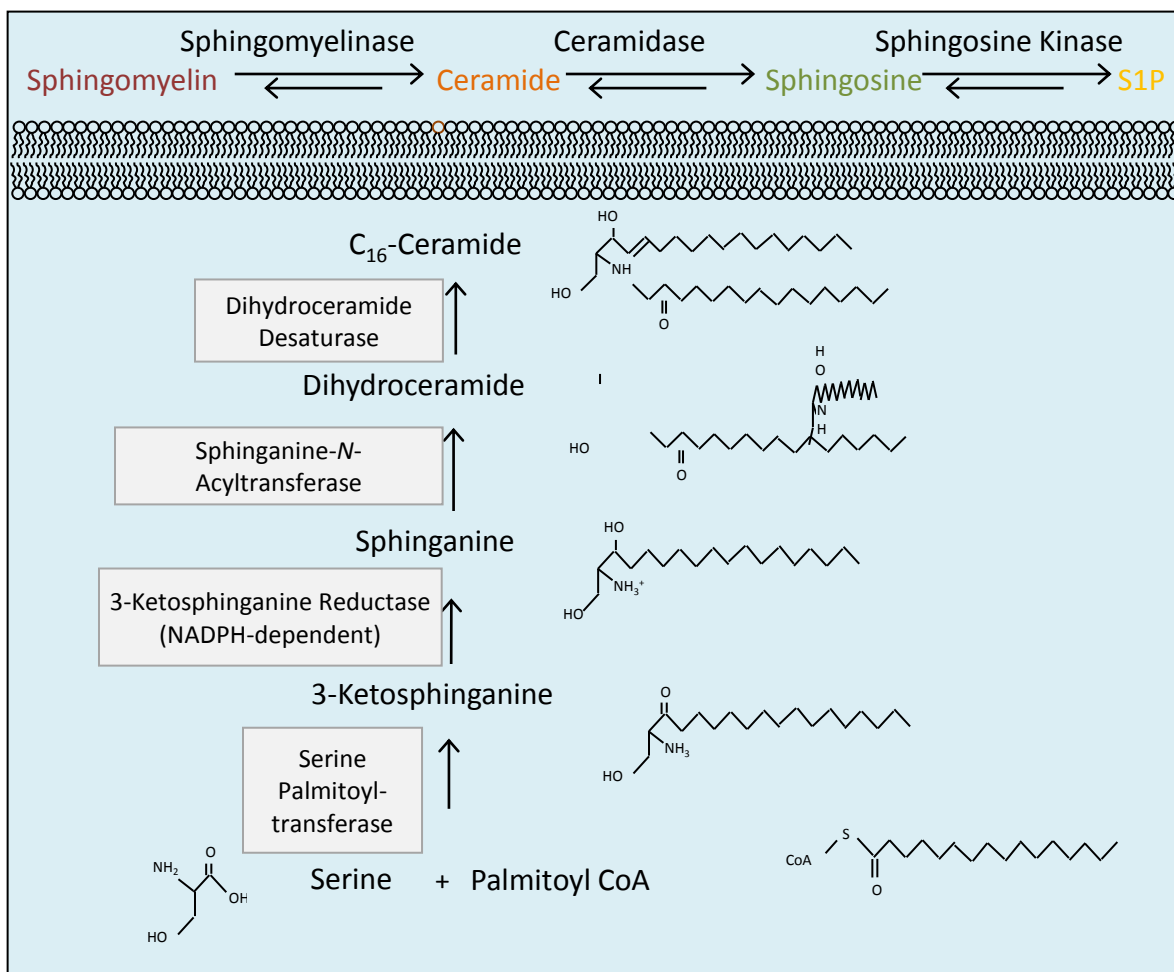


Figure 2: *De novo* biosynthesis and metabolism of ceramide. Generation of ceramide at the plasma membrane can occur through *de novo* synthesis beginning with the condensation of palmitoyl coA with serine in the sarcoplasmic/endoplasmic reticulum. Breakdown of plasma membrane pools of sphingomyelinase can also lead to the formation of ceramide and subsequent formation of sphingosine and sphingosine-1-phosphate. The enzymes that facilitate each reaction are shown in the boxes.

membrane. Ceramide can also be generated directly on the plasma membrane through breakdown of sphingomyelin pools by the enzyme sphingomyelinase (either neutral or acidic sphingomyelinases; N- or A-SMase). Ceramide can then further undergo deacylation to sphingosine, which is rapidly phosphorylated by sphingosine kinase to generate sphingosine-1-phosphate (33, 66-67, 114). Given that the rate of *de novo* ceramide synthesis is coupled to the relative concentration of intramyocardial fatty acid, changes in fatty acid uptake or utilization can have a direct effect on the amount of ceramide present. This has received considerable interest recently, as accumulation of ceramide has been linked to the development of cardiac disease (24, 78, 142, 217), which will be discussed in subsequent sections.

B. The Sarcomere and Energy Utilization

1. Excitation-Contraction Coupling

Excitation-contraction coupling is the process by which electrical impulses are propagated inward to allow for rapid mechanical force production. The “system” is designed such that the physico-chemical process is not limited by the properties of diffusion, an idea first recognized by A.V. Hill in 1949 (76). Action potentials are transmitted inward through the t-tubule system (41) where they promote Ca^{2+} -induced Ca^{2+} release from abutting subsarcolemmal cisternae. The local concentration of ion channels and pumps act as a functional cluster (51) and further highlight the interdependent nature of the excitation-contraction coupling process (185).

Generation of the cardiac action potential occurs through a coordinated sequence of sodium (Na^+), Ca^{2+} and potassium (K^+) fluxes across the plasma membrane, leading to opening of the L-type Ca^{2+} channel found in the t-tubular network. Voltage-dependent conformational changes in the L-type channel allow for a relatively small influx of Ca^{2+} that promotes opening of the sarcoplasmic reticulum (SR)-bound ryanidine receptor (RyR). This, in turn, causes a rapid and substantial release of Ca^{2+} from the SR pools through the process collectively referred to as Ca^{2+} -induced Ca^{2+} release (42). Intracellular Ca^{2+} then binds to cTnC, inducing a series of conformational change within the thin filament proteins. These conformational changes promote force generation through the strong binding of myosin cross-bridges to actin.

During the transition to diastole, Ca^{2+} is removed from the cytosolic compartment to facilitate relaxation. Densely packed SR Ca^{2+} ATPase (SERCA2a) pumps located on the sarcotubular network aid in cytosolic Ca^{2+} removal by promoting re-uptake of Ca^{2+} into the SR. Unphosphorylated phospholamban pentamers bound to SERCA2a regulate this process and further provide a mechanism for regulation of Ca^{2+} fluxing by signaling molecules. Extrusion of cytosolic Ca^{2+} also occurs through the $\text{Na}^+/\text{Ca}^{2+}$ exchanger (NCX), whose ability to transport Ca^{2+} back into the extracellular milieu is driven by the electrogenicity of the myocyte. This is important to note, as changes in intracellular Na^+ , K^+ or Ca^{2+} concentrations can affect the direction of transport through the NCX (10). While these two transporters are the major means for Ca^{2+} removal from the cytosol, plasma membrane Ca^{2+} pumps and mitochondrial

uptake of Ca^{2+} also play minor roles in reducing cytosolic Ca^{2+} during diastole. Interestingly, mitochondrial Ca^{2+} concentrations are known to regulate oxidative phosphorylation (13, 26) and mitochondrial transport of Ca^{2+} could have a significant impact on energy supply in the context of the Ca^{2+} overloaded myocyte.

While it is clear that the processes of excitation-contraction coupling consume large amounts of energy in the form of ATP, as mentioned before, energy consumption by the contractile machinery account for majority of this expenditure. In the next section, I will introduce the sarcomere in more detail and elaborate on the cross-bridge cycle, which is the dynamic process whereby the sarcomeric energy demands are made.

2. Sarcomeric Structure

The myofilaments consist of highly organized thick and thin filament proteins that facilitate, in a Ca^{2+} -dependent manner, contraction and relaxation of the sarcomere (Figure 3). Through the hydrolysis of ATP and resulting cross-bridge cycling, the cardiac sarcomere elegantly coordinates the transduction of elevated intracellular Ca^{2+} into the mechanical work of contraction and relaxation necessary for proper cardiac pump function.

The myofilaments consist of both thick and thin filament proteins that span the sarcomere. The hexameric myosin macromolecular complex is the major component of the thick filament, accounting for roughly 30% of the sarcomeric mass (196). Each individual complex of myosin consists of two globular heavy chains (containing S1 and S2 regions) and two pair of light chains (essential light

chain, MLC1, and regulatory light chain, MLC2), extending from the coiled-coil tail domain to the globular N-terminal head region. Within the “rod-like” structure of the coiled-coil tail domain, neighboring myosin molecules anneal to form the thick filament backbone. Within the bare zone, or M-line, myosin molecules overlap one another in an anti-parallel fashion, resulting in myosin heads that project from the backbone with opposite polarity. This unique organization allows for shortening of the sarcomere during cross-bridge cycling.

Further regulation of myosin structure and function occurs via the myosin associated proteins, myosin binding protein-C (cMyBP-C) and titin. cMyBP-C collars the myosin head and acts to both tether the cross-bridge to the tail region, promoting greater order of the myosin heads along the thick filament (119), and connects myosin to the cytoskeletal proteins through titin binding. As a consequence of binding to cMyBP-C, myosin’s kinetics are constrained (92, 183-184). Titin is a giant filamentous protein that extends from the Z-disk to the center of the sarcomere, where it interacts with myosin within the M line (60, 116). Titin also provides elasticity and is further responsible for most of the passive tension within the sarcomere (58-59).

Actin monomers, self-assembled into a filamentous structure, form the major portion of the thin filament and are critical for enhancing myosin ATPase activity during cross-bridge cycling. The functional unit of the thin filament is comprised of seven actin monomers, one tropomyosin (Tm) dimer and one troponin complex (cTn) that includes the Ca^{2+} -binding subunit, cTnC, the inhibitory subunit, troponin I (cTnI) and the tropomyosin binding subunit, troponin T (cTnT). This

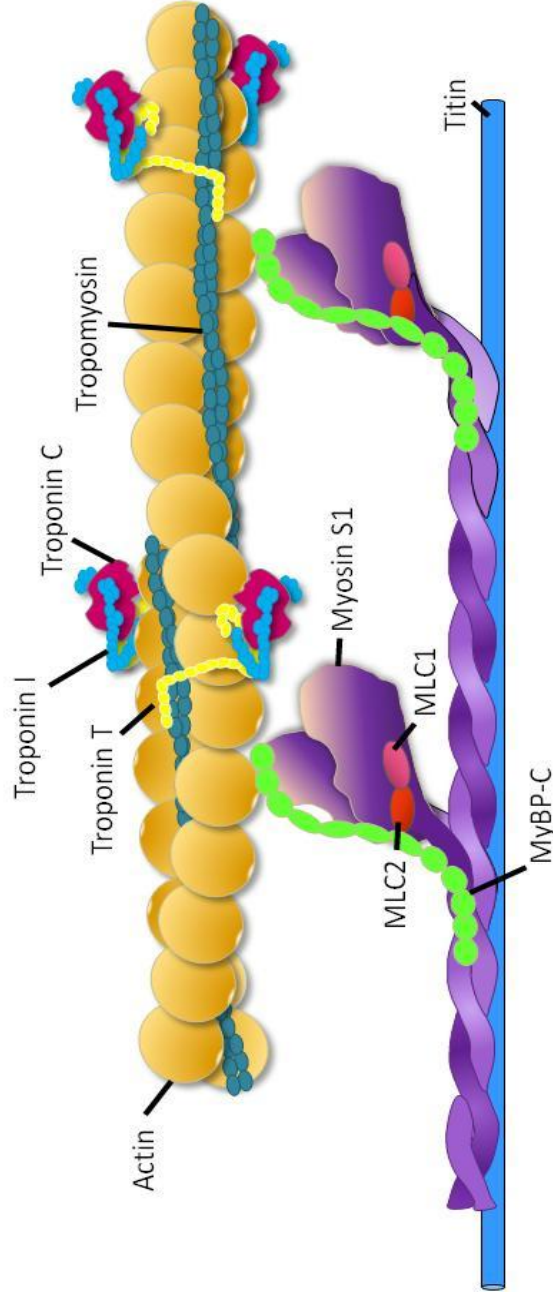


Figure 3: Schematic of cardiac myofilament proteins. The cartoon illustrates the major proteins found in the cardiac myofilament during diastole, prior to crossbridge activation. The myofilament is comprised of both thick (myosin – shown in purple) and thin (actin – shown in yellow) filament proteins, as well as regulatory proteins such as the troponin complex, tropomyosin, myosin light chains (MLC1 & MLC2) and myosin binding protein-C (MyBP-C). See *text for more detail*.

multimeric cTn complex is crucial for binding Ca^{2+} and allowing for the regulation of cross-bridge cycling in a Ca^{2+} -dependent manner, which it does by modulating Tm's position on the actin thin filament.

During diastole, intracellular Ca^{2+} concentrations are low and the binding of Ca^{2+} to the regulatory site on cTnC is not favored. Furthermore, in this state the cTn complex acts to prevent actomyosin formation via cTn-Tm interactions that form an ordered structure along the actin filament. This structure promotes the positioning of Tm along the actin groove, resulting in either blockage of myosin binding to actin ("blocked" state) or weak cross-bridge attachment ("closed" state) (118). As suggested by the three-state model of muscle contraction (123), such positioning of Tm does not allow for significant force generation and the requirement of ATP for myosin binding and hydrolysis is minimal. It is also possible that the cTn complex itself may block the interaction between actin and myosin directly (202).

During systole, intracellular Ca^{2+} levels rise promoting the binding of Ca^{2+} to cTnC. This binding induces a conformational change within the cTn complex resulting in strong binding of cTnI, both the inhibitory region and the C-terminal domain, to cTnC. As a result, cTnI is released from actin and the interaction between cTnT and Tm becomes significantly weaker (178). This change in cTnT-Tm interaction facilitates the movement of Tm into the "open" state. In this state, myosin binding sites on actin are exposed allowing for the strong binding of myosin cross-bridges to actin, which greatly enhances actomyosin ATPase activity leading to cross-bridge cycling and force generation (29, 97, 118). The formation of

strong, force generating cross-bridges also promotes the binding of additional cross-bridges and enhances Ca^{2+} binding to cTnC (141). This interdependence results in a relationship between Ca^{2+} concentration and isometric force that is very steep and shows a highly cooperative character.

The interaction between the thick and thin filament is dependent on both the intracellular milieu, as well as the state of each protein within the sarcomere. Moreover, the functional interaction of these proteins involves multiple mechanisms, including allosteric, steric and cooperative activation. It is this complex relationship within the sarcomere that makes the transition of the myofilaments from the relaxed state to the contractile (or activated) state highly sensitive to regulation at multiple points. Moreover, alterations in sarcomeric function can occur via regulation of practically any of the sarcomeric proteins.

3. The Cross-bridge Cycle

The cross-bridge cycle is the means by which the heart couples the hydrolysis of ATP to positive work production and produces force. It is driven by several thermodynamically favorable reactions. Cross-bridge cycling is dependent upon the ability of the myocyte to maintain sufficient levels of reactants (MgATP and H_2O) and products (MgADP, P_i and H^+), thereby generating continual force production. A simplified schematic of the critical steps involved in cross-bridge cycling are shown in Figure 4.

As mentioned, the myosin globular head domain contains an S1 region where both nucleotide binding and subsequent hydrolysis occurs (Figure 4, Step 1). At

this point, myosin remains bound to the hydrolysis products, MgADP and inorganic phosphate (P_i), with some myosin S1 heads binding weakly to actin. According to the three-state model of thin filament activation, this state of weakly bound myosin with a strongly bound nucleotide represents the “closed” state (122). Further isomerization of the myosin head results in stronger binding to actin and a weakening of the associated nucleotide to form the “open” state. It is this transition from the closed to the open state that is regulated by the binding of Ca^{2+} to cTnC and subsequent movement of Tm away from myosin’s binding sites along the actin thin filament (72, 123). Following formation of the open state, P_i is quickly released from the actomyosin complex (Figure 4, Step 2). At this step along the cross-bridge cycle the potential energy generated from ATP hydrolysis is transferred to the myosin “lever arm” and harnessed to produce the power stroke, which drives sliding of the thick and thin filament past one another (155, 205). Under steady-state isometric force, ADP release from the actomyosin complex is rate-limiting and results in the formation of a rigor cross-bridge (Figure 4, Step 3). At this point, given the high local concentration of MgATP, myosin undergoes rapid nucleotide binding followed by detachment of the myosin head from actin (Figure 4, Step 4).

Modulation of the parameters that define cross-bridge dynamics can be both Ca^{2+} -dependent and Ca^{2+} -independent. MgATP binding and the resulting detachment of myosin from actin determines the maximal velocity of the cross-bridge cycling. The regulation of this process is Ca^{2+} -independent and depends on the ability of the myocyte to maintain high levels of MgATP and low levels of

MgADP, P_i and H^+ (116). In a state of energy deprivation, as observed in end-stage heart failure, the altered velocity of cross-bridge cycling becomes a significant contributor to the overall contractile dysfunction (63). Maximal force production is determined by Ca^{2+} regulated mechanisms that include the number of rigor cross-bridges formed and the time these cross-bridges spend in the rigor state (known as the duty ratio). Any observed change in contractile function associated with the sarcomere ultimately alters cross-bridge dynamics (kinetic properties of the cross-bridge cycle). These properties include changes to the velocity of shortening, the duty cycle and/or the unitary force generated by the strongly bound cross-bridges, intrinsically related to the state of both the thick and thin filament.

C. Heart Disease

Shown in Figure 5 is a schematic representation of the myocardial responses to physiological stress, as mentioned at the beginning (see figure legend for further details). In pathological states, we see a failure of these responses to compensate for the presence the stressor, leading to decompensation, exacerbation of the stress and abnormal cardiac function. Late-stage heart failure is associated with abnormalities in all of the above mentioned processes (energy production, excitation-contraction coupling, modifications to the sarcomere) as a result of the progressively declining ability for the heart to compensate for persistent hemodynamic stress (in the case of non-ischemic heart disease) or for the loss of viable myocardial cells (in the case of ischemic heart disease). Alterations in myofilament protein modifications are believed to play a significant role in the development of cardiac dysfunction underlying the

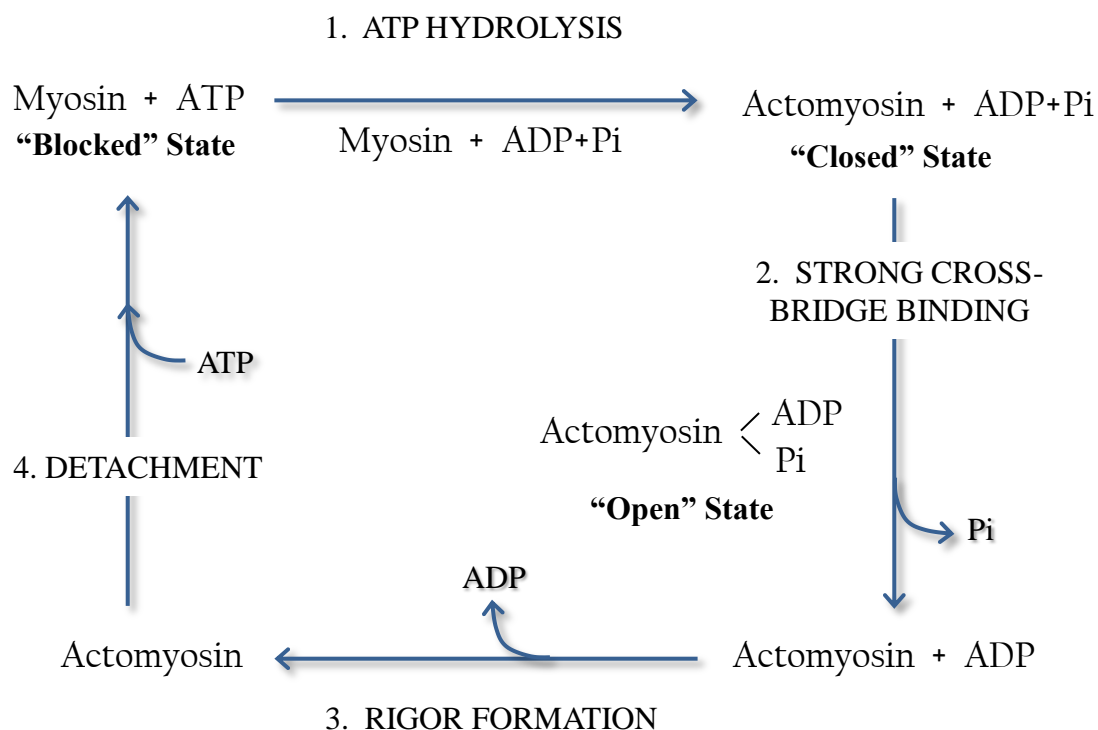


Figure 4: Schematic diagram of crossbridge cycling. The 4-step process for actomyosin ATPase-dependent cycling. Step 1 begins with hydrolysis of myosin-bound ATP and transition of the thin filament to the closed state allowing for weak actomyosin interaction. Step 2 proceeds with the transfer of energy of the nucleotide to facilitate strong cross-bridge binding and transition of the thin filament to the open, fully activated state. The release of ADP in Step 3 allows for the myosin power stroke, rigor cross-bridge formation and the production of work followed by the binding of ATP to the actomyosin complex in Step 4, resulting in dissociation of the myosin head from actin.

progression to heart failure (37). Moreover, our understanding of the mechanisms underlying cardiac dysfunction associated with heart failure have broadened in recent years to include maladaptive changes to the sarcomere and cross-bridge dynamics caused by genetically-linked mutations, or so-called intrinsic stressors.

1. Hypertrophic Cardiomyopathy

Hypertrophic cardiomyopathy is defined clinically by the presence of unexplained hypertrophy (wall thickness >15 mm) which may be accompanied by myocyte disarray, fibrosis and diastolic dysfunction. This disease affects roughly 1 in 500 people (109) and is the leading cause of sudden cardiac death (SCD) in young individuals (111-112). Although first described in 1986 by Teare (198), it was not linked to mutations in sarcomeric proteins until 4 years later, with the identification of a HCM-causing mutation in β -MHC (54). Today, there are more than 1,400 disease causing mutations identified, with majority linked to missense mutations, deletions or truncations in sarcomeric proteins (110). However, despite our rapidly growing body of knowledge with regard to HCM, the mechanistic links which underlie the disease are still unclear.

Our understanding of the genotype-phenotype relation is muddled by the fact that the same mutation can induce differing phenotypes (107) and by the finding that the disease severity can depend on the specific amino acid substituted at a particular site (49, 160). Nevertheless, several mechanisms have been proposed to underlie HCM phenotype, including: 1) higher energetic cost independent of hypertrophy, 2) alterations in Ca^{2+} buffering by the myofilament, 3) poison peptide (dominate negative function of mutant protein), and 4) haploinsufficiency

(insufficient quantity of sarcomere protein) (5, 30, 87, 89, 113, 172). The commonality among these mechanisms is their relation to altered properties inherent to sarcomeric function, but our global understanding of how this relates to phenotype is superficial at best. Ultimately, deciphering the genotype-phenotype link at a molecular level will serve to enhance our ability to increase risk assessment and help implement specific treatments for delaying or preventing HCM.

Of relevance to this thesis is HCM associated with mutations in Tm. As mentioned earlier, Tm is a coiled coil protein that lays along the actin filament grooves where it serves to regulate actin-myosin interactions in a Ca^{2+} -dependent manner. In order to form a continuous strand neighboring Tm form head-to-tail overlaps of 8-9 amino acid residues (96). Characteristic of coiled-coiled structures, Tm contains heptad repeats of nonpolar and polar amino acid (designated *a*, *b*, *c*, *d*, *e*, *f*, and *g* – see Figure 6). The arrangement of these amino acid repeats is such that polar and ionic side chains (*b*, *c* and *f* position) situate themselves on the exterior of the coiled-coil where they are able to interact with proteins and solvent. Nonpolar amino acids (*a* and *d* position) pack the interior forming a hydrophobic core, while charged amino acids (*e* and *g* position) stabilize the coiled-coil structure by forming interhelical salt bridges (15, 186). A strand of Tm also has 7 “zones” that facilitate actin binding (15). Unlike other coiled-coils, however, Tm has two highly conserved residues (D137 and E218 in the *a* and *d* positions, respectively) that act to increase Tm flexibility which allows for a bent conformation thought to be important for winding of Tm along the actin thin

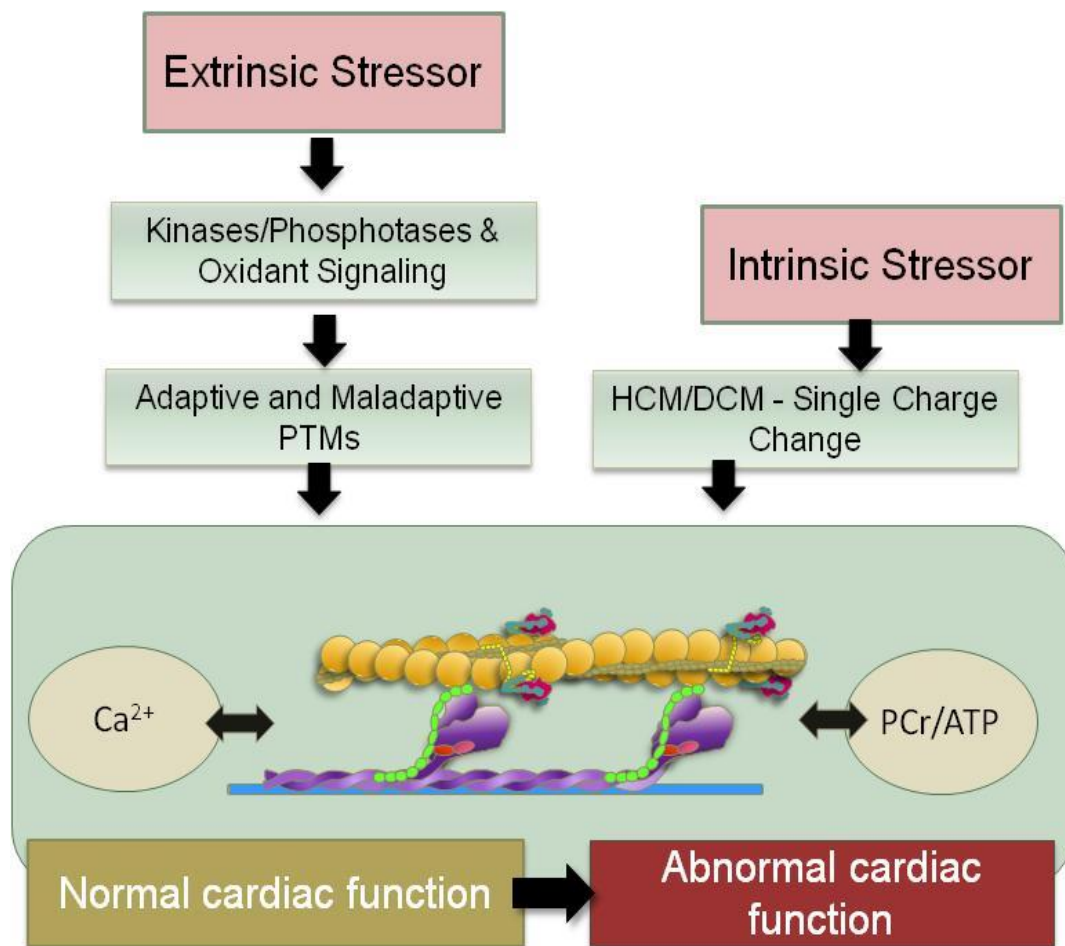


Figure 5: Regulatory mechanisms of cardiac function by extrinsic and intrinsic stressors. *Left*, The presence of extrinsic stressors evoke signal transduction mechanism which alter the post-translational state of proteins of the myofilament, as well as proteins involved in excitation-contraction coupling, thereby altering the dynamic interactions between the sarcomere and the intracellular milieu. All of this is done as a compensatory response to the extrinsic stressor, allowing for the maintenance of normal cardiac function. However, in the pathological state, we see a failure of these responses to compensate for the extrinsic stress, leading to decompensation, exacerbation of the stress and transition to abnormal cardiac function. *Right*, this can also be observed in response to intrinsic stressors, as in the case of hypertrophic cardiomyopathy (HCM) and dilated cardiomyopathy (DCM)-linked mutations, which are, most often sarcomeric single point mutations or truncations. (Figure modified from Solaro & de Tombe (2008) *Cardiovasc Res*)

filament (15, 131, 192). Moreover, changes in Tm's inherent flexibility have been shown to be important in the mechanism by which Tm mutations cause HCM, the specifics of which will be discussed further in Chapter IV.

2. Cardiac Lipotoxicity

With the increasing rate of obesity in industrialized countries, the incidence of heart disease due to increased intramyocardial lipid accumulation is growing at an alarming rate. In 2001 it was estimated that half of all Americans were overweight, however this number is likely to be higher now (181). Lipotoxicity, in general is associated lipid-induced dysfunction occurring in any non-adipose tissue; however, important to this thesis is lipotoxicity of the heart, or cardiac lipotoxicity. Clinically, cardiac lipotoxicity is more loosely described as heart disease associated with the metabolic syndrome (hyperlipidemia, cardiomyopathy, insulin resistance and diabetes), while in animal models, cardiac lipotoxicity is much more clearly defined as the cardiac phenotype associated with models in which fatty acid uptake is increased (206). These lipotoxic models have provided key insights into the mechanisms involved in altered lipid handling, insulin resistance and myocardial loss and have defined a causal role for ceramide in mediating these effects (180, 217, 224).

As mentioned earlier, increases in fatty acid uptake, either through transport-mediated uptake or by an increase in fatty acid flip-flop, results in accumulation of long-chain acyl CoA and intramyocardial TAG. When uptake exceeds the ability for the mitochondria to oxidize the intramyocardial TAG, non-oxidative

intermediates, such as ceramide, begin to accumulate. While not all studies have assessed ceramide levels in the lipotoxic heart, elevations in TAG are clearly associated with the depressed contractile function characteristic of the disease (106, 130, 224, 228). In most cases, the cardiomyopathy is associated with apoptosis and is linked to or suggested to be due to accumulation of ceramide. Despite this, Chiu et al (22) demonstrated that in transgenic mice overexpressing FATP, increases in fatty acid uptake were associated with altered electrical conductance and diastolic dysfunction without apoptotic induction. This model suggests that alterations in contractile function observed under states of high intramyocardial fatty acids are not solely dependent on myocardial loss. However, no studies have been conducted to date to determine the underlying cause of contractile impairment in cardiac lipotoxic models.

In humans, increases in either TAG or ceramide are associated with systolic impairment as a result of diabetes (120) or obesity (108). Ceramide has also been shown to underlie insulin resistance in late-stage heart failure patients, by inhibiting insulin-dependent signaling through activation of protein kinase C (PKC) (24). Interestingly, in the same study unloading of hearts with a left ventricular assisted device (LVAD) reduced ceramide levels, ameliorated insulin resistance and improved contractile function. In mice with angiotensin II-induced heart failure, high-fat feeding resulted in ceramide accumulation and further contractile dysfunction (144). It seems that in both instances an overall reduction in β -oxidation in the failing heart contributed to the intramyocardial lipid imbalance, whereas lipid imbalance associated with metabolic syndrome is due

to elevations in lipid availability to a degree which exceeds the hearts capacity to oxidize fatty acids.

These “newly” defined cardiac disorders (by new I mean that we have only begun to discover their pathogenesis and clinical relevance) have already provided insight into the cross-talk that exists between processes within the heart. However, we have far more to learn. The objective of this thesis was to define how alterations in the post-translational state of the myofilament proteins play a role in regulation of cardiac function when cardiomyocytes are exposed to ceramide (Chapters II and III) or when charge changes due to HCM mutations alter thin filament structure (Chapter IV).

CHAPTER II

ACUTE EXPOSURE OF CARDIOMYOCYTES TO CERAMIDE CAUSES NEGATIVE INOTROPY MEDIATED BY PKC ϵ

A. Introduction

There is emerging evidence that increased myocardial lipid accumulation is correlated to the increased incidence of heart failure associated with obesity and diabetes mellitus. Ceramide, which has been deemed a cardiotoxin, is elevated in animal models of obesity (23, 142, 228) as well as in heart failure patients (24). In addition, studies have identified ceramide as a significant contributor to the development of dilated cardiomyopathy in animal models of lipotoxicity (142), as well as to the worsening of contractile impairment in the progressively failing heart under high levels of circulating fatty acids (144). Despite these findings, surprisingly little is known about ceramide's effects in directly altering cardiac contractility.

Our current knowledge of ceramide's ability to alter myocellular mechanics is based on studies using exogenous application of the short-chain analog C₂-ceramide to isolated rat cardiomyocytes. These studies reported a positive inotropic response to ceramide treatment, which was associated with both alterations in Ca²⁺ fluxes and the sensitivity of the myofilaments to Ca²⁺ (101, 158). However, these studies were unable to determine the mechanism underlying such alterations. Moreover, treatment of cells with C₂-ceramide has been shown to produce effects that are either less potent than endogenous ceramide (65) or non-specific due to its highly hydrophilic nature (9, 214). C₆-ceramide, which mimics endogenous ceramide generation (44), is now recognized

as a more physiologically-relevant means to assess the effects of ceramide *in vitro*. Studies in skeletal muscle using either C₆-ceramide or endogenously generated ceramide have shown reductions in maximal tetanic force production (44-45), findings that are more consistent with the depressed contractile force typically associated with myocardial ceramide accumulation.

B. Materials and Methods

1. Isolation of Adult Rat Cardiomyocytes

Adult male Sprague-Dawley rats (Harlan) between 180-200 g were used for cell isolation experiments. All animal procedures were conducted according to the guidelines instituted by the Animal Care and Use Committee at the University of Illinois at Chicago (ACC# 11-229). Myocytes were isolated as previously described by (104). Rats were injected intraperitoneally with heparin sulfate (5000 U/kg BW) and then 30 mins later were anesthetized by intraperitoneal injection of pentobarbital sodium (100 mg/kg BW). Animals were assessed for proper depth of anesthesia and then hearts were quickly excised, weighed in a pre-tared petri dish and then cannulated via the ascending aorta. Hearts were perfused at 37°C for 3 mins with a Ca²⁺-free control solution (BSA-CS) containing 133.5 mM NaCl, 4 mM KCl, 1.2 mM NaH₂PO₄, 10 mM HEPES, 1.2 mM MgSO₄, 11.1 mM glucose (pH 7.4 using NaOH) with addition of bovine serum albumin (1 mg/mL). Hearts were then perfused with oxygenated BSA-CS containing 0.25 mg/mL type II collagenase (Worthington Biochemical) and 0.03 mg/mL protease (Sigma-Aldrich) for 15 to 20 mins (perfusion time = 16 min/mg heart weight). After the heart was well-digested, the ventricles were removed, collected in a petri dish containing BSA-CS with 50

$\mu\text{M Ca}^{2+}$, and cut into small pieces. The ventricles were then incubated for 10 mins at 37°C , at which time they were gently triturated with a transfer pipette. Following this, the resulting cell suspension was filtered through a $250\ \mu\text{m}$ mesh collector and transferred into centrifuge tubes. The cells were allowed to sediment by gravity for 7 mins, the supernatant fraction was removed, and cells were resuspended in fresh BSA-CS containing $100\ \mu\text{M Ca}^{2+}$. Sedimentation was repeated 3 more times with the cells introduced to sequentially higher concentrations of Ca^{2+} ($200\ \mu\text{M}$, $500\ \mu\text{M}$, and finally $1\ \text{mM Ca}^{2+}$) each time.

2. Perfusion Solutions

The cell-permeable ceramide analog C_6 -ceramide (*N*-hexanoyl-D-erythro-sphingosine, Sigma-Aldrich) and the inactive ceramide analog C_6 -dihydroceramide (*N*-hexanoyl-D-erythro-sphinganine, Avanti Polar Lipids) were exogenously applied to cardiomyocytes at the indicated concentrations. Both stock solutions of $10\ \text{mM C}_6$ -ceramide and $10\ \text{mM C}_6$ -dihydroceramide were prepared using 100% dimethylsulfoxide (DMSO). Two inhibitors were used to assess the role of PKC in mediating C_6 -ceramide's functional effects. The general PKC inhibitor Chelerythrine chloride (Sigma-Aldrich) was used at a concentration of $1\ \mu\text{M}$ diluted from a stock solution prepared in distilled water. This concentration has been shown to be sufficient to inhibit $\text{PKC}\alpha$, δ and ϵ translocation in the rat myocardium (86). Go6976 (Tocaris) is a selective inhibitor for Ca^{2+} -dependent isoforms of PKC ($\text{PKC}\alpha$ and $\text{PKC}\beta$) and was used at a concentration of $5\ \mu\text{M}$ diluted from a stock solution prepared in 100% DMSO.

3. Simultaneous Cell Shortening and Ca²⁺ Transient Measurements

After isolation an aliquot of cells was placed in a small perfusion chamber mounted on the stage of an inverted microscope, the cells were allowed to settle to the bottom and any unattached cells were washed off with dye-free Control Solution (CS) containing 133.5 mM NaCl, 4 mM KCl, 1.2 mM NaH₂PO₄, 10 mM HEPES, 1.2 mM MgSO₄, 11.1 mM glucose (pH 7.4 using NaOH) and 1.5 mM Ca²⁺. A background fluorescent recording was taken and used for each emission spectra to reduce noise. The perfusion chamber was then cleaned of the cells and washed briefly to remove any debris. An aliquot of cells was then loaded within the perfusion chamber for 10 mins with 3 μM fura 2-AM (Invitrogen), which was made from a DMSO-based stock, diluted in 1 mM Ca²⁺ containing CS-BSA. Following loading, de-esterification of the fura 2 indicator was accomplished with a 10 min perfusion with CS. Cells were field stimulated at 0.5 Hz using parallel platinum electrodes submerged in the bathing solution and base-line intracellular Ca²⁺ ([Ca²⁺]_i) transients and unloaded cell shortening were recorded simultaneously. For [Ca²⁺]_i transient measurements, myocytes were alternately excited with light at a wavelength of 340 and 380 nm and the emitted fluorescence was collected at a wavelength of 505 nm by a photomultiplier tube. Unloaded cell shortening assessment was carried out using edge detection. Cell images were collected by the 40X Nikon objective and transferred to a multi-image module. From here, images were separated from the fluorescence using a 580-nm dichroic mirror and projected onto a TV monitor. A video-edge detector (Crescent Electronics) was

used to monitor cell length and recordings were stored in an acquisition software program (Felix32, Photon Technology International) for later analysis offline.

4. Treatment of Isolated Cardiomyocytes

To measure the direct effects of C₆-ceramide on cell shortening and [Ca²⁺]_i transients, treatment was carried out on the same cell following base-line measurements. Initial experiments were performed with different concentrations of ceramide (between 1-5 μM) to determine the concentration and time for treatment. All further studies were carried out with 5 μM C₆-ceramide (or DMSO control) for a period of 2 mins. In separate experiments, cells were also exposed to the inactive ceramide analog C₆-dihydroceramide (5 μM) to assess the bioactive specificity of C₆-ceramide treatment (8). Likewise, to measure the role of PKC in mediating ceramide's effects, following base-line measures cells were exposed to inhibitor only (either 1 μM Chelerythrine chloride or 5 μM Go6976) and measurements were taken after 2 minutes. After 5 mins of exposure to the inhibitor, the perfusion solution was changed to inhibitor + 5 μM C₆-ceramide and measurements were repeated after 2 minutes.

5. Cell Shortening and Ca²⁺ Transient Analysis

The peak percentage of cell shortening was calculated from 5 individual shortening peaks and expressed as an average percentage of shortening. To determine the shortening and relengthening velocities, the first derivative of the cell shortening trace was calculated using Felix32 (Photon Technology International), and the maximal velocity peak was determined from the average of 5 individual

peaks. The $[Ca^{2+}]_i$ transient was measured as a function of the ratio of emissions from 340/380 excitation wavelength after subtraction of the background fluorescence. The baseline and peak $[Ca^{2+}]_i$ transient was manually determined from the average of 5 individual tracings. The decay times (τ_{decay} , ms) were evaluated by a monoexponential fit to the declining phase of the $[Ca^{2+}]_i$ transient using pClamp 9.0 (Molecular Devices).

6. Cell Culturing and Treatment

Short term culturing conditions follow methods previously established (104). Isolated cells were plated on 60-mm dishes pre-coated with 10 $\mu\text{g}/\mu\text{L}$ mouse laminin (Sigma-Aldrich) for 1 hr in Medium 199, Cellgrow) supplemented with 5 mM creatine, 2 mM L-carnitine, 5 mM taurine, 10 mM Na_2HCO_3 , 10 mM HEPES, 50 U/mL penicillin and 50 U/mL streptomycin (pH 7.4) to make creatine-carnitine-aurine (CCT) medium. After the initial plating time, plates were washed twice with CCT medium to remove any unattached cells and the medium was replaced with either 10 μM C_6 -ceramide treatment medium, 100 nM phorbol 12-myristate 13-acetate (PMA), or normal CCT. Plates were incubated for 5 mins in the selected condition medium at 37°C, 5% CO_2 .

7. Subcellular Fractionation of Adult Rat Cardiomyocytes

Subcellular fractionation methods were modified from (182), and all steps were carried out on ice or at 4°C. Following treatment, cells were quickly washed in with CCT and then manually scraped using 120 μL of ice cold fractionation buffer (FB; 20 mM Tris-HCl, 2 mM EDTA, 0.5 mM EGTA, 0.3 mM sucrose, pH 7.4 with

mammalian protease inhibitor cocktail (Sigma, 1:100) and phosphatase inhibitor cocktail (Calbiochem, 1:100) and centrifuged for 5 mins at 20,000 x g to wash and collect cells. The supernatant was removed and cell pellets were resuspended in 30 μ L of FB. Samples were then homogenized with a micro ground glass Dual homogenizer for 1 min (*Fraction a – whole cell homogenate*) and centrifuged at 1,000 x g for 5 mins. The supernatant fraction was saved and the pellet re-homogenized 3 additional times with the final pellet (*Fraction b – nuclear and sarcomeric*) ultimately discarded. Supernatant fractions from each homogenization were pooled together (*Fraction c – enriched sample*). Cytosolic and particulate fractions were then separated by ultracentrifugation at 40,000 x g for 30 mins. The resulting supernatant fraction was kept as the cytosolic fraction (*Fraction d – cytosolic*) and the pellet was resuspended in sucrose-free FB with 1% Triton, incubated for 1 hr (*Fraction e – particulate*), then centrifuged at 80,000 x g for 15 mins. The resulting supernatant fraction was kept as the membrane fraction (*Fraction f – membrane*) and pellets were discarded (*Fraction g – insoluble particulate*). Prior to experimentation, successful fractionation of the cytosol and membrane was confirmed using Western blotting with antibodies against the cytosolic protein GAPDH (Santa Cruz; 1:500) and the membrane protein Na⁺/K⁺ ATPase (Millipore; 1:5,000) (See Figure 7). Protein samples (20 μ g) of cytosolic and membrane fractions were separated by SDS-PAGE and protein was transferred to 0.2 μ m nitrocellulose membrane. Membranes were stained with MemCode (Pierce Biotechnology) and imaged on a Chemidoc XRS+ imager (BioRad) to quantitate total protein. After the stain was removed, membranes

were blocked in 5% milk in TBS-T and then incubated overnight at 4°C in primary antibody [PKC ϵ (Millipore), 1:1,500; PKC δ (Santa Cruz), 1:500; PKC ζ (Santa Cruz), 1:500] diluted in TBS-T with 2.5% milk. Membranes were washed for 30 mins in TBS-T and incubated in secondary antibody (goat anti-mouse (Sigma) 1:50,000 for Na⁺/K⁺ ATPase; goat anti-rabbit (GE Healthcare), 1:40,000 for all others) conjugated to horseradish peroxidase for 1 hr at room temperature. Membranes were then washed for 30 mins in TBS-T and developed by ECL Plus on the ChemiDoc XRS+ imager (BioRad). Band densities were analyzed using ImageLab software (BioRad) and normalized to the total protein density in each respective lane, acquired from the MemCode stained images. Cytosolic and membrane fractions from each sample were expressed as the percentage of total (i.e. % cytosolic = density of band in cytosolic fraction/(density of cytosolic + membrane fraction bands)).

8. Statistical Analysis

Values are expressed as mean \pm S.E. For measures of unloaded cell shortening and [Ca²⁺]_i transients where 3 or more groups were compared statistical analyses were performed using one-way ANOVA along with a multi-comparison Newman-Keul's post-hoc test to make comparisons among groups. Statistical differences for all other functional data were determined using a paired Student's *t* test. For subcellular fractionations, statistical differences between the percentage of PKC isoform within the cytosolic or membrane fraction were compared using an unpaired Student's *t* test. A level of $p < 0.05$ was considered significant throughout.

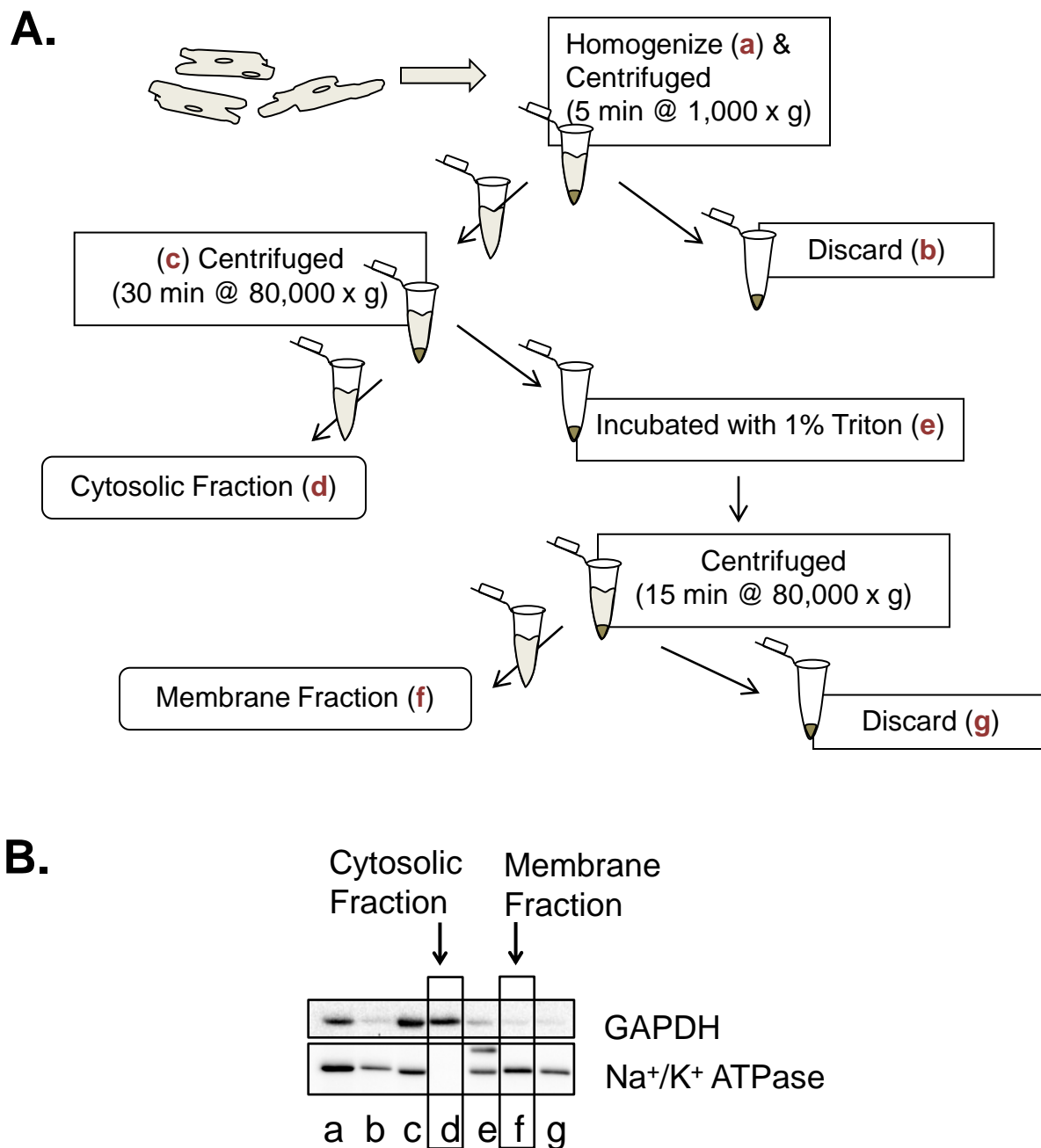


Figure 7: Preparation of subcellular fractions from isolated rat cardiomyocytes. A, Schematic of the protocol developed for subcellular fractionation of adult rat cardiomyocytes. The letters in parentheses correspond to each fraction used for Western blotting. B, Representative Western blot of GAPDH and Na⁺/K⁺ ATPase performed on samples taken during each step of the subcellular fractionation protocol (see *Materials and Methods*). The presence of GAPDH predominately within the cytosolic fraction (fraction d) and Na⁺/K⁺ ATPase only within the corresponding membrane fraction (fraction f) confirms proper subcellular fractionation.

C. Results

1. Acute ceramide treatment of isolated cardiomyocytes depresses contractility without altering Ca^{2+} transients

First we assessed the functional consequence of exogenous ceramide exposure in both a concentration-dependent and a time-dependent manner. As depicted in Figure 8, treatment of isolated rat cardiomyocytes for 2 min with C_6 -ceramide decreased the peak amplitude of cell shortening in a concentration-dependent manner, with a maximal decrease of $26.7 \pm 4.0\%$ at $5 \mu\text{M}$ concentration. Importantly, treatment with vehicle (0.05% DMSO) had no effect on cell shortening (see also Figure 11 for more details). The ceramide-mediated decrease in peak amplitude of shortening was also time-dependent, as shown in Figure 9. Regardless of time or concentration studied, ceramide exposure had no effect on the peak Ca^{2+} transient or the rate of transient decline (τ), as assessed by the Fura 2 ratio (Figure 8A *Insert*). Based on these initial studies, further characterization of the functional effects of ceramide on cell mechanics and intracellular $[\text{Ca}^{2+}]$ was conducted using 2 min exposure of myocytes to $5 \mu\text{M}$ C_6 -ceramide.

After establishing the dose and time course for treatment, we performed further experiments for a more complete characterization of ceramide-mediated effects. Figure 10A shows an overlay of pacing-stimulated cell shortening and $[\text{Ca}^{2+}]_i$ transient measures taken simultaneously in the same cell at base-line (control) and after ceramide treatment. In these experiments, the average cell length at base-line was $103.5 \pm 7.3 \mu\text{m}$ and did not differ with ceramide treatment. Acute exposure of isolated cardiomyocytes to ceramide resulted in a significant depression in the peak

amplitude of unloaded cell shortening (base-line = $11.4 \pm 0.8\%$ vs. ceramide = $9.8 \pm 0.9\%$). The peak rate of contraction was also reduced following ceramide treatment (base-line = $109.5 \pm 6.7 \mu\text{m/s}$ vs. ceramide = $96.3 \pm 6.9 \mu\text{m/s}$), whereas the peak rate of relaxation remained unaltered (base-line = $65.6 \pm 9.6 \mu\text{m/s}$ vs ceramide = $59.2 \pm 9.7 \mu\text{m/s}$) (Figure 10B). These changes in cellular mechanics following ceramide treatment occurred independent of changes in $[\text{Ca}^{2+}]_i$, demonstrated by the lack of an effect of ceramide treatment on the resting $[\text{Ca}^{2+}]_i$ (base-line = 0.31 ± 0.03 vs ceramide = 0.31 ± 0.03), peak $[\text{Ca}^{2+}]_i$ amplitude (Δ fura ratio; base-line = 0.34 ± 0.06 vs ceramide = 0.36 ± 0.07) and the decay time constant, τ (base-line = 808.5 ± 81.2 ms vs ceramide = 839.0 ± 75.1 ms) (Figure 10C). Table I shows the effects of ceramide, along with treatments discussed in subsequent sections, on the parameters of cell shortening and $[\text{Ca}^{2+}]_i$ expressed as a percentage of base-line measures.

2. Ceramide-mediated effects are specific to ceramide's known bioactivity

To test the specificity of ceramide's functional effect, we exposed cardiomyocytes to C₆-dihydroceramide, an inactive ceramide analog (8), or 0.05% DMSO (the concentration of DMSO present in the dihydroceramide perfusion buffer) and measured cell shortening and $[\text{Ca}^{2+}]_i$ transients. As shown in Figure 11, both DMSO and dihydroceramide failed to alter any of the parameters of cell shortening or $[\text{Ca}^{2+}]_i$ transients. These findings indicate that the negative inotropic response, in the presence of unaltered $[\text{Ca}^{2+}]_i$, induced by ceramide is specific to ceramide's known bioactivity.

3. PKC ϵ mediates ceramide's negative inotropic response

To examine the potential involvement of PKC in the ceramide-mediated effects we repeated measures of intact cell shortening and $[Ca^{2+}]_i$ transients in isolated myocytes in the presence of ceramide + the general PKC inhibitor chelerythrine chloride. Cardiomyocyte contractile parameters were unchanged from base-line levels when exposed to ceramide in the presence of chelerythrine chloride (Figure 12A; peak shortening = $10.7 \pm 1.2\%$, vs base-line = $10.5 \pm 1.5\%$), demonstrating the global inhibition of PKC attenuates the ceramide-mediated depression of cardiomyocyte contractility. Measurements of $[Ca^{2+}]_i$ transients were also unchanged among all groups (See Figure 12B and Table I). Through use of the conventional PKC inhibitor, Go6976, we were able to demonstrate that ceramide mediates its negative inotropic effects through one of the Ca^{2+} -independent isoforms of PKC (Figure 13). Treatment of cardiomyocytes with Go6976 alone had no effect on cell shortening parameters (peak shortening = $8.6 \pm 0.8\%$ vs base-line = $8.9 \pm 0.8\%$, velocity of shortening = $98.9 \pm 10.2 \mu\text{m/s}$ vs. base-line = $100.3 \pm 9.9 \mu\text{m/s}$, velocity of relengthening = $76.6 \pm 11.6 \mu\text{m/s}$ vs base-line = $75.8 \pm 11.1 \mu\text{m/s}$) or $[Ca^{2+}]_i$ transients (peak fura amplitude = 0.44 ± 0.07 vs base-line = 0.43 ± 0.06 , decay time constant (τ) = $685.1 \pm 54.1 \text{ ms}$ vs base-line = $640.7 \pm 45.3 \text{ ms}$). Moreover, Go6976 was unable to block ceramide's functional effects when cells were exposed to Go6976 + ceramide. This is observed by ceramide's ability to depress peak shortening amplitude ($7.2 \pm 0.8\%$ vs base-line = $8.9 \pm 0.8\%$) and the maximal velocity of shortening ($83.5 \pm 10.3 \mu\text{m/s}$ vs base-line = $100.3 \pm 9.9 \mu\text{m/s}$) with no change in the relengthening velocity (ceramide + Go6976 = $66.0 \pm 10.6 \mu\text{m/s}$

vs base-line = 75.8 ± 11.1 $\mu\text{m/s}$) or $[\text{Ca}^{2+}]_i$ transient (peak fura amplitude for ceramide + Go6976 = 0.41 ± 0.06 vs base-line = 0.43 ± 0.06 , decay time constant (τ) for ceramide + Go6976 = 709.1 ± 56.9 vs base-line = 640.7 ± 45.3 ms) in the presence of Go6976.

Based on these findings, we assessed activation of the Ca^{2+} -independent PKC isoforms following ceramide treatment of isolated cardiomyocytes. Inactive PKCs are found predominately in the cytosol and require membrane translocation for activation (79). Therefore, use of subcellular fractionation and immunoblotting of the Ca^{2+} -independent PKC isoforms were used to indirectly measure PKC activation through translocation in untreated and C_6 -ceramide treated myocytes. Our values for subcellular distribution of untreated (control) samples shown here are consistent with values previously published (148). Cardiomyocytes were also treated with PMA, a potent activator of conventional and novel PKCs, as a positive control for PKC δ and ϵ . As expected, treatment of cardiomyocytes with 100 nM PMA resulted in translocation of virtually all of PKC ϵ and PKC δ into the membrane fraction ($98.60 \pm 0.58\%$ and $91.50 \pm 0.05\%$, respectively), while the subcellular distribution of PKC ζ remained unchanged by PMA treatment (membrane fraction = $33.60 \pm 2.92\%$) (Figure 14A). Interestingly, ceramide treatment resulted in a significant shift in the subcellular distribution of PKC ϵ , with $28.80 \pm 3.80\%$ localized within the membrane fraction compared to $16.67 \pm 1.90\%$ in untreated (control) samples. The distribution of PKC δ (membrane fraction = $55.32 \pm 3.60\%$ in ceramide treated vs $63.01 \pm 2.60\%$ in untreated controls) and PKC ζ (membrane fraction = $20.23 \pm 6.72\%$ in ceramide treated vs $37.53 \pm 8.51\%$ in untreated controls) within the myocytes remained

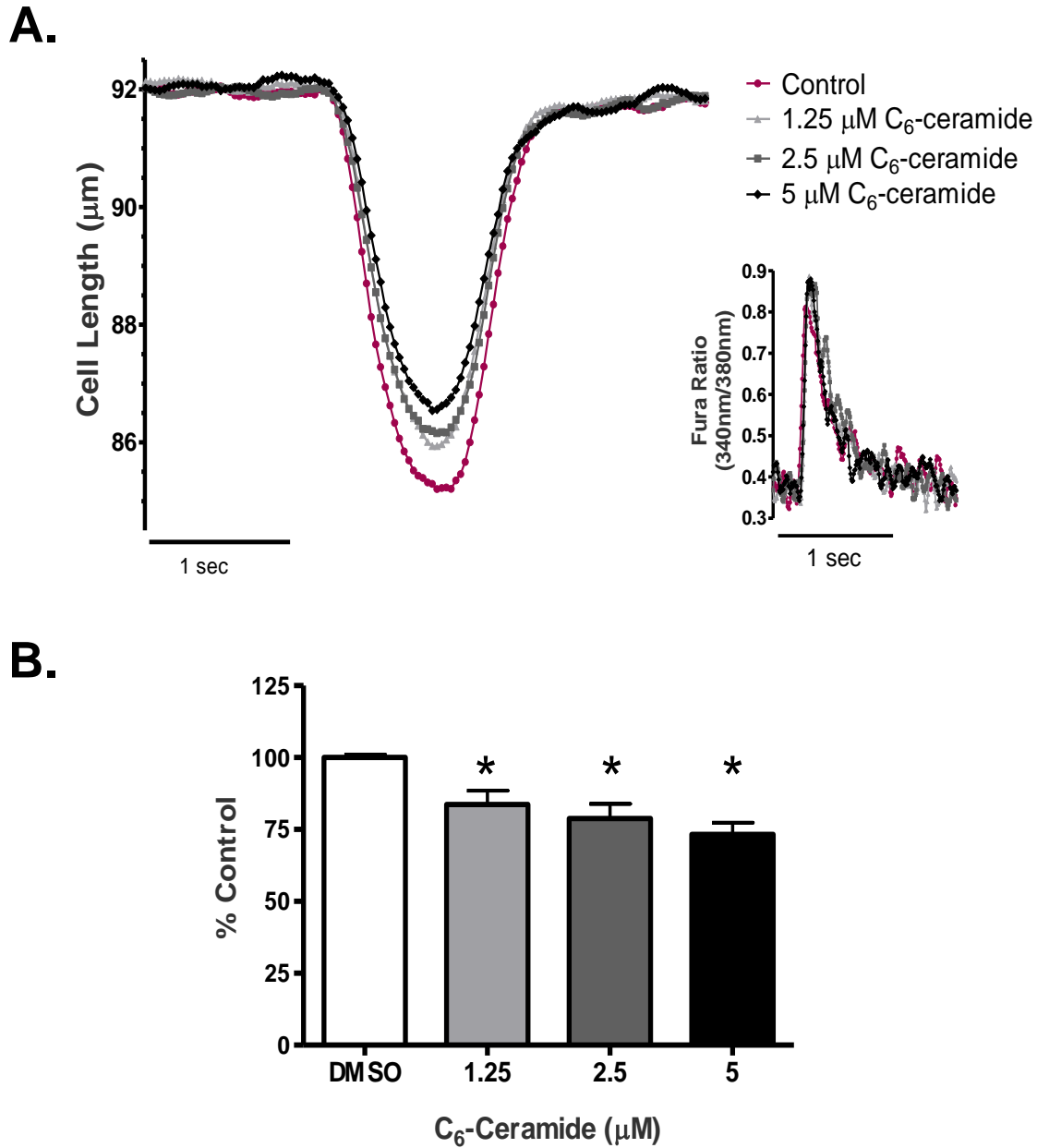


Figure 8: Concentration-dependent effects of exogenous C₆-ceramide treatment on contractile mechanics and [Ca²⁺]_i in ventricular cardiomyocytes.

A, Overlay of unloaded cell shortening measurements from a single cardiomyocyte under field stimulation at 0.5 Hz at base-line (control) and during treatment with sequentially increasing concentrations of C₆-ceramide. *Insert*, overlay of simultaneous Ca²⁺-transient measures corresponding to each cell shortening measure. No difference was observed in the peak amplitude or time for decay between groups. B, The quantified change in the percentage of cell shortening relative to control following treatment with vehicle (DMSO) and each concentration of C₆-ceramide. $F_{(3,15)} = 10.32$, * $p < 0.05$ vs DMSO; $n = 4$.

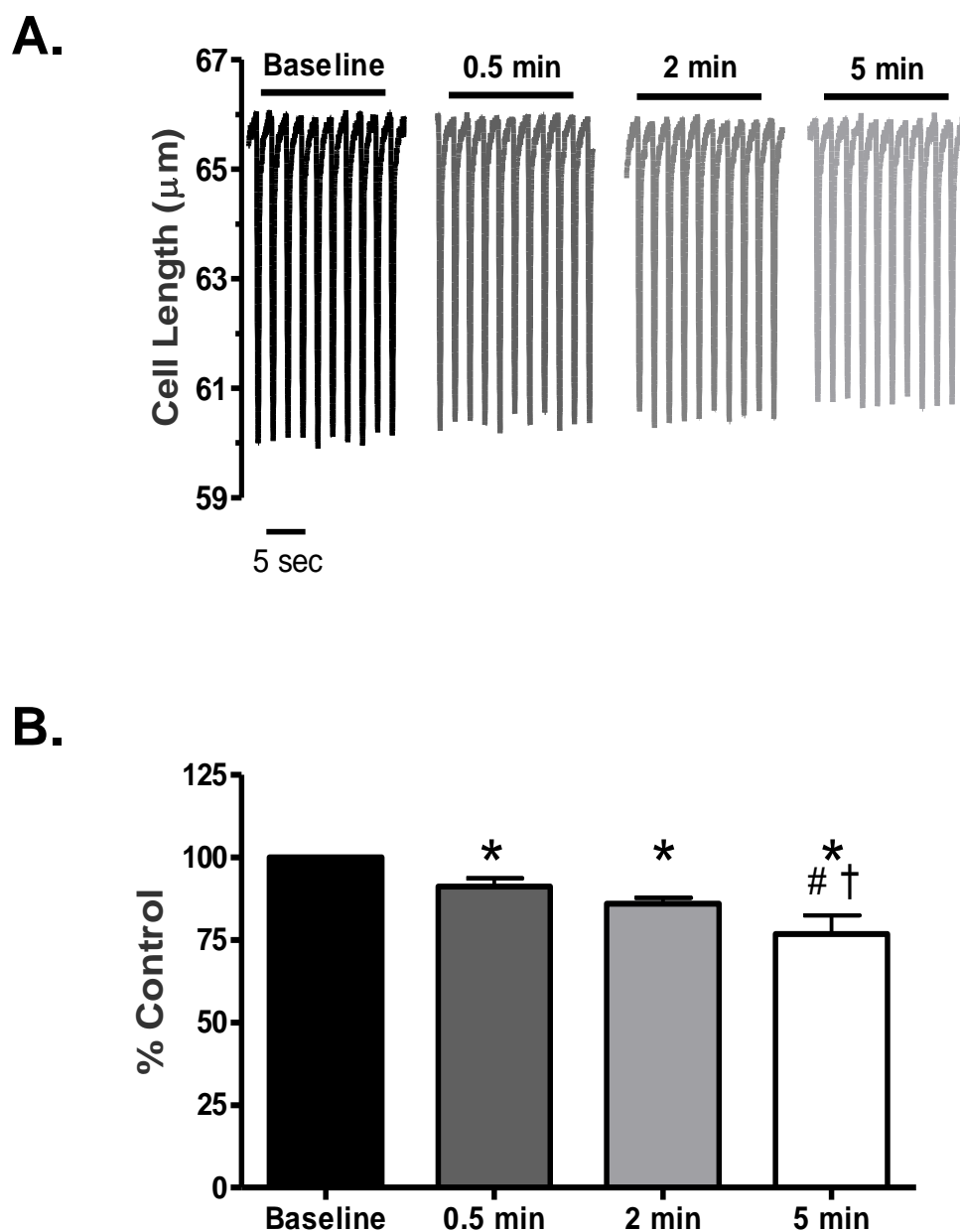


Figure 9: Time-dependent effects of exogenous C_6 -ceramide treatment on contractile mechanics in ventricular cardiomyocytes. A, Representative cell shortening measurements taken under steady-state pacing at base-line conditions and following 30 sec, 2 min and 5 min of exogenous C_6 -ceramide treatment. B, The quantified change in the percentage of cell shortening relative to control during the time course for C_6 -ceramide treatment. $F_{(3,12)} = 16.70$ * $p < 0.05$ vs. Base-line, # $p < 0.05$ vs. $1.25 \mu\text{M}$ C_6 -ceramide, † $p < 0.05$ vs. $2.5 \mu\text{M}$ C_6 -ceramide, $n = 3$.

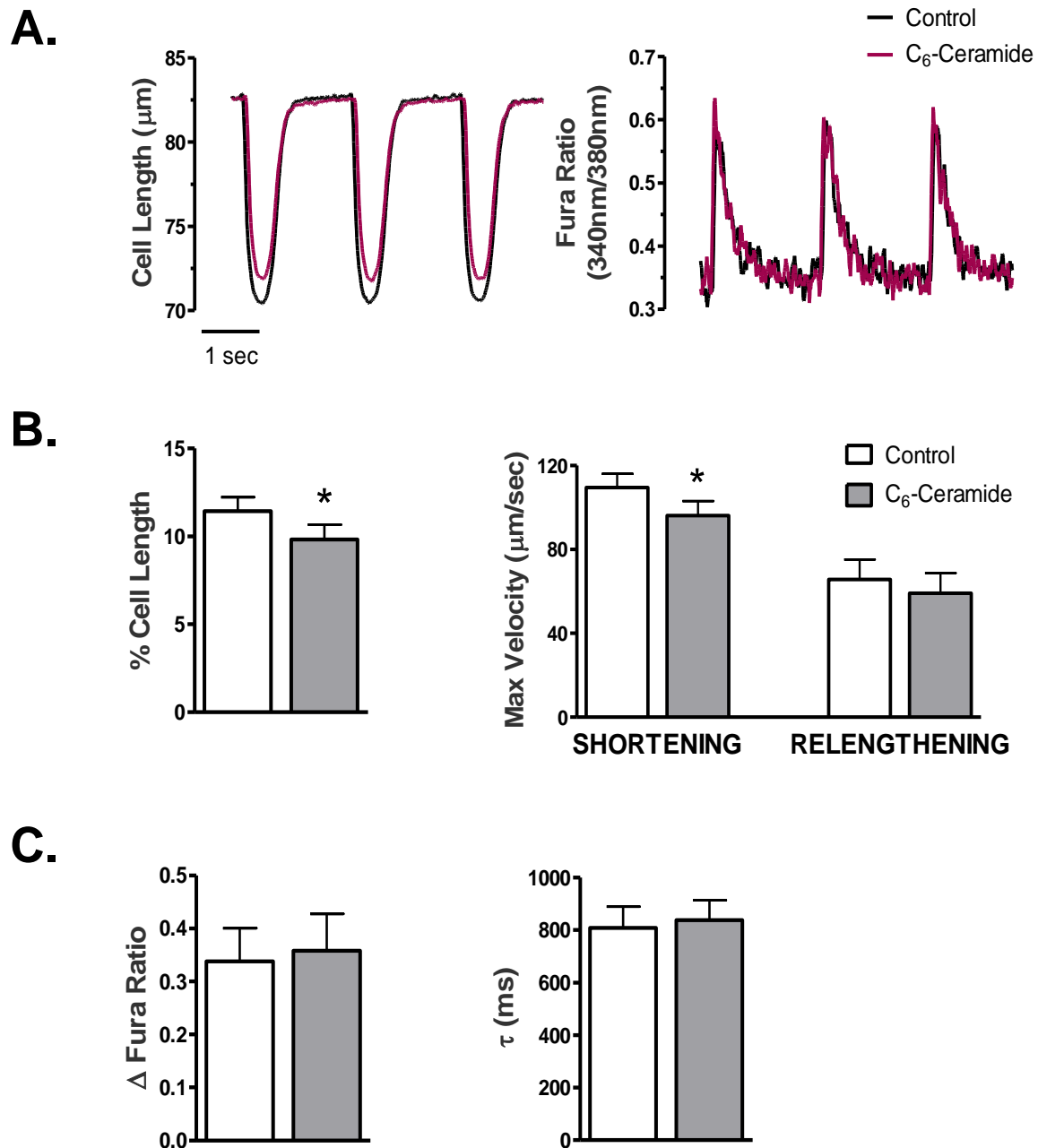
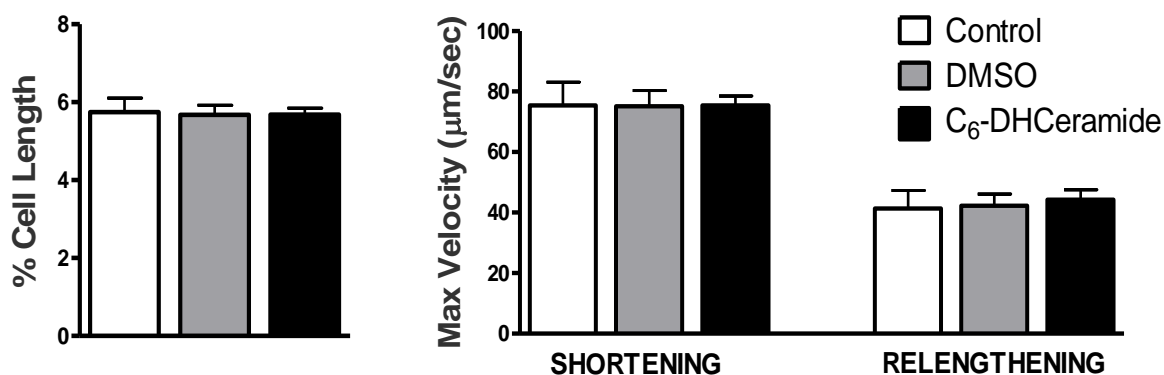


Figure 10: Effects of acute C₆-ceramide treatment on contractile mechanics and [Ca²⁺]_i in ventricular cardiomyocytes. A, Overlay of representative unloaded cell shortening measurements with simultaneous Ca²⁺ transient measurements in a single cardiomyocyte under field stimulation (0.5 Hz) before (black) and after (red) exogenous treatment with 5 μM C₆-ceramide. B, Quantification of the contractile parameters (percent of shortening and maximal rates of contraction and relaxation) and C, Ca²⁺ transient parameters (peak amplitude of the Fura ratio (340 nm/380 nm) and the time constant, τ, for the declining phase of the transient). **p*<0.05 vs Control; *n*=6.

A.



B.

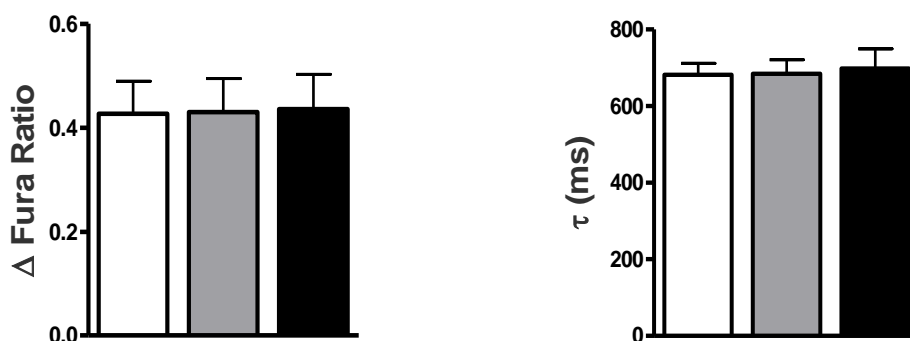


Figure 11: Assessment of functional specificity using the non-bioactive sphingolipid C₆-dihydroceramide. A, Quantification of the percent of cell shortening and the maximal rates of contraction and relaxation before treatment, with 0.05% DMSO (vehicle) and then following treatment with 5 μM C₆-dihydroceramide. B, Quantification of the Ca²⁺ transient peak amplitude (Δ Fura ratio, 340 nm/380 nm) and the time constant, τ, for the declining phase of the transient before treatment, with 0.05% DMSO and then following treatment with 5 μM C₆-dihydroceramide. $F_{(2,12)} = 0.05$, $n = 4$.

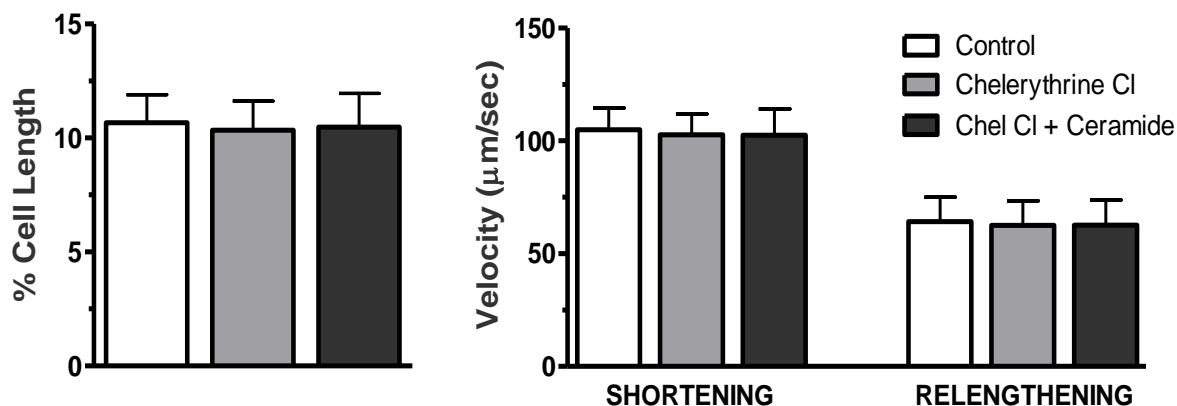
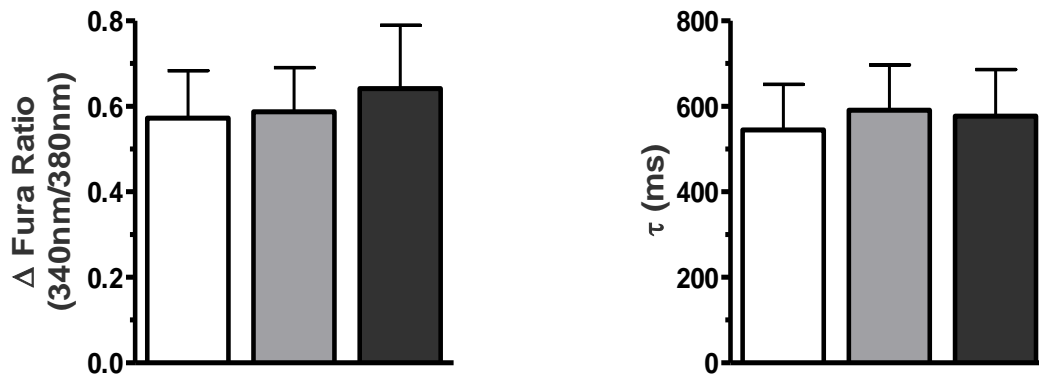
A.**B.**

Figure 12: Attenuation of the functional effects of acute C₆-ceramide treatment by inhibition of PKCs. A, Quantification of the percent of cell shortening and the maximal rates of contraction and relaxation before treatment, with 1 μM chelerythrine chloride and then following treatment with 1 μM chelerythrine chloride + 5 μM C₆-ceramide. B, Quantification of the Ca²⁺ transient peak amplitude (Δ Fura ratio, 340 nm/380 nm) and the time constant, τ, for the declining phase of the transient before treatment, with 1 μM chelerythrine chloride and then following treatment with 1 μM chelerythrine chloride + 5 μM C₆-ceramide. $F_{(2,12)} = 1.01$, $n = 4$.

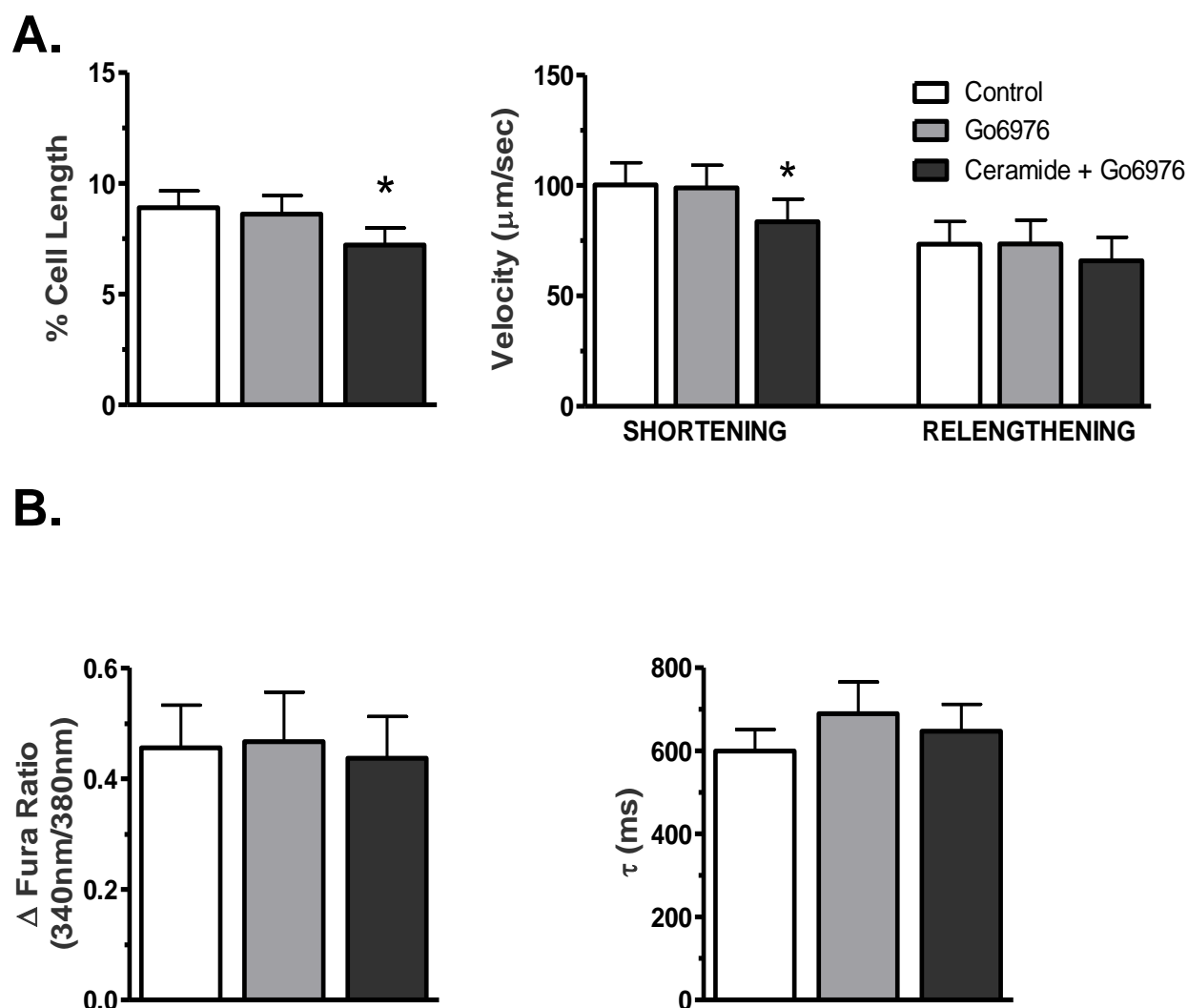


Figure 13: Inhibition of Ca^{2+} -dependent PKCs in the presence of C_6 -ceramide has no effect on cardiomyocyte shortening or $[\text{Ca}^{2+}]_i$. A, Quantification of the percent of cell shortening and the maximal rates of contraction and relaxation before treatment, with 5 μM Gö6976 and then following treatment with 5 μM Gö6976 + 5 μM C_6 -ceramide. B, Quantification of the Ca^{2+} transient peak amplitude (Δ Fura ratio, 340 nm/380 nm) and the time constant, τ , for the declining phase of the transient before treatment, with 5 μM Gö6976 and then following treatment with 5 μM Gö6976 + 5 μM C_6 -ceramide. $F_{(2,16)} = 28.89$, * $p < 0.05$ vs Control; $n = 6$.

Table B: Parameters of Cellular Mechanics and Intracellular Ca²⁺ Transients (% Control)

	DMSO (n = 5)	5 μ M C ₆ - dihydroceramide (n = 5)	5 μ M C ₆ - ceramide (n = 6)	1 μ M Chelerythrine Cl (n = 4)	5 μ M C ₆ -ceramide + Chelerythrine Cl (n = 4)	5 μ M Go6976 (n = 6)	5 μ M C ₆ -ceramide + 5 μ M Go6976 (n = 6)
Peak Shortening	98.9 \pm 1.3	103.0 \pm 1.8	82.7 \pm 3.3*	93.4 \pm 2.6	93.4 \pm 3.1	96.3 \pm 1.5	80.4 \pm 3.4*
- dL/dt	101.2 \pm 1.8	106.0 \pm 6.12	85.7 \pm 3.6*	96.1 \pm 2.8	97.8 \pm 2.0	98.7 \pm 2.1	81.9 \pm 4.1*
+ dL/dt	105.2 \pm 3.5	110.3 \pm 7.9	89.9 \pm 3.3	96.0 \pm 4.5	98.6 \pm 4.7	98.2 \pm 3.6	89.6 \pm 5.2
Peak [Ca ²⁺] Amplitude	99.9 \pm 2.9	102.0 \pm 5.0	102.0 \pm 3.9	102.5 \pm 2.6	108.3 \pm 4.1	102.1 \pm 4.7	100.3 \pm 7.8
Tau (τ)	98.4 \pm 2.4	102.4 \pm 6.2	105.6 \pm 5.6	116.5 \pm 8.6	110.4 \pm 12.2	107.7 \pm 5.8	111.1 \pm 6.3

Results are means \pm S.E.M. * $p < 0.05$ where paired observations are found to be statistically different based on a one-way ANOVA with a Newmann-Keuhl's post-hoc analysis.

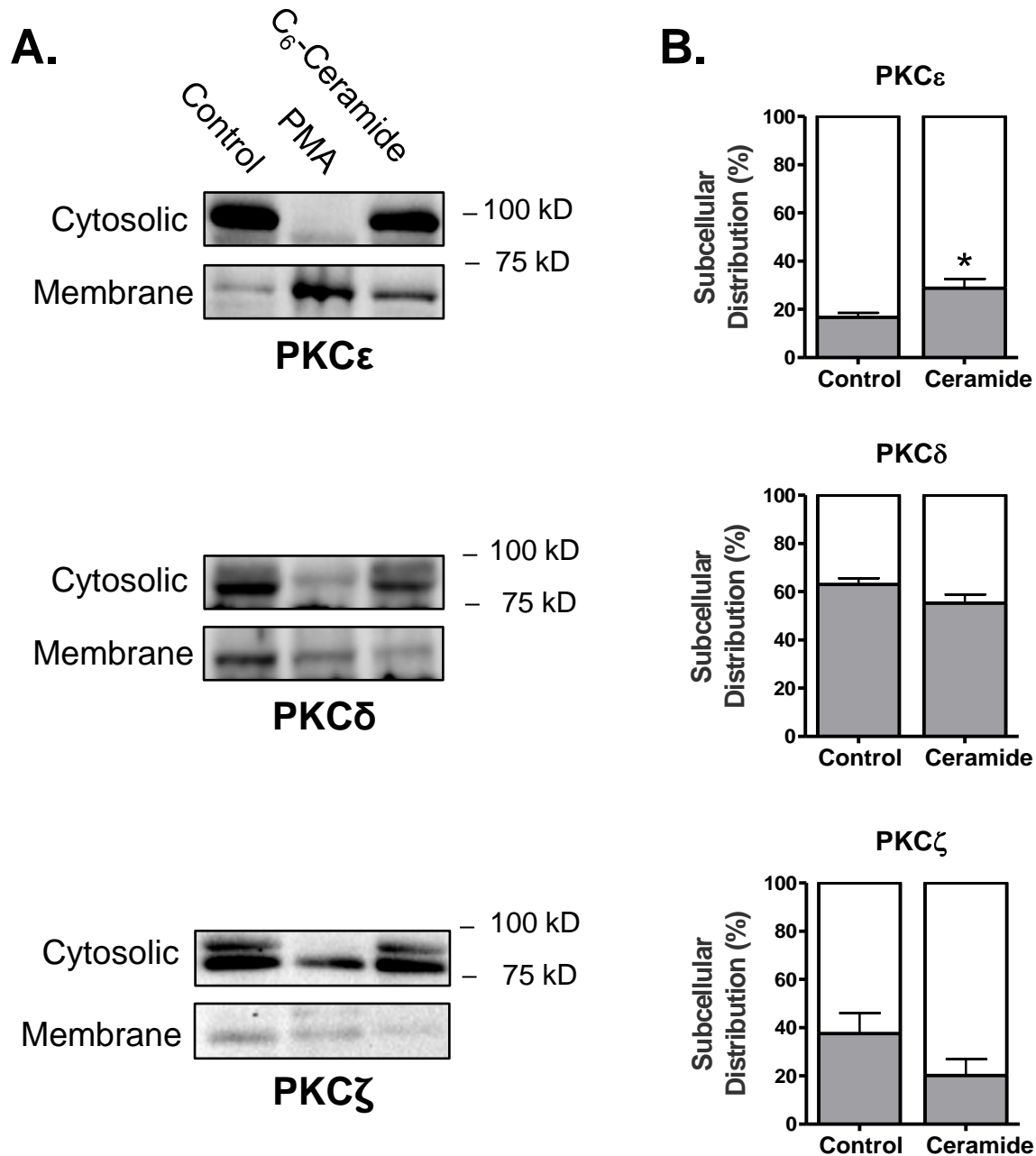


Figure 14: Translocation of the Ca²⁺-independent PKC isoforms. A, Representative Western blots of the Ca²⁺-independent PKC isoforms in the cytosolic and membrane subcellular fractions of isolated cardiomyocytes treated with medium only (control), myocytes treated with 100 nM PMA, and myocytes treated with 10 μ M C₆-ceramide. B, Quantification of the cytosolic and membrane subcellular fractions from control and C₆-ceramide treated samples. White bars represent the amount of PKC in the cytosolic fraction and grey bars represent the amount of PKC within the membrane fraction. Each band density was normalized to the total protein within that lane. An $n=3$, * $p<0.05$ vs Control.

insignificant by ceramide treatment (Figure 14B). These results suggest that ceramide signals through PKC ϵ to alter myofilament properties and depress contractility.

D. Discussion

Although ceramide accumulation in the heart is known to adversely affect cardiac function, the present study demonstrates for the first time that ceramide directly alters cardiomyocyte contractility through ceramide signaling to the myofilament via PKC ϵ . Previous studies have concluded that depressions in contractility observed when ceramide levels are elevated are due primarily to cell death via ceramide-stimulated apoptosis. However, our functional observations in intact cardiomyocytes revealed that ceramide directly regulates contractile function. This was demonstrated by a depression in shortening amplitude and velocity following ceramide exposure, which occurred despite unaltered $[Ca^{2+}]_i$ levels or kinetics. While these changes were modest (15-20% reduction), these observations would be projected to reduce force production and power output (the product of force and velocity) in the intact myocardium and contribute significantly to depressed contractile function.

The mechanism by which ceramide-mediated activation of PKC might alter contractile mechanics is likely to involve both the allosteric regulation of crossbridges reacting with the thin filament and crossbridge dynamics independent of thin filament activation. PKC dependent phosphorylation of the myofilament *in vitro* has been shown to reduce Ca^{2+} -activated actomyosin ATPase, myofilament Ca^{2+} sensitivity and cooperativity with observed depressions in the maximal tension generation (17, 83, 91, 126, 133-136, 152, 190). Functionally, these changes are associated with reduced

force production and shortening velocity, both loaded and unloaded (98, 187), resulting in depressed power output (77). While reductions in isometric tension generation can be attributed to an altered activation state of the myofilament, previous studies demonstrate that shortening velocities at zero load are unaffected by myofilament activation (40, 57) and are more likely to depend on crossbridge cycling (80). However, exactly how PKC-dependent phosphorylation of the myofilament modifies crossbridge dynamics is unclear. Whereas earlier studies by Pyle et al (153) identify PKC-mediated effects on crossbridge detachment rates, as demonstrated by increased tension cost (an estimate of the crossbridge detachment rate (14, 36)) in transgenic mice expressing an unphosphorylatable mutant cTnI (cTnI-S43A/45A), more recent studies have shown unaltered tension costs, and therefore unaltered crossbridge detachment rates in transgenic (TG) mice in which all 3 PKC sites were pseudophosphorylated by glutamic acid substitution (88). The authors, instead, attributed the negative inotropic response in TG mice to a decreased rate of crossbridge formation and a Ca^{2+} -independent persistence of the active state. Despite the discrepancy, in general PKC-mediated phosphorylation has been shown to reduce crossbridge cycling rate (133-134, 136) and would be expected to prolong the duty cycle, consequently reducing shortening kinetics during ejection. This is likely also to be true for the PKC-dependent effects we observed following ceramide treatment. Moreover, evidence from others would suggest that the effects we observed in isolated cardiomyocytes may be more pronounced in the intact, auxotonically-loaded heart (95), translating to a marked reduction in pressure development, decreased extent of shortening during ejection and overall impairment of systolic function.

Beyond the acute effects shown here, ceramide-induced activation of PKC may also be of significance in cardiac remodeling and the development of dilated cardiomyopathy associated with long-term elevations in ceramide (46, 142, 224, 228). Activation of PKCs directly by ceramide has been shown to occur in the heart, leading to both insulin resistance (24) and reduced β -adrenergic signaling (38). Likewise, it is well known that PKC activation induces hypertrophic growth within the heart (12, 159, 194, 218) and may further play a role in modifying actin capping dynamics (69) to promote addition of new sarcomeres into the myofilament lattice. It is enticing, therefore, to speculate that chronic elevations in ceramide may be one of the mechanistic triggers of cardiac decompensation which leads to contractile dysfunction, ventricular dilation and the progression to failure. This hypothesis is certainly supported by studies from Park et al (142) who found that inhibition of *de novo* ceramide biosynthesis in LpL_{GPI} overexpressing mice, which develop lipotoxic-induced dilated cardiomyopathy, resulted in reduced apoptosis, enhanced myocardial energetic and improved overall systolic function and survival. Interestingly, in a rat model of metabolic syndrome, elevations in TAG and long-chain acyl CoAs (ceramide content was not measured) caused membrane translocation and activation of PKC ϵ leading to contractile dysfunction (34). Nevertheless, future studies examining ceramide accumulation in human diseases of cardiac lipotoxicity will be critical for establishing a role for ceramide as a lipotoxic mediator in human pathology.

Although novel, these findings are limited by the use of exogenous treatment of a non-biological ceramide analog. While use of C6-ceramide has been shown to illicit responses similar to endogenously generated ceramide (45), we do not assess the

Beyond the acute effects shown here, ceramide-induced activation of PKC may also be of significance in cardiac remodeling and the development of dilated cardiomyopathy associated with long-term elevations in ceramide (46, 142, 224, 228). Activation of PKCs directly by ceramide has been shown to occur in the heart, leading to both insulin resistance (24) and reduced β -adrenergic signaling (38). Likewise, it is well known that PKC activation induces hypertrophic growth within the heart (12, 159, 194, 218) and may further play a role in modifying actin capping dynamics (69) to promote addition of new sarcomeres into the myofilament lattice. It is enticing, therefore, to speculate that chronic elevations in ceramide may be one of the mechanistic triggers of cardiac decompensation which leads to contractile dysfunction, ventricular dilation and the progression to failure. This hypothesis is certainly supported by studies from Park et al (142) who found that inhibition of *de novo* ceramide biosynthesis in LpL_{GPI} overexpressing mice, which develop lipotoxic-induced dilated cardiomyopathy, resulted in reduced apoptosis, enhanced myocardial energetic and improved overall systolic function and survival. Interestingly, in a rat model of metabolic syndrome, elevations in TAG and long-chain acyl CoAs (ceramide content was not measured) caused membrane translocation and activation of PKC ϵ leading to contractile dysfunction (34). Nevertheless, future studies examining ceramide accumulation in human diseases of cardiac lipotoxicity will be critical for establishing a role for ceramide as a lipotoxic mediator in human pathology.

Although novel, these findings are limited by the use of exogenous treatment of a non-biological ceramide analog. While use of C6-ceramide has been shown to illicit responses similar to endogenously generated ceramide (45), we do not assess the

functional effects of naturally generated ceramide in these studies. Future studies aimed at assessing the functional effects of endogenously generated ceramide, through use of ceramidase inhibitors (i.e. DMAPP) or compounds that inhibit the conversion of ceramide to sphingomyelinase (i.e. D609), would serve to overcome this limitation.

CHAPTER III

**IDENTIFICATION OF POST-TRANSLATIONAL MODIFICATIONS TO
MYOFILAMENT PROTEINS FOLLOWING CERAMIDE TREATMENT**

A. Introduction

Charge modifications, such as phosphorylation, are known to alter the protein-protein interactions within the sarcomere and are well correlated with altered myocardial dynamics (including the myofilament response to Ca^{2+} and cross-bridge cycling rate). In the healthy heart, this helps to finely tune cardiac performance on a beat-to-beat basis; however, persistence of myofilament protein phosphorylation has been shown to contribute greatly to the decline in cardiac function associated with cardiac disorders (6, 91, 208). Disturbances in myocardial metabolism leading to accumulation of ceramide have been linked to cardiac dysfunction and our work presented in Chapter 2 of this thesis provides evidence in support of altered myofilament mechanics as the underlying cause. Moreover, the rapid responses to ceramide treatment we observed point to transient changes in the post-translational state of the myofilament proteins.

We have hypothesized that ceramide confers its negative inotropic response through enhanced phosphorylation of the myofilament, specifically at PKC sites. Evidence indicates that phosphorylation of the myofilament by PKC can have differential effects on contractile mechanics, depending on the specific PKC isoform. PKC δ is unique in its ability to phosphorylate cTnI at the conventional PKA-specific sites, serine 23/24, leading to reduced Ca^{2+} -sensitivity (83). Phosphorylation of these sites is believed to be critical for the increased maximal force and enhanced relaxation kinetics associated

with adrenergic stimulation. PKC δ is also able to phosphorylate cTnI at Ser-43 and 45, as well as cTnT (83), modifications that have been shown to reduce contractility (88, 153, 190). PKC ϵ and α target for phosphorylation cTnI, specifically at Ser-43/45, cTnT and cMyBP-C (152, 190, 219). Phosphorylation of the myofilament proteins by either PKC α or ϵ *in vitro* reduces maximum Ca²⁺-activated force and shortening kinetics (83, 91, 98, 136). Transgenic mouse models have confirmed many of these *in vitro* findings and further indicate that persistent phosphorylation of the myofilament leads to the development of dilated cardiomyopathy (55, 174). The significant contribution of PKC-mediated myofilament phosphorylation to depressions in tension generation is further emphasized by studies in failing human hearts (11, 91).

Here we provide new evidence on the role of ceramide in regulating myofilament phosphorylation. We determined the extent to which ceramide may alter the phosphorylation state of the myofilament proteins by both 2-dimensional difference in-gel electrophoresis (2D-DIGE) and Western blotting. Our data show that ceramide mediates the decline in cardiomyocyte function through PKC-dependent phosphorylation of cTnI, cTnT and cMyBP-C, providing a novel mechanism by which ceramide may depress cardiac contractility.

B. Materials and Methods

1. Isolation of Adult Rat Cardiomyocytes

Rat ventricular cardiomyocytes were isolated from adult male Sprague-Dawley rats (Harlan) weighing between 180 - 200 g as previously described (See Chapter 2 and (104)). In brief, cells were isolated from excised hearts that were cannulated via the ascending aorta onto a Langendorff apparatus. Initially, hearts were

perfused for 3 mins with a Ca^{2+} -free control solution (BSA-CS) containing 133.5 mM NaCl, 4 mM KCl, 1.2 mM NaH_2PO_4 , 10 mM HEPES, 1.2 mM MgSO_4 , 11.1 mM glucose (pH 7.4 using NaOH) with added bovine serum albumin (1 mg/mL), followed by perfusion with oxygenated BSA-CS containing 0.25 mg/mL type II collagenase (Worthington Biochemical) and 0.03 mg/mL protease (Sigma-Aldrich) for 15 to 20 mins (perfusion time = 16 min/mg heart weight). Following digestion, myocytes are re-introduced to Ca^{2+} in a step-wise fashion with BSA-CS containing Ca^{2+} in concentrations of 50 μM through to a final concentration of 1 mM.

2. Cell Culturing and Treatment

Short term culturing conditions follow methods previously established (104). Isolated cells were plated on 60-mm dishes pre-coated with 10 $\mu\text{g}/\mu\text{L}$ mouse laminin (Sigma-Aldrich) for 1 hr in Medium 199 (Cellgrow) supplemented with 5 mM creatine, 2 mM L-carnitine, 5 mM taurine, 10 mM Na_2HCO_3 , 10 mM HEPES, 50 U/mL penicillin and 50 U/mL streptomycin (pH 7.4) to make creatine-carnitine-taurine (CCT) medium. After the initial plating time, plates were washed twice with CCT medium to remove any unattached cells and the medium was replaced with either 10 μM C_6 -ceramide treatment medium or normal CCT. Plates were incubated for 5 mins in the selected condition medium at 37°C, 5% CO_2 , at which time the treatment was removed and cells were washed quickly with PBS. In later experiments, an additional treatment group was added with cells pre-treated for 10 mins with 1 μM Chelerythrine chloride followed by 5 mins of treatment with 1 μM Chelerythrine chloride + 10 μM C_6 -ceramide.

3. Western Blot

a. Preparation of Protein for Biochemical Analysis

Cell culture plates were manually scraped in 500 mL of ice-cold CCT and the resulting suspension was transferred into a 1.5 mL microcentrifuge tube and pelleted by centrifugation at 12,000 rpm for 5 mins. The pellets were lysed in UTC Buffer (8 M urea, 2 M thiourea, 4% CHAPS) with bath sonication. Sample protein concentrations were determined using a modified Lowry's protein assay (RC-DC Assay, BioRad) and concentrated samples were stored at -80°C until used.

b. SDS-PAGE and Western Blot

Protein lysates (20µg) from cells were separated on 12% SDS gels followed by transfer of the protein to a 0.2 µm polyvinylidene difluoride (PVDF) membrane for Western blot analysis. Membranes were blocked in 5% milk in Tris-Buffered saline with 0.1% Tween-20 (TBS-T) and then incubated overnight at 4°C in primary antibody, with the exception of phospho-Tm which was incubated for 1 hr at room temperature [GAPDH (Santa Cruz) 1:500; phospho-cTnI (Ser23/24) (Cell Signaling), 1:400; cTnI (C5 clone, Fitzgerald) 1:5,000; phospho-Tm (Ser283) 1:10,000; Tm (CH-1, Iowa Hybridoma) 1:1,000]. Following incubation, membranes were washed for 30 mins in TBS-T and then incubated in secondary antibody [goat anti-mouse (Sigma-Aldrich) 1:40,000 for cTnI; goat anti-rabbit (GE Healthcare) 1:20,000 for all others] conjugated to horseradish peroxidase for 1 hr at room temperature. Membranes were then

washed for 30 mins in TBS-T and developed by enhanced chemiluminescence (ECL Plus, GE Healthcare) on a ChemiDoc XRS+ imager (BioRad). Band densities were analyzed using ImageLab software (BioRad).

c. Myosin Binding Protein-C Western Blot

Following cell culture treatment, the plates were washed once with PBS and 60 μ L of Urea buffer (50 mM Tris-HCl, pH 7.5, 4 M urea, 1 M thiourea, 0.4% CHAPS, 20 mM Spermine, 20 mM DTT) was added, plates were manually scraped and cells were lysed by sonication. Lysates were centrifuged for 10 mins at 14,000 rpm and the supernatant fraction was removed and kept as sample. Sample protein concentration was determined using the Bradford assay. Protein (10 μ g) was then loaded onto 4-15% gradient SDS gels followed by transfer to 0.45 μ m nitrocellulose membrane for Western blot analysis. Membranes were blocked in 1X Roche Western Blocking Reagent (Roche) diluted in TBS-T and then incubated overnight at room temperature (22-23°C) in primary antibody [cMyBP-C (C0-C1), 1:10,000; phospho-cMyBP-C (Ser273), 1:2,000; phospho-cMyBP-C (Ser282), 1:2,000; phospho-cMyBP-C (Ser302), 1:10,000 all a generous gift from Dr. Sakthivel Sadayappan at Loyola University Chicago; GAPDH (Santa Cruz), 1:1,000] diluted in 1X Blocking Reagent in TBS-T. Membranes were washed for 30 mins in TBS-T and then incubated in secondary antibody [donkey anti-rabbit (Santa Cruz) 1:10,000 for phospho-cMyBP-C (Ser273), and 1:20,000 for all others] conjugated to horseradish peroxidase for 1 hr at room temperature. Membranes were washed for 30 minutes in TBS and developed by ECL Plus on a ChemiDoc

XRS+ imager (BioRad). Band densities were analyzed using ImageLab software (BioRad).

4. **2-Dimensional Difference In-Gel Electrophoresis (2-D DIGE)**

Protein lysates (100 µg) were cleaned of any interfering substances that would produce high conductivity during isoelectric focusing using a 2D Clean-up Kit (GE Healthcare) and the precipitated protein was resuspended in UTC buffer. Samples were then labeled for 2 hrs with cyanine dyes (CyDye, GE Healthcare) at 100 pmol/50 µg of protein. In individual experiments CyDye labeling was randomized to eliminate bias based on dye affinity or sensitivity. Reactions were quenched on ice with 0.2 mM of L-lysine and 40 µg of each sample was mixed with IEF buffer containing 8 M urea, 2 M thiourea, 4% (w/v) Chaps, 130 mM DTT, 1% (v/v) Destreak (GE Healthcare), plus 0.25% (v/v) immobilized pH gradient (IPG) 7-11 ampholytes (for IPG 7-11 pH strips) or 0.5% (v/v) IPG 3-11 ampholytes (for IPG 3-11 pH strips) and loaded onto the Protean IEF tray. Both Nonlinear 3-11 IPG strips and 7-11 IPG strips (GE Healthcare) were passively re-hydrated for 10 hrs at 50 V and 20 °C and proteins were focused using a linear method [250 V for 15 mins, 10,000 V for 3 hrs, 10,000 V until 60,000 Vh]. For 7-11 pH strips, a wick soaked in 5% (w/v) DTT was added at 55,000 Vhrs to the negative end of the strip for 5 mins to replenish DTT at the basic end of the IPG strip. After focusing, samples were equilibrated in 1% DTT (w/v) dissolved in IEF Equilibration buffer (IEF-EQ; 6 M Urea, 5% SDS (w/v), 30% glycerol (v/v)) for 10 mins then in 2.5% iodoacetamide (w/v) dissolved in IEF-EQ. The second dimension electrophoresis was run on a 12% total acrylamide (0.5% crosslinking) SDS resolving gel. After

running, the gels were washed in ddH₂O for 30 mins and imaged using a Typhoon 9410 Imager (GE Healthcare) with Cy3 (532-nm laser), Cy5 (633-nm laser) and Cy2 (488-nm laser). Images were analyzed using PDQuest v8 advanced (Biorad), with spot intensities normalized to total gel density to reduce gel-to-gel variability. Percent phosphorylation was calculated using ratiometric analysis (% of phosphorylation = density of spot/total density of all spots for a given myofilament protein).

5. Statistical Analysis

Values are expressed as mean \pm S.E. For measures of unloaded cell shortening and [Ca²⁺]_i transients where 3 groups were compared, statistical analyses were performed using one-way ANOVA along with a multi-comparison Newman-Keul's post-hoc test to make comparisons among groups. Statistical differences for all other data were determined using an unpaired Student's *t* test. A level of $p < 0.05$ was considered significant throughout.

C. Results

We tested whether acute exposure of cardiomyocytes to ceramide had an effect on the post-translational state of myofilament proteins using 2D-DIGE, which allows for analysis of the post-translational state of the sarcomeric proteome on a global level. Figure 15 shows merged images of regions of interest from representative 2D-DIGE scans of a Cy3-labeled untreated (control) sample and a Cy5-labeled ceramide treated sample. Spots associated with Tm, RLC and cTnT are labeled in Figure 15A with migration of phosphorylated spots appearing toward the acidic region of the strip.

Analysis of the samples showed a significant increase in cTnT phosphorylation in samples treated with ceramide ($69.9 \pm 2.28\%$ vs control = $62.7 \pm 1.99\%$), while no changes were observed in RLC (control = 17.74 ± 3.16 vs ceramide = 19.80 ± 2.56) or Tm (control = 43.60 ± 4.19 vs ceramide = 35.54 ± 2.64).

Figure 15B shows the 2D-DIGE region-of-interest for cMyBP-C in which cMyBP-C modification spots occur in an additive fashion, (i.e. acidity of M3>M2, etc.). As opposed to the other myofilament proteins whose isoelectric shifts have been proven to be phosphorylation modifications (88, 173, 213), there is no conclusive evidence that the pattern of spots that occurs when cMyBP-C is isoelectrically focused are due solely to phosphorylation modifications, therefore spots are only considered as post-translational modifications versus phosphorylation. In any case, analysis of the samples showed no difference in the post-translational modification of cMyBP-C in any of the isoelectrically focused spots. However, 10 distinct charge species are visible on the 2D-DIGE gels for cMyBP-C and it may be assumed that small, but significant changes could not be evident in the 2D-DIGE analysis. To circumvent this possibility, we used phospho-peptide antibodies (a generous gift from Dr. Sakthivel Sadayappan) against 3 of the known phosphorylation sites for cMyBP-C. Figure 16A shows a dose-dependent increase in the intensity of the immunoblot signal for Ser-273 and Ser-302 without changes in the Ser-282 signal in ceramide treated samples. Quantification of samples treated with $10 \mu\text{M}$ C₆-ceramide confirmed an increase in the phosphorylation state of Ser-273 (1.7 ± 0.2 -fold) and Ser-302 (1.6 ± 0.2 -fold) with no difference in Ser-282 phosphorylation (1.1 ± 0.1 -fold). 2D-DIGE results for Tm, although not significant, appeared to show a trend toward reduced phosphorylation ($F_{(1,10)} = 1.755$, $p = 0.13$).

Therefore, we assessed the phosphorylation state using the phospho-peptide antibody against Ser-283 of Tm (a generous gift from Dr. David Wiczorek at the University of Cincinnati). Immunoblotting confirmed a lack of effect of ceramide treatment on Tm phosphorylation (Figure 16B).

In separate 2D-DIGE experiments we determined if treatment of cardiomyocytes to ceramide altered cTnI phosphorylation. Analysis of the samples showed an increase in the tris-phosphorylated (P3) spot alone in samples treated with ceramide ($22.83 \pm 1.35\%$ vs control = $13.99 \pm 2.22\%$, n=6) (Figure 17A). Subsequent immunoblotting with anti-phospho-peptide antibodies for Ser-23/24 of cTnI showed no difference in untreated vs. ceramide treated cardiomyocytes (Figure 17B). Taken together, these findings imply that ceramide treatment leads to increased phosphorylation of cTnI at sites other than the putative protein kinase A (PKA) sites. These findings, coupled with earlier functional studies (shown in Chapter 2 of this thesis) demonstrating that ceramide's negative inotropic effects are mediated through PKC suggest that the increase in cTnI phosphorylation may occur at PKC sites. To determine this, we assessed cTnI phosphorylation by 2D-DIGE in untreated samples and in samples treated with either ceramide alone or samples treated with ceramide in the presence of the general PKC inhibitor Chelerytherine chloride. As shown in Figure 18, PKC inhibition by Chelerytherine chloride was sufficient to prevent ceramide-mediated phosphorylation of cTnI at the 3P site.

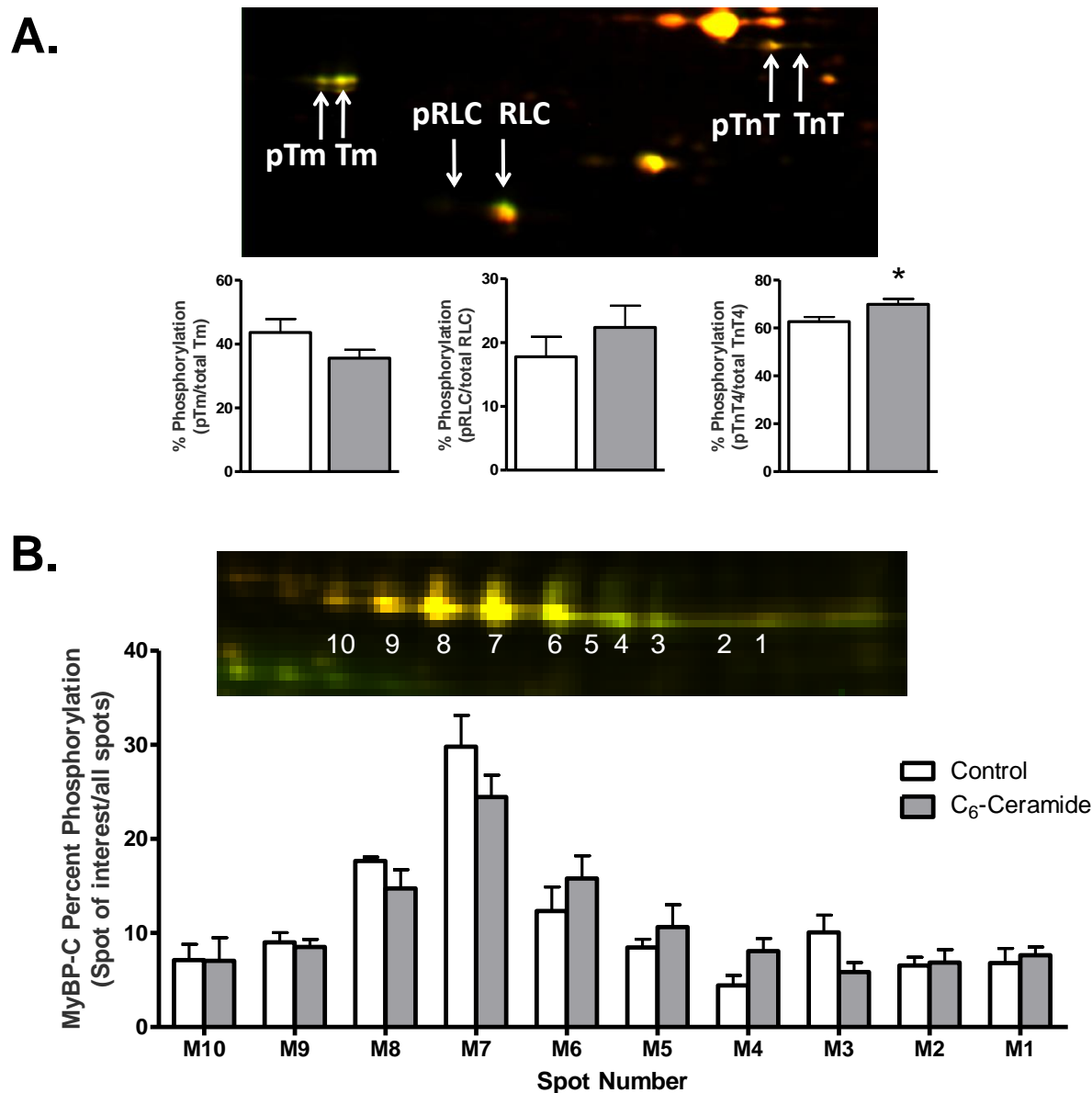


Figure 15: 2D-DIGE of myofilament protein phosphorylation for Tm, RLC, cTnT and cMyBP-C. Tm, tropomyosin; RLC, regulatory light chain; cTnT, cardiac troponin T, MyBP-C, myosin binding protein-C; P, phosphorylation, M, modification. A, *Top*, representative gel images for the region of interest including Tm, RLC and cTnT are shown in a merged image of control samples labeled with Cy3 (pseudo-colored green) and C₆-ceramide treated samples labeled with Cy5 (pseudo-colored red). *Bottom*, Results from the quantification of phosphorylation sites from Tm, RLC and cTnT expressed as a percentage of all spot density for the protein of interest. B, *Top*, representative gel image for cMyBP-C shown as a merged image of control samples labeled with Cy3 and C₆-ceramide treated samples labeled with Cy5. *Bottom*, Results from the quantification of modification sites on cMyBP-C expressed as a percentage of all spot density. * $p < 0.05$ vs Control; $n = 7$.

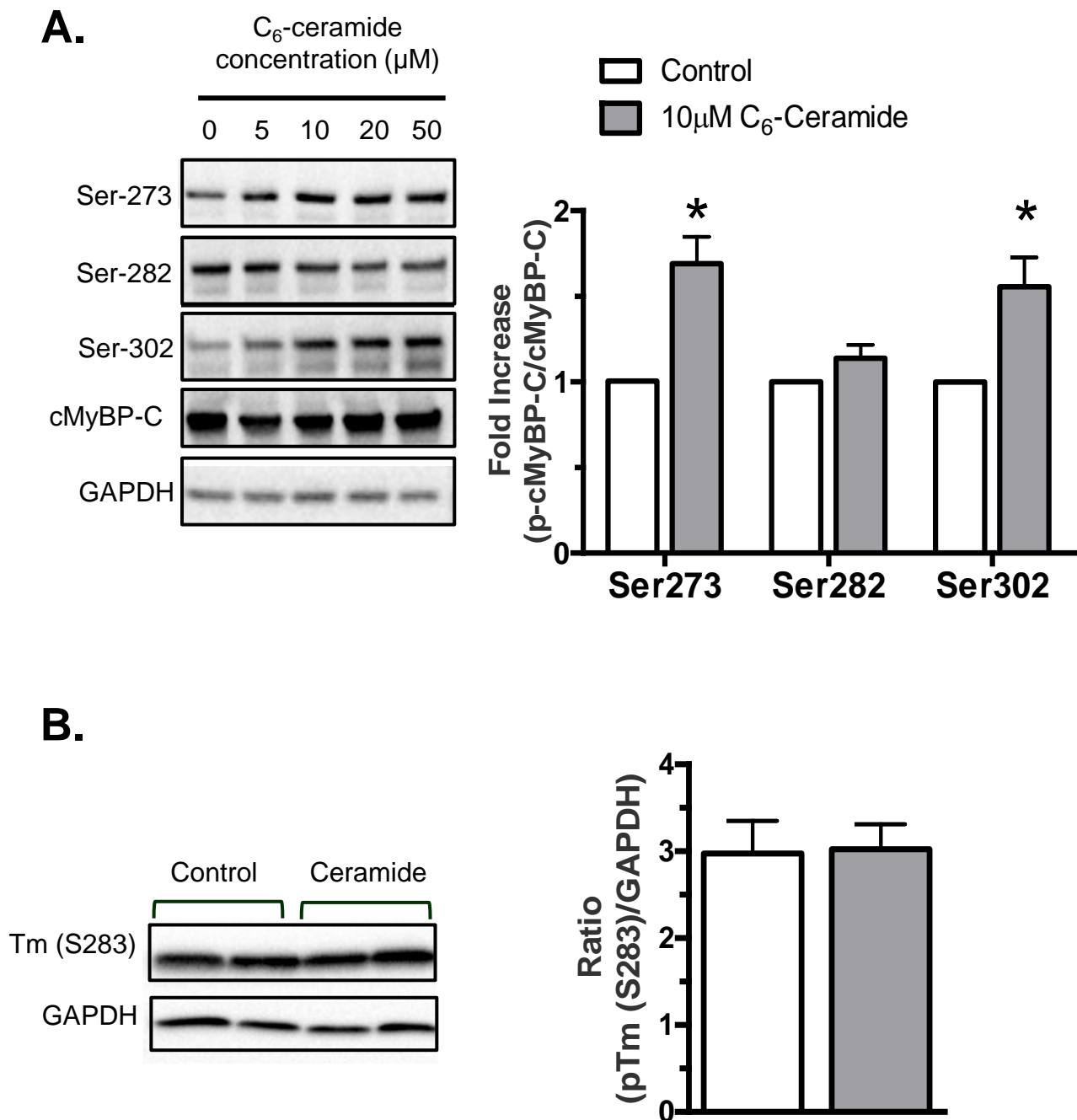


Figure 16: Site-specific immunoblotting for cMyBP-C and Tm phosphorylation. A, Representative images and quantification of Western blots using cMyBP-C phospho-peptide antibodies against Ser-273, Ser-282 and Ser-302 in untreated samples and in samples treated with increasing doses of C₆-ceramide. $n=3$. B, Representative images and quantification of Western blots using a Tm phospho-peptide antibody against Ser-283 in untreated and 10 μM C₆-ceramide treated samples. $n=5$. * $p<0.05$ vs Control.

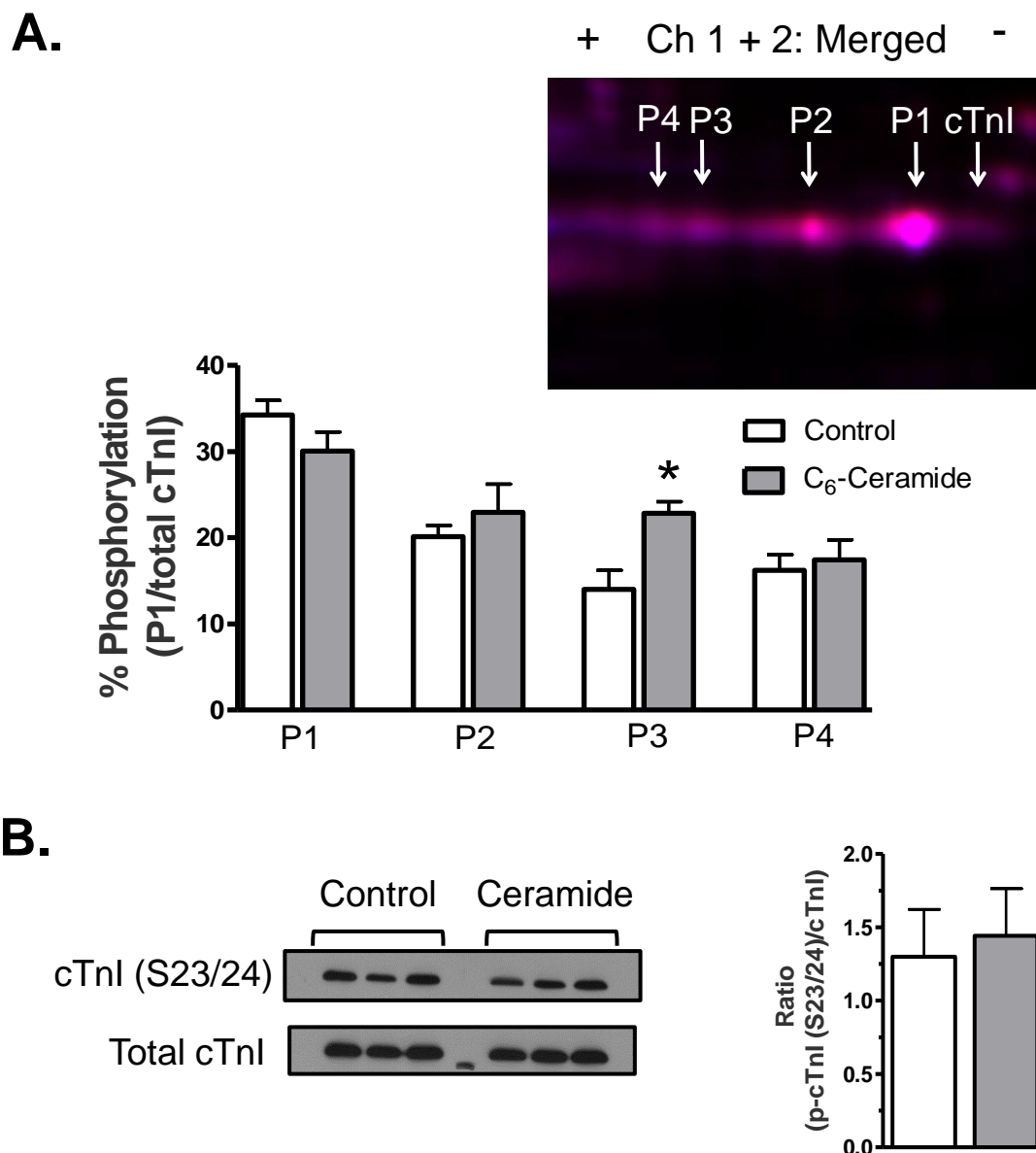


Figure 17: 2D-DIGE and Western blotting of cTnI phosphorylation. cTnI, cardiac troponin I; P, phosphorylated cardiac troponin I. A, *Top*, untreated and C₆-ceramide treated cells were labeled with Cy2 (pseudo-colored blue) and Cy5 (pseudo-colored red), respectively, and focused in the first dimension on a 18 cm nonlinear IPG 7-11 pH strip followed by standard 12% SDS-PAGE for the second dimension. The representative merged image of the cTnI region of interest is shown with phosphorylation sites labeled. *Bottom*, results for cTnI phosphorylation spots 1-4 in which each spot density is shown relative to the total density for all cTnI spots. B, Results from Western blot analysis using the phospho-peptide cTnI (Ser23/24) antibody following treatment of isolated cells with or without 10 μ M C₆-ceramide. * $p < 0.05$ vs Control; $n = 6$.

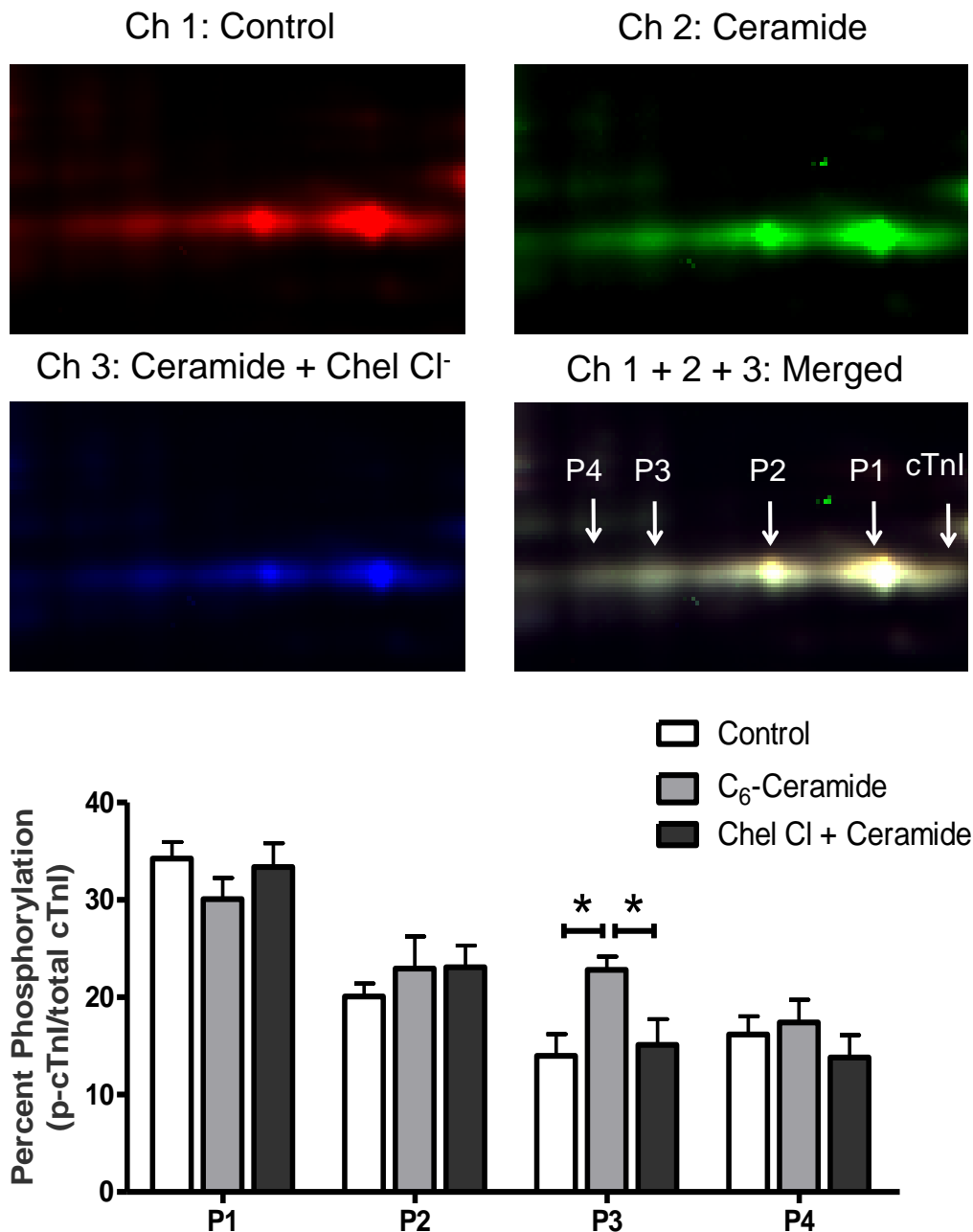


Figure 18: The role of PKC in C₆-ceramide-mediated effects on cTnI phosphorylation. cTnI, cardiac troponin I; P, phosphorylated cardiac troponin I. *Top*, images of the cTnI region of interest from Cy5 labeled control samples (channel 1), Cy2 labeled samples treated with 10 μ M C₆-ceramide (channel 2) and Cy3 labeled samples treated with 10 μ M C₆-ceramide in the presence of 1 μ M Chelerytherine chloride (Channel 3) are shown individual along with a merged image (channel 1 + 2 + 3). *Bottom*, quantitative results for cTnI phosphorylation spots 1-4 in which each spot density is shown relative to the total density for all cTnI spots. * $p < 0.05$ as indicated; $n = 6$.

Discussion

Our data provide a novel mechanism by which ceramide targets the myofilament proteins for phosphorylation to evoke a negative inotropic response. Our biochemical assessment revealed increases in the phosphorylation of cTnT and cMyBP-C upon ceramide treatment, as well as increases in the phosphorylated form (P3) of cTnI which was prevented by inhibition of PKC. Previous studies support our conclusion that the phosphorylated P3 spot likely contains phosphorylation of cTnI on Ser-43/45 (2, 169, 174, 225). Specifically, it has been shown that the higher charged, more acidic cTnI species identified by isoelectric mobility in IEF gels includes phosphorylation on the PKC sites (174), while the vast majority of mono-phosphorylated (cTnI_p) and bis-phosphorylated (cTnI_{pp}) cTnI found in the basal state contain cTnI phosphorylated at Ser-23/24 (2, 169, 225).

Although it is likely that the net phosphorylation state of all three substrates are critical for determining the overall contractile effect in the intact heart, charge changes at the PKC-sites of cTnI and cTnT found here are likely to govern the negative inotropic effects of ceramide treatment observed in the previous chapter. PKC-mediated phosphorylation of cTnI *in vitro*, specifically at Ser-43/45, has been shown to reduce isometric tension and the Ca²⁺-activated ATPase rate by promoting the blocked state of thin-filament activation (83, 136, 153), an effect which is likely to alter the economy of muscle contraction. Indeed, a recent study by Hinken et al (77) showed PKC treatment of skinned rat cardiomyocytes reduced force production and loaded shortening velocity resulting in depressed power output. Phosphorylation of cTnI was shown to play a dominant role in these responses. cTnT phosphorylation has also been shown to

depress Ca^{2+} -dependent ATPase rate and maximal tension development (135, 190), however, earlier studies suggest that the phosphorylation of cTnT alone cannot account for the full reduction in actomyosin ATPase rate (135). Rather, PKC-mediated phosphorylation of cTnT and cTnI act in concert within the myofilament to alter contractility (126). *In vivo* phosphorylation of cTnI at Ser43/45 has been shown to play a main role in contractile dysfunction (88, 162) and in the progression to failure associated with PKC ϵ overexpression, demonstrated by rescue of the PKC ϵ overexpressing mouse phenotype when endogenous cTnI was partially replaced with a non-phosphorylatable cTnI at Ser43/45 (S43/45A) (174). Interestingly, a study using mice which constitutively express pseudo-phosphorylated cTnI at Ser43/45 and Thr144 (cTnI_{PKC-P}) showed that minimal changes (7%) in cTnI phosphorylation at the PKC sites were sufficient to cause contractile dysfunction (88). It is worth noting here that the observed increase in phosphorylation induced by ceramide treatment in the current study was roughly 8%. The aforementioned study would suggest that even in the context of the whole heart this degree of modification would be sufficient to impair contractility.

Nevertheless, understanding the significance of cTnI-Ser43/45 phosphorylation in humans remains an evolving pursuit (179). While phosphorylation of cTnI has been shown to be altered in human heart failure (91, 226-227), use of top-down proteomics has demonstrated that this is primarily due to a reduction in cTnI-Ser23/24 phosphorylation, while detection of cTnI-Ser43/45 was not observed (226). However, a more recent study employing multiple reaction monitoring tandem mass spectrometry (MRM-MS/MS) analysis has shown a shift from PKA to PKC-mediated phosphorylation

of cTnI in human heart failure samples as well as the presence of several newly identified phosphorylation sites (227). Interestingly, although phosphorylation of Ser43 and Ser45 were both elevated in that study, Thr144 was shown to have the highest level of phosphorylation overall. Based on this, we cannot rule out the possibility that the elevated P3 spot in our cTnI 2D-DIGE is due to an increase in cTnI-Thr144, although *in vitro* phosphorylation of Thr144 has been primarily attributed to a decreased Ca^{2+} sensitization and slowed relaxation (88) which we did not observe.

Unexpectedly, our observed increase in cMyBP-C phosphorylation was not associated with an increase in the rate of contraction or relaxation, as has been previously described (27, 167, 203). This lack of increase in contraction and relaxation rates can be explained in the following ways. First is that increases in phosphorylation of the PKC sites at Ser273 and Ser302 without changes in Ser-282 may impact contractile mechanics differently than when all three sites on cMyBP-C are phosphorylated. In fact, studies examining the role of cMyBP-C phosphorylation on contractile mechanics have focused solely on PKA-mediated phosphorylation of cMyBP-C, in which case all three sites, Ser273, Ser282 and Ser302, are phosphorylated (ref). However, Sadayappan et al (166) have shown that pseudo-phosphorylation of cMyBP-C at the PKC sites was not sufficient to rescue contractile dysfunction in the cMyBP-C null background, while Ser282 alone was. The authors suggest that phosphorylation of Ser282 is essential for cMyBP-C's ability to regulate contractility and may be the major determinate of cMyBP-C phosphorylation-induced alterations. Moreover, Florea et al (48) found that constitutive phosphorylation of PP1 I-1 at its PKC sites resulted in depressed systolic function that was associated, in part,

with reduced phosphorylation of cMyBP-C at Ser282. Future studies examining the functional differences between PKA and PKC-mediated phosphorylation of cMyBP-C may shed light on more recent findings. A second explanation is that perhaps phosphorylation of cMyBP-C does little to change relengthening kinetics in *unloaded* cell measurements. The notion of a load-dependence of relaxation under auxotonic conditions has long been established (16). Moreover, in the unphosphorylated state cMyBP-C has been proposed to conform to a 'viscous-load model' in which it produces an opposing drag-force through its ability to bind actin. This effect is reduced when phosphorylation of cMyBP-C blunts its binding to actin, allowing for less force-opposition and faster contraction and relaxation kinetics (216). In this case, the observed effects of cMyBP-C phosphorylation may be reduced in the context of unloaded cardiomyocytes used here, particularly in terms of relengthening and may, therefore, account for our lack of change in relengthening velocity following ceramide treatment, despite an increase in cMyBP-C phosphorylation.

While our results provide strong evidence that ceramide alters the post-translational state of the myofilament proteins directly through PKC-mediated phosphorylation, we cannot exclude the possibility that ceramide may also have induced oxidative modifications to the myofilament. Ceramide is well-known to provoke oxidative stress in striated muscle (45, 189), as well as several other tissues (52, 115, 146). Diaphragm fiber bundles exposed to C₆-ceramide show increased oxidant activity which resulted in a depression in maximal isometric force (45). The decline in force could be blunted by pretreatment of the fibers with the nonspecific antioxidant NAC but not by the NO synthase inhibitor L-NAME. Of the sarcomeric proteins, actin, Tm, titin, cMyBP-C and

myosin all have been shown to be modified by ROS. Oxidation of actin was associated with reduced contractility via a reduction in the maximal force production and a depression in the force-frequency relationship (31). Cys-374 on actin is likely the modified residue, as oxidation at this site is associated with reduced ATPase activity and sliding velocity (31). Actin was also shown to be carbonylated in human heart failure patients, as was Tm. These two modifications, along with Tm disulfide cross-bridge formation strongly correlated with the associated cardiac contractile impairment (18). Oxidation of Tm, presumably at Cys-190, has also been shown to occur in mice following MI (1). Cys-190 is located within the TnT interacting region of Tm and oxidation at this site is likely to decrease contractility through altered Tn-Tm interaction, as well as affecting Tm flexibility during the development of heart failure (19-20, 74). The same study by Avner et al that demonstrated Tm oxidation also showed increased S-glutathionylation of a high molecular weight protein that they suggest is likely titin (1). Interestingly, *in vitro* studies have pointed to three residues in titin that contain disulfide bridges under oxidative conditions. These modifications were localized to the N2B region of titin and resulted in increases in passive stiffness due to a reduction in the extensibility of titin (61). S-glutathionylation of MyBP-C was shown to correlate with diastolic dysfunction in a hypertensive mouse model, suggesting such oxidative modifications may mediate contractile dysfunction (105). Myosin has also been shown to be S-glutathionylated, specifically at Cys-400 and Cys-695 within the myosin head region, and Cys-947 resulting in reduced ATPase activity (143). Acutely, following an MI, myosin heavy chain was shown to be oxidized at Cys-707 and Cys-697. This was associated with reduced sliding velocity, suggestive of reduced unloaded shortening

velocity of the cross-bridge. In addition, following the acute phase post-MI, MyBP-C carbonylation was shown to be increased (154). While it is plausible that in our experiments ceramide's effects may have occurred, in part, due to oxidative modifications of the sarcomere, our ability to completely abolish ceramide's negative inotropic response through PKC inhibition (Chapter 2, Figure 12) supports a predominate role for PKC-mediated phosphorylation as the underlying mechanism.

CHAPTER IV

CHRONIC MODIFICATION TO THE MYOFILAMENT BY A HYPERTROPHIC CARDIOMYOPATHY-LINKED MUTATION IN TROPOMYOSIN (TM K70T) CAUSES MALADAPTIVE REMODELING OF EXCITATION-CONTRACTION COUPLING

A. Introduction

To this point, the predominating theme of my thesis has been in linking the functional consequences of acute cellular stress (i.e. ceramide exposure) with transient phosphorylation modifications among the myofilament proteins. This chapter expands this theme to encompass the functional consequences of chronic modification to the myofilament by way of mutationally-induced charge changes associated with HCM resulting from the missense mutation in Tm at position 70 (Tm K70T).

Activation of the thin filament is dependent on coordinated structural movements within the cTn complex following Ca^{2+} binding to its single regulatory binding site on cTnC. These structural changes are transduced through the cTn complex to regulate the position of Tm along the actin filament. Ultimately, it is the position of Tm which dictates the interaction between actin and myosin leading, in turn, to force production. Given the fact that regulation of contraction is highly dependent on the precise interactions of several proteins, it is not surprising that single amino acid substitutions caused by genetic mutations (or even charge changes mediated by post-translational modifications) have significant effects on contractility.

Structural and biochemical studies have provided unique insight into both the interactions which dictate thin filament activation as well as how cardiomyopic mutations

disrupt them. HCM mutations localized to cTn have been shown to cluster within the mobile domains and alter the dynamic protein-protein interactions critical for thin filament activation. Likewise, mutations in Tm also cluster to 2 specific regions of periodic amino acid repeats, or so-called 'periods', which are important for interactions with both actin and the cTn complex (period 5), as well as regions critical for the head-to-tail overlap (period 2) of neighboring Tm filaments (197). Period 5 mutations E180G and D175N have been shown to increase global Tm flexibility as well as local flexibility in the case of E180G (100, 102). Such effects are likely to alter the azimuthal positioning of Tm along the actin filament in favor of myosin head binding at lower $[Ca^{2+}]$. Mutations in period 2, K70T and A63V, have also been shown to alter the flexibility of Tm but at the N-domain which is important for head-to-tail interactions with neighboring Tm. These mutations increase Ca^{2+} sensitivity (124), but have surprisingly little effect on thin-filament cooperativity (73, 75).

Use of transgenic animals has extended these *in vitro* findings, showing that mutationally-induced effects on flanking residues may be an important determinant of altered function. Mouse models of the E180G and D175N mutations demonstrate divergent phenotypes, despite the close proximity of these residues (with E180G being markedly more severe than D175N) (127, 149). These findings are in line with the *in vitro* studies which consistently show greater local structural influence by the E180G mutation compared with the D175N mutation (56, 93, 100). While the molecular mechanisms involved are still unclear, what is apparent from these studies is that single charge changes in the Tm supercoil are sufficient to alter Tm flexibility, be it global or

local, with profound, albeit diverse, effects on the biophysical properties of the myofilament.

Despite this, the clinical phenotype of patients with HCM linked to Tm mutations demonstrates heterogeneity among carriers (See Table II). Patients often present with varying degrees of hypertrophy, fibrosis and cardiac dysfunction with prognostic outcomes differing, even amongst family members with the same mutation (107). The evident dissociation between hypertrophy and the clinical severity is suggestive of an inherently cellular mechanism underlying the disease outcome. A common link among thin filament mutations has been the apparent increase in the myofilament Ca^{2+} -sensitivity, albeit to varying degrees. Recently, Bai et al (3) showed that this increase in the myofilament response to Ca^{2+} resulted in a greater number of cross-bridges cycling at low levels of Ca^{2+} , concluding that this effect provides a catalyst for initiation of hypertrophic remodeling and is a major cause of Tm mutation-related pathogenesis. Moreover, evidence from mouse models of HCM linked to mutations in cTnT suggest that the degree of myofilament Ca^{2+} -sensitization is likely to determine the susceptibility to cardiac arrhythmias, particularly in the absence of gross anatomical remodeling (5, 172). Whether this holds true for other HCM related thin filament mutations is yet to be determined.

Human carriers of the Tm K70T mutation present with relatively mild hypertrophy but lack other obvious signs of structural remodeling. Despite this, the Tm K70T mutation was associated with a high incidence of sudden cardiac death (SCD), with all carriers demonstrating premature ventricular contractions (PVC) (221). In studies reported here we use a newly developed mouse model which bears the Tm K70T mutation to

Table II: Known Hypertrophic Cardiomyopathy mutations in α Tm

Mutation	Helical Position	Charge change	Type of charge Δ	Phenotype	Reference Human HCM
<i>Mutations near N-terminus</i>					
A22T	<i>a</i>	No		Hypertrophy SCD	(139)
E62Q	<i>f</i>	Yes	-1 to 0	Hypertrophy Arrhythmias & SCD	(84)
A63V	<i>g</i>	No		Hypertrophy Progressive LV dilation SCD	(129) (221)
K70T	<i>g</i>	Yes	+1 to 0	Heart failure Arrhythmias	(221)
V95A	<i>d</i>	No		Mild hypertrophy Abnormal EKG	(85)
A107T	<i>b</i>	No		Hypertrophy SCD	(139)
<i>Mutations in Period 5</i>					
I172T	<i>d</i>	No		Abnormal EKG	(209)
D175N	<i>g</i>	Yes	-1 to 0	Heart failure SCD Hypertrophy Fibrosis Mild hypertrophy	(129, 221) (81, 139) (28) (199-200)
E180G	<i>e</i>	Yes	-1 to 0	Mild hypertrophy Arrhythmias	(199-200)
E180V	<i>e</i>	Yes	-1 to 0	Hypertrophy Progressive LV dilation	(157)
L185R	<i>c</i>	Yes	0 to +1	Arrhythmias SCD	(107, 209-210)
E192K	<i>c</i>	Yes	-1 to +1	Fibrosis Interventricular septal hypertrophy	(150)
M281T	<i>a</i>	No		Hypertrophy Arrhythmias	(139) (209)

SCD, sudden cardiac death; EKG, electrocardiogram

investigate the molecular changes underlying the disease phenotype. Our findings offer novel insight into the pathogenesis of HCM and the increased risk for sudden cardiac death (SCD) in patients bearing the Tm70 mutation.

B. Materials and Methods

1. Generation of α Tm K70T Transgenic Mice

Transgenic mice (FVB/N background) were generated in the laboratory of Dr. David F. Wieczorek at the University of Cincinnati using a cDNA-encoding mutated α Tm, in which the nucleotides encoding for lysine at position 70 were mutated to nucleotides encoding for threonine. The mutated α Tm cDNA was cloned downstream of the cardiac expressing α -myosin heavy chain (α -MHC) expression vector and upstream of the human growth hormone poly(A) signal sequence using methods previously published (188). Founder mice were identified by PCR and four lines of transgenic mice with varied copy numbers of the transgene were confirmed by Southern blot analysis. Expression of the transgenic protein in the heart was confirmed by Western blot analyses. All animal procedures were conducted according to the National Institutes of Health *Guide for the Care and Use of Laboratory Animals* and approved by the Institutional Animal Review Board (ACC #12-063) at the University of Illinois at Chicago. All experiments were carried out in 4 and 10 month animals with an equal distribution of male and female mice.

2. Immunohistochemical Analysis

Excised hearts were cannulated via the aorta and the coronary arteries retrogradely perfused with ice-cold saline followed by several mL of Formalin (Sigma). The heart was then transversely sliced into four pieces and each piece

placed into a labelled cassette. Cassettes were kept in Formalin overnight at 4° C and then samples were shipped to the University of Illinois in Urbana for further sectioning and staining. Hematoxylin & Eosin (H & E) and Masson's trichrome staining were conducted on 5 µm sections.

3. Hydroxyproline Content Assay

Hydroxyproline (HOP) content was determined using methods previously published (145). A small piece (15-20 mg) of mouse cardiac tissue previously frozen in liquid nitrogen was minced into a pre-weighed Pyrex (#9826, Fisher Scientific) screw cap vial to determine the wet weight. The tissue was hydrolyzed overnight in 200 µL of 6 M HCl in an oven set to 110°C. After the hydrolysis, 80 µL of isopropanol was added to 5 µL of the hydrolysate, followed by addition of 40 µL of chloramine-T solution (7% chloramine-T in water) mixed with acetate citrate buffer (0.695M anhydrous C₂H₃O₂Na, 0.174M C₆H₈O₇, 0.435M NaOH, and 38.5% [v/v] 2-propanol) in a 1:4 ratio. Samples were vortexed and allowed to incubate to oxidize for 5 min at room temperature. Next 0.5 mL of Ehrlich's reagent (3g of 4-(dimethylamino) benzaldehyde, 10 ml ethanol, 675 µl sulfuric acid) mixed with 2-propanol in a 3:13 ratio was added, vortexed, and incubated for 30 min at 55°C. The reaction was quenched in an ice bath and the samples were centrifuged at 5,000 × g for 1 min. The optical density of the supernatant was determined at 558 nm. A standard curve of *trans*-4-hydroxy-L-proline (0–500 nM) was included in each assay to determine the nM HOP/mg of tissue.

4. Transthoracic Echocardiography

Mice were anesthetized with isoflurane (1.0-1.5%) in 100% oxygen using a face mask. Animals were placed in a supine position and body temperature was maintained at 37°C. Transthoracic echocardiographic recordings were then obtained using a 30-MHz high resolution transducer with an integrated rail system (Vevo 770 High-Resolution Imaging Systems). AM Mode images of the left ventricle (LV) outflow tract (LVOT), ascending aorta (AO) and left atrium (LA) were taken from the parasternal long axis view. The parasternal short axis view at the level of the papillary muscles was used to measure the LV internal dimension (LVID), interventricular septum (IVS) and posterior wall (PW) thicknesses. Pulsed Doppler was performed with the apical four-chamber view. The mitral inflow was recorded with the Doppler sample volume at the tip level of the mitral valve leaflets to obtain the peak velocities of flow in the early phase of diastole (E) and after LA contraction (A). Then, the Doppler sample volume was moved toward the LVOT and both the mitral inflow and LV outflow were simultaneously recorded to measure the isovolumic relaxation time (IVRT). Additional information about the diastolic function was obtained with tissue Doppler imaging (TDI). Peak myocardial velocities in the early phase of diastole (E') and after LA contraction (A') were obtained with the sample volume at the septal side of the mitral annulus in the four chamber view. All measurements and calculations were averaged from 3 consecutive cycles as previously described (207) and performed according to the American Society of Echocardiography guidelines (94, 128). Data analysis was performed offline with the Vevo 770 Analytic Software.

5. Skinned Fiber Preparations

Left ventricular papillary muscles were isolated, cut into fiber bundles approximately 200 μm in width and 3-4 mm in length and detergent extracted in a high relaxing solution (HR: 10mM EGTA, 41.89mM K-Prop, 100mM BES, 6.75mM MgCl_2 , 6.22mM Na_2ATP , 10mM Na_2CrP , 5mM NaAzide) with 1% Triton X-100 for 3-4 hours at 4°C. Fibers were then mounted between a micromanipulator and a force transducer and bathed in HR solution. After baseline force stabilized, fibers were sequentially bathed in a series of solutions containing increasing Ca^{2+} concentrations (pCa 8 to 4.5) and their developed force was recorded on a chart recorder. Isometric tension measurements were plotted as a function of Ca^{2+} and fit by a nonlinear least-squares regression analysis to the Hill equation using Graph Prism 5. From this fitted curve, we derived the pCa_{50} (pCa required to produce 50% of the maximal force obtained), maximal force and the Hill coefficient (n_H).

6. Programmed Electrical Stimulation

Mice were sedated with isoflurane via nose cone until loss of the pedal reflex. Following sedation, mice were placed supine on a temperature-controlled (37°C) plate, intubated, and mechanically ventilated with supplemental oxygen mixed with isoflurane using a rodent ventilator (Harvard Apparatus). A minute ventilation of 100/min at a tidal volume of 0.3 mL was used to maintain anesthesia with isoflurane (1.0 and 1.5% titrated to effect) via intubation. Needle electrodes were placed subcutaneously to record Lead II of an electrocardiogram (EKG). A base-line EKG was acquired for 2 minutes and then the chest cavity was cut open to expose the heart. A bipolar countercurrent electrode (World Precision Instruments) was used to

record left and right ventricular monophasic action potentials (MAP) at both the base and apex and then the electrode was positioned on the left ventricle to record MAPs throughout the stimulation protocol. A constant-current stimulator (A320, World Precision Instruments) connected to a laptop computer was used for cardiac stimulation which was delivered through a custom-made silver wire bipolar electrode placed on the right ventricle. Inducibility of ventricular arrhythmias was determined using a series of 8, 1 ms (4000 mV threshold) pacing trains at a fixed pacing cycle length (PCL) of 80 ms coupled with a shorter S2, S3 and S4 premature stimulus, beginning at 60 ms, 50 ms and 40 ms, respectively. The S4 stimulus was progressively reduced by 2-ms in each pacing train from 40 ms to 30 ms until the effective refractory period (ERP) was reached. The same sequential reduction was repeated for the S2 and the S3 stimulus. This was again repeated using an S1 pacing train with a PCL of 60 ms (See Figure 19 for reference). Successful induction of an arrhythmia was defined by 2 criteria: 1) the presence of 2 or more extra beats following the pacing train, with or without the return of a normal sinus rhythm and 2) the ability to evoke the arrhythmia in 3 consecutive trials.

7. Isolation of Mouse Cardiomyocytes

Hearts from anesthetized (pentobarbital sodium; 50 mg/kg) and heparinized (5,000 U/kg) mice were quickly removed and put into ice cold, nominally Ca^{2+} -free perfusion buffer (PB) containing: 113 mM NaCl, 4.7 mM KCl, 0.6 mM Na_2HPO_4 , 0.6 mM KH_2PO_4 , 1.2 mM MgSO_4 , 0.032 mM phenol red, 12 mM NaHCO_3 , 10 mM KHCO_3 , 30 mM taurine, 10 mM HEPES, 5.5 mM glucose, 10 mM and 2,3-butanedione monoxime (BDM), pH 7.4 at 37°C. The aorta was cannulated and the

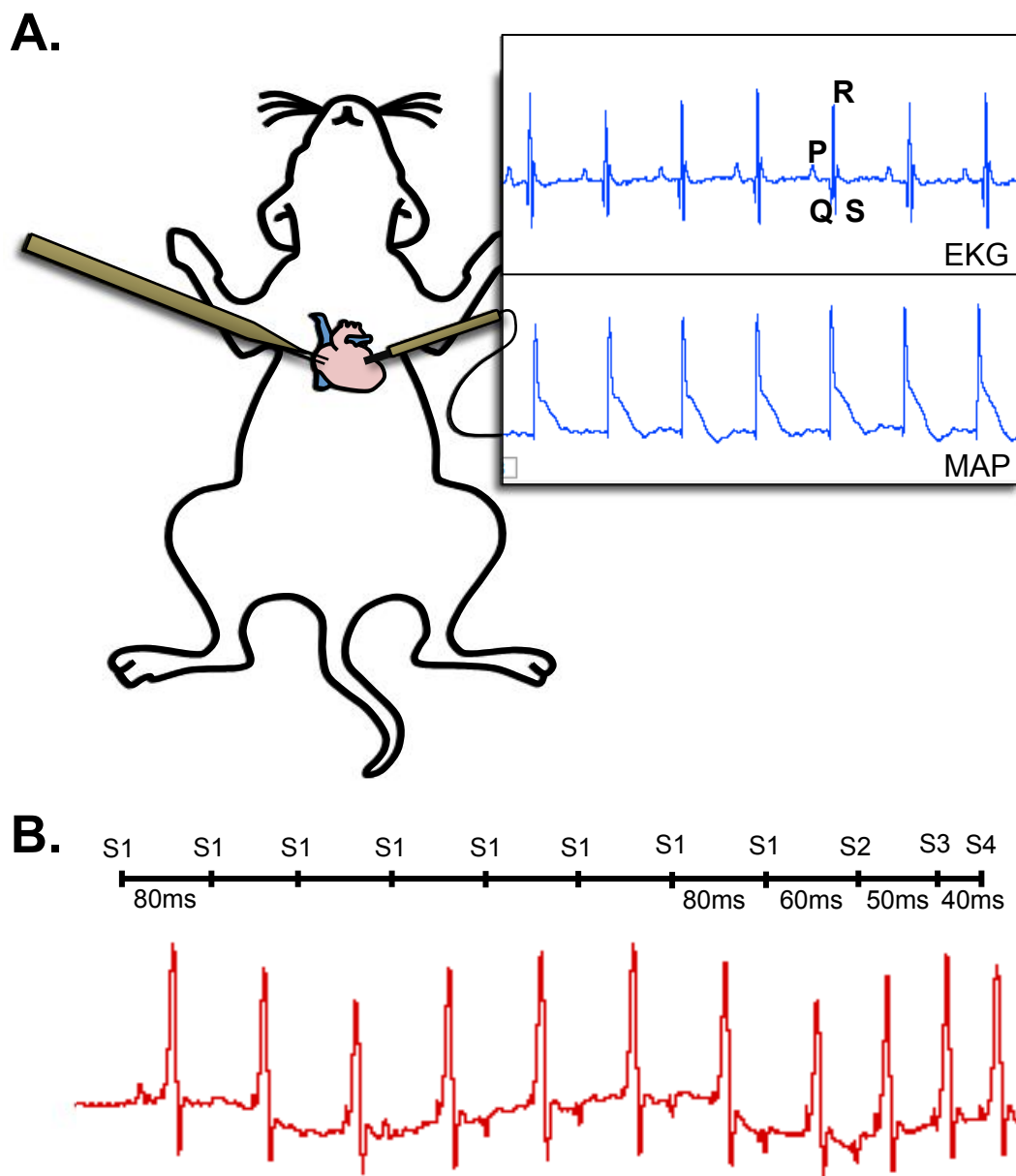


Figure 19: Protocol summary for programmed electrical stimulation. A, Cartoon depicting the placement of the bipolar countercurrent stimulating electrode on the right ventricle with the monophasic action potential (MAP) recording electrode on the left ventricle. The sample electrocardiogram (EKG) and MAP recording was taken from a 4 mo NTG mouse and indicates the P wave (atrial depolarization) and the QRS complex (ventricular depolarization) within the EKG recording. B, Actual EKG tracing from a 4 mo NTG mouse heart undergoing programmed electrical stimulation (PES). The marked time intervals show a PES protocol in which 8 -1 ms pulses are delivered in 80 ms intervals (S1), with single S2-S3-S4 pulses occurring at sequentially shorter intervals (60 ms, 50 ms, 40 ms, respectively).

heart mounted on a Langendorff perfusion system. Hearts were perfused for 4 min with Ca^{2+} -free PB and subsequently for 8–12 min with digestion buffer (DB) containing PB and $12.5 \mu\text{M Ca}^{2+}$ together with 0.15 mg/ml blendzyme 2 (Roche) and 0.14 mg/ml trypsin (Invitrogen, Carlsbad, CA). Hearts were then removed and transferred to a dish containing DB, and the ventricles were cut into small pieces and gently triturated. At the end of the trituration period, the cell suspension was filtered through a mesh collector and placed into centrifuge tubes, and the digestion process was stopped with an equal volume of PB containing $12.5 \mu\text{M Ca}^{2+}$ plus 10% bovine calf serum (v/v). The cells were then permitted to settle under gravity for 5–7 min. The supernatant fraction was removed, and the cells were resuspended in fresh PB containing $12.5 \mu\text{M Ca}^{2+}$ and 5% bovine calf-serum (v/v). Cells were allowed to settle under gravity, the supernatant was removed, and the cells were resuspended in fresh control solution (CS) of the following composition: 133.5 mM NaCl, 4 mM KCl, 1.2 mM MgSO_4 , 1.2 mM NaH_2PO_4 , 10 mM HEPES, and various Ca^{2+} concentrations; first, $200 \mu\text{M Ca}^{2+}$ followed by $500 \mu\text{M}$ and then 1 mM Ca^{2+} . The cells were stored at room temperature (22–23°C) until used.

8. Simultaneous Cell Shortening and Ca^{2+} Transient Measurements

After isolation an aliquot of cells was placed in a small perfusion chamber mounted on the stage of an inverted microscope and the cells were allowed to settle to the bottom. A background fluorescent recording was taken and used for each fura emission spectra to reduce noise. The perfusion chamber was then cleaned of the cells and washed briefly to remove any debris. An aliquot of cells was then loaded within the perfusion chamber for 10 mins with $3 \mu\text{M}$ fura 2-AM

(Invitrogen), which was made from a DMSO-based stock, diluted in 1 mM CS-BSA. Following loading, de-esterification of the fura 2 indicator was accomplished with a 10 min perfusion using dye-free Control Solution (CS) containing 133.5 mM NaCl, 4 mM KCl, 1.2 mM NaH₂PO₄, 10 mM HEPES, 1.2 mM MgSO₄, 11.1 mM glucose (pH 7.4 using NaOH) and 1.2 mM Ca²⁺. Cells were field stimulated at 0.5 Hz using parallel platinum electrodes submerged in the bathing solution and base-line intracellular Ca²⁺ ([Ca²⁺]_i) transients and unloaded cell shortening were recorded simultaneously. All measurements were taken at room temperature (22-23°C). For [Ca²⁺]_i transient measurements, myocytes were alternately excited with light at a wavelength of 340 and 380 nm and the emitted fluorescence was collected at a wavelength of 505 nm by a photomultiplier tube. Unloaded cell shortening assessment was carried out using edge detection. A video-edge detector (Crescent Electronics) was used to monitor cell length and recordings were stored in an acquisition software program (Felix32, Photon Technology International) for later analysis offline.

9. Western Blot Analysis

Apexes from the left ventricle of transgenic Tm70 or non-transgenic (NTG) frozen hearts were homogenized in industrial strength sample buffer (8 M urea, 2 M thiourea, 0.05 M Tris, pH 6.8, 75 mM DTT, 3% (w/v) SDS, 0.05% (w/v) bromophenol blue) using a Duall ground-glass homogenizer. Protein lysates (20µg) from cells were separated on 12% (200:1 acrylamide-to-bisacrylamide) SDS gels followed by transfer of the protein to a 0.2 µm polyvinylidene difluoride (PVDF) membrane for Western blot analysis. Membranes were blocked in 5% milk in tris-buffered saline

with 0.1% Tween-20 (TBS-T) and then incubated overnight at 4°C in primary antibody [SERCA2 (ABR Laboratories) 1:2,000; phospho-Akt (Ser473) (Cell Signaling), 1:1,000; total Akt (Cell Signaling) 1:1,000; Tm (CH-1, Iowa Hybridoma) 1:1,000]. Following incubation, membranes were washed for 30 mins in TBS-T and then incubated in secondary antibody [goat anti-mouse (Sigma-Aldrich) 1:40,000 for SERCA2a and Tm; goat anti-rabbit (GE Healthcare) 1:20,000 for all others] conjugated to horseradish peroxidase for 1 hr at room temperature. Membranes were then washed for 30 mins in TBS-T and developed by enhanced chemiluminescence (ECL Plus, GE Healthcare) on a ChemiDoc XRS+ imager (BioRad). Band densities were analyzed using ImageLab software (BioRad).

10. Statistical Analysis

Values are expressed as mean \pm S.E. To make statistical comparisons between NTG and Tm70 mice at different ages a two-way ANOVA with a Bonferroni post-hoc test was used, both for making comparisons among genotypes within age and to make age-dependent comparisons within genotype. An exact Fisher's test was used to determine statistical differences in arrhythmia inducibility. For AP duration statistical differences were determined using an unpaired Student's *t* test. A level of $p < 0.05$ was considered significant throughout.

C. Results

1. Generation of Tm70 Mice

In order to unveil the molecular mechanisms underlying the Tm K70T missense mutation that has been identified in human patients (221), several lines of transgenic

mice expressing various percentages of the Tm K70T transgene (see Figure 20B) were generated at the University of Cincinnati in Dr. David Wieczorek's laboratory. Two independent lines (Line 51 and Line 230) were sent to us for preliminary characterization. Line 51 showed 51% replacement of endogenous Tm protein with the Tm70 mutant protein compared to 81.2% replacement in Line 230 (Figure 20C). Tm70 mice were grouped into younger (4-7 mo) and older (11-10 mo) mice for investigation based on phenotypic differences. Following initial echocardiographic assessment, we found that Line 230 displayed the greatest disease phenotype (diastolic impairment), therefore the remainder of our experiments were conducted using Line 230. Interestingly, we found that the phenotype was only present in the older animals (Line 230), similar to disease development in the human carriers with this particular mutation. With this in mind, we sought to determine if there were early adaptations which accounted for the age-dependent progression of the disease, grouping our animals into pre-phenotype, young mice (4 mo) and post-phenotype, older mice (10 mo).

2. Age-dependent Alterations in Morphology and Hemodynamics in Hearts from Tm70 Mice

Overall, Tm70 mice display mild age-dependent hypertrophy and impaired relaxation without signs of structural remodeling. Representative images of ventricular histological sections of 10 mo old mice stained with Hematoxylin & Eosin or Masson's trichrome to characterize gross cardiac morphology are shown in Figure 21A. Hearts from NTG and Tm70 animals showed unaltered cardiomyocyte architecture and a lack of fibrosis, regardless of age. To confirm the lack of fibrosis

quantitatively, we measured collagen deposition using the HOP assay (initially described by (151) and found no differences in HOP content among groups (Figure 21B).

Morphometric data obtained using echocardiography are shown in Table III and Figure 22 and demonstrate no difference in left ventricular (LV) mass or relative wall thickness (RWT) between younger or older NTG and Tm70 mice; however, Tm70 mice had a significantly greater age-dependent increase (20%) in LV mass whereas NTG mice showed no significant changes in LV mass (7%) with age (Figure 22C). Moreover, when broken down by gender, only the male Tm70 mice had significant age-dependent LV hypertrophy (Figure 22E). Nevertheless, we consider this to be an indication of mild hypertrophy as heart weight to tibia length ratios, an index of the overall cardiac mass, were unchanged among groups (Figure 22D). Consistent with the age-dependent increase in LV mass, activation of hypertrophic signaling through phosphorylation of Akt was also shown to be increased in the hearts of older Tm70 mice relative to younger mice (Figure 23).

Hemodynamic measures at 4 mo (Table III) showed no differences in systolic or diastolic parameters between Tm70 mice and NTG controls. However, at 10 mo Tm70 mice had impaired relaxation, as evidenced by the measured diastolic parameters, with no differences in systolic parameters compared to NTG controls (Figure 24 and Table III). Across groups there was no difference in heart rate or gender-dependent differences beyond LV mass.

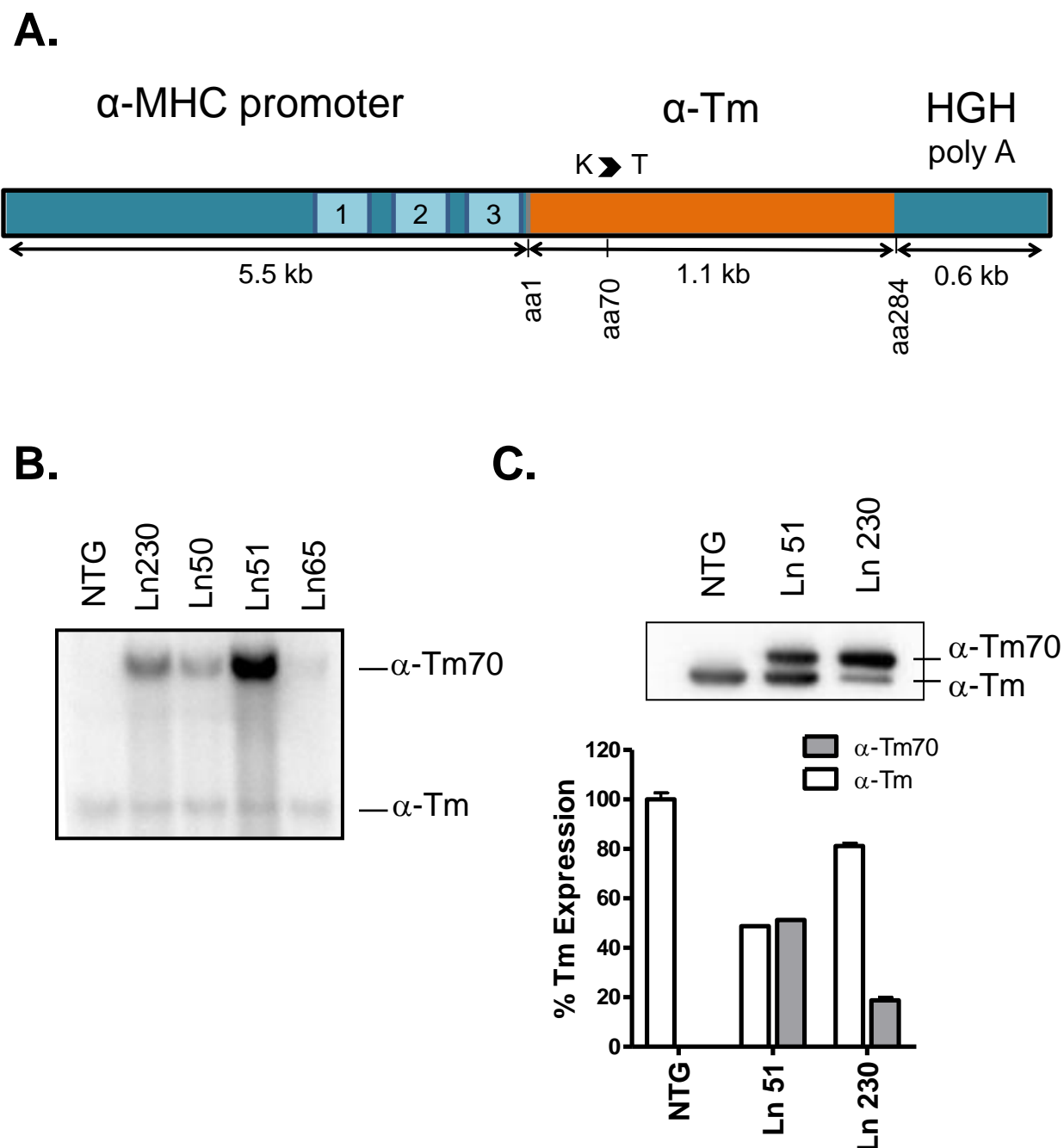


Figure 20: Endogenous transgene transcript and protein levels in α -Tm70 mice. A, The construct used for generation of the transgene is shown. Site-directed mutagenesis at codon 70 in α -Tm was made as described in the Materials and Methods section. B, Representative Southern blot showing PCR products for the endogenous α -Tm gene and the α -Tm70 transgene in 4 separate mouse lines. C, Western blot from NTG and α -Tm70 hearts, *top*, and quantification of the α -Tm content, *bottom*, showing the percentage of transgene protein expressed. Line 51, $n = 1$, Line 230 $n = 6$.

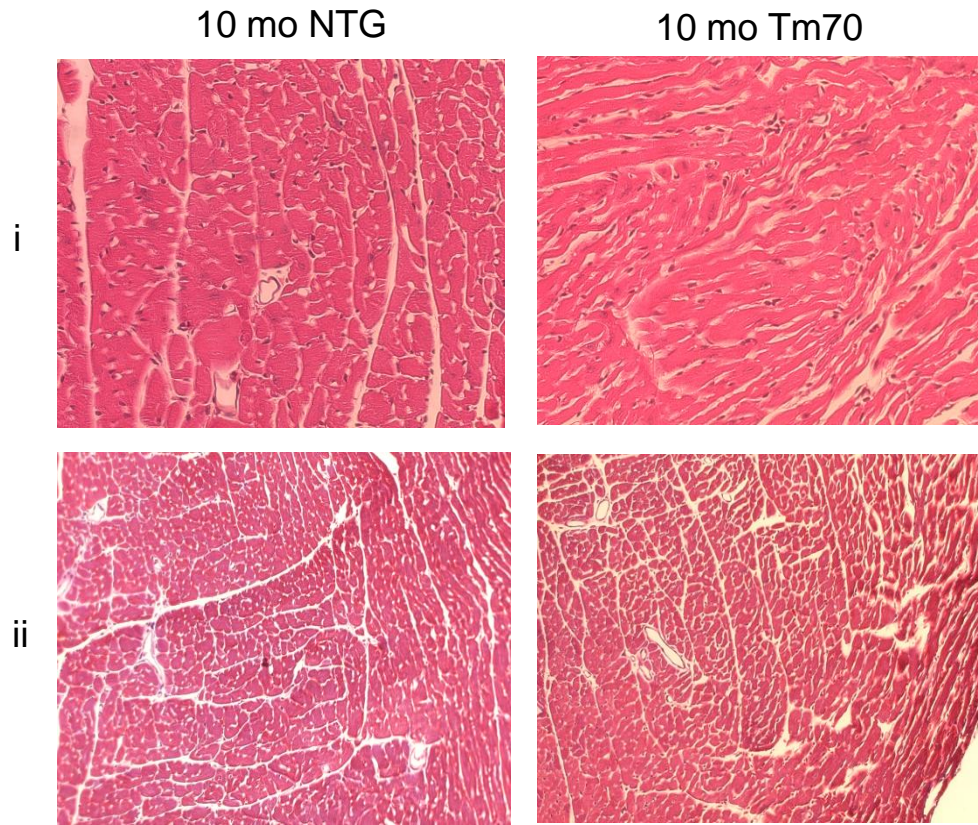
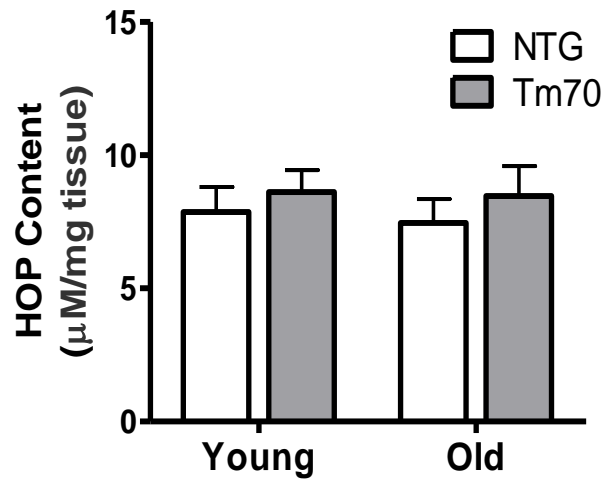
A.**B.**

Figure 21: Histological assessment of NTG and Tm70 hearts. A, Ventricular sections of NTG and Tm70 hearts were stained with (i) Hematoxylin & Eosin (H & E) to qualitatively assess myocyte architecture or (ii) Masson's trichrome to qualitatively assess fibrosis. Images were taken at 20x and 10x magnification, respectively. B, Quantitative measurement of the hydroxyproline content, an indicator of interstitial collagen, in 4 mo (young) and 10 mo (old) NTG or Tm70 mice. $n = 4$

Table III: Echocardiography of NTG and Tm70 mice at 4 mo and 10 mo of age

	NTG at 4 mo (n = 9)	Tm70 at 4 mo (n = 9)	NTG at 10 mo (n = 10)	Tm70 at 10 mo (n = 14)
Morphology				
LV Mass, mg	81.02 ± 4.22	76.35 ± 4.92	88.25 ± 4.97	96.15 ± 6.02
LA, mm	1.93 ± 0.08	1.88 ± 0.11	2.08 ± 0.06	2.07 ± 0.08
LVIDd, mm	3.89 ± 0.06	3.81 ± 0.12	4.10 ± 0.11	4.03 ± 0.09
RWT	0.38 ± 0.01	0.38 ± 0.02	0.36 ± 0.01	0.40 ± 0.01
Systole				
HR, bpm	481.67 ± 13.6	497.56 ± 8.16	480.80 ± 11.6	465.93 ± 11.0
FS, %	38.03 ± 1.20	38.49 ± 1.42	37.32 ± 1.83	38.22 ± 1.32
EF, %	68.67 ± 1.48	69.30 ± 1.80	67.38 ± 2.50	68.61 ± 1.82
V _{cf} , circ/s	6.82 ± 0.35	7.13 ± 0.36	6.93 ± 0.49	7.02 ± 0.25
CO, mL/min	22.56 ± 0.81	22.14 ± 1.24	23.97 ± 1.02	22.65 ± 1.45
Diastole				
E/A Ratio	1.54 ± 0.18	1.45 ± 0.16	1.78 ± 0.19	1.12 ± 0.04*
E/Em Ratio	30.93 ± 1.80	34.50 ± 2.14	33.87 ± 2.92	26.66 ± 1.55*#
E wave DT, ms	24.35 ± 0.85	21.42 ± 1.43	20.04 ± 0.73†	24.36 ± 0.84*
IVRT, ms	11.07 ± 0.35	12.21 ± 0.81	10.54 ± 0.62	15.41 ± 0.55*#

Results are means ± S.E.M. NTG, non-transgenic; Tm, α -tropomyosin; LV, left ventricle; LVIDd, LV internal dimension (diastole); RWT, relative wall thickness; FS, fractional shortening; EF, ejection fraction; V_{cf}, velocity of circumferential shortening; E/A ratio, maximal velocity of blood flow in early LV filling (E)/ maximal velocity of blood flow after atrial contraction (A); E-wave DT, E-wave deceleration time; IVRT, isovolumic relaxation time. * $p < 0.05$ vs NTG 10 mo, # $p < 0.05$ vs Tm70 4 mo, † $p < 0.05$ vs NTG 4 mo.

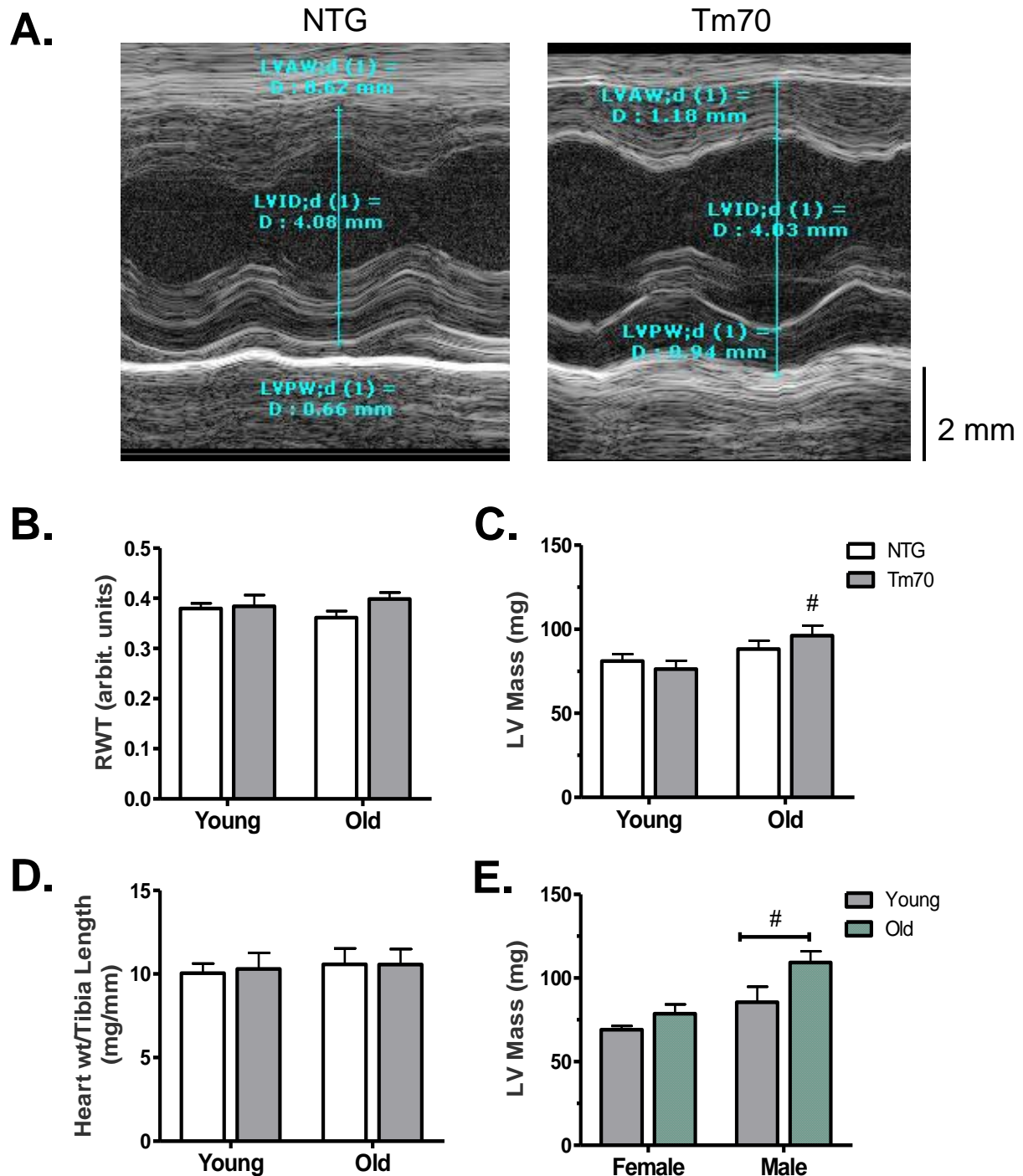


Figure 22: Morphology of NTG and Tm70 hearts. A, Representative M-Mode echocardiography of 10 mo old mice. B, Quantification of relative wall thickness (RWT) and C, left ventricular (LV) mass as assessed by M-Mode echocardiography in 4 mo and 10 mo old NTG and Tm70 mice. D, The ratio of heart weight to tibia length in 4 mo and 10 mo old NTG and Tm70 mice as an indicator of cardiac hypertrophic growth. E, LV mass of Tm70 mice by gender. # $p < 0.05$ vs 4mo Tm70 mice.

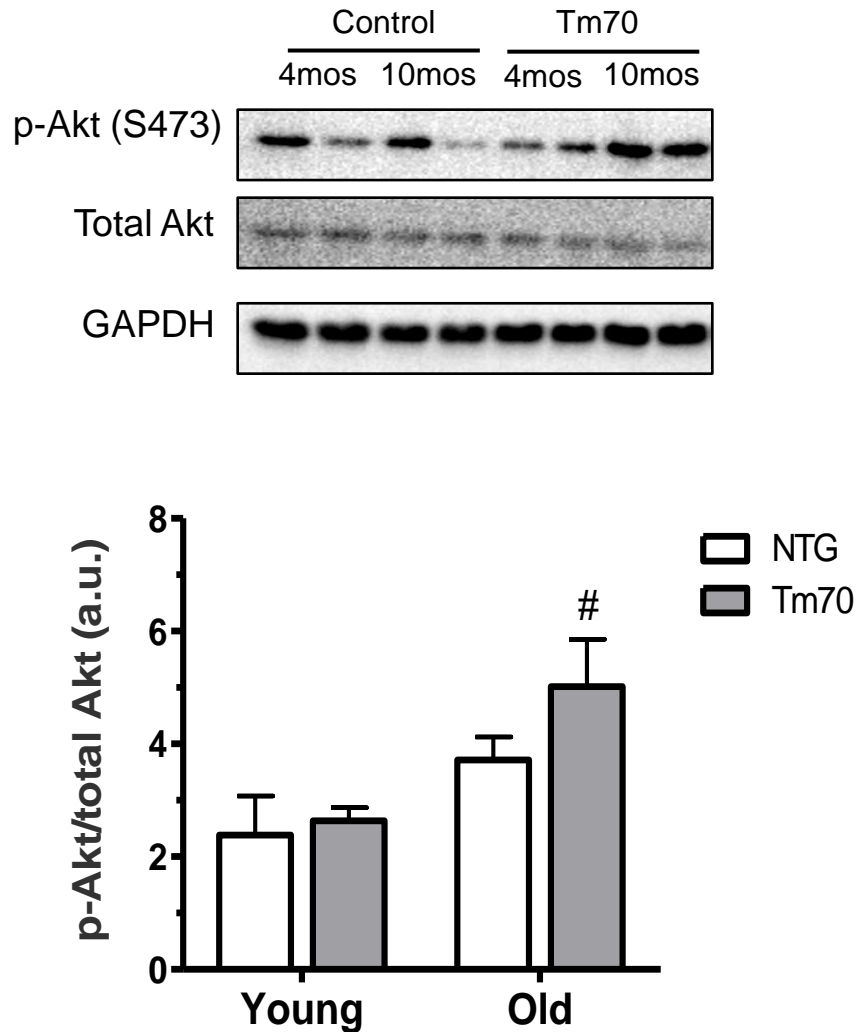


Figure 23: Hypertrophic signaling through activation of Akt. Representative Western blot showing relative phospho-Akt in heart samples from 4 mo and 10 mo NTG and Tm70 mice with quantification of the ratio of phospho-Akt to total Akt. Immunoblotting for GAPDH on the same membrane was used to confirm equal loading. # $p < 0.05$ vs 4mo Tm70 mice. $n = 6$

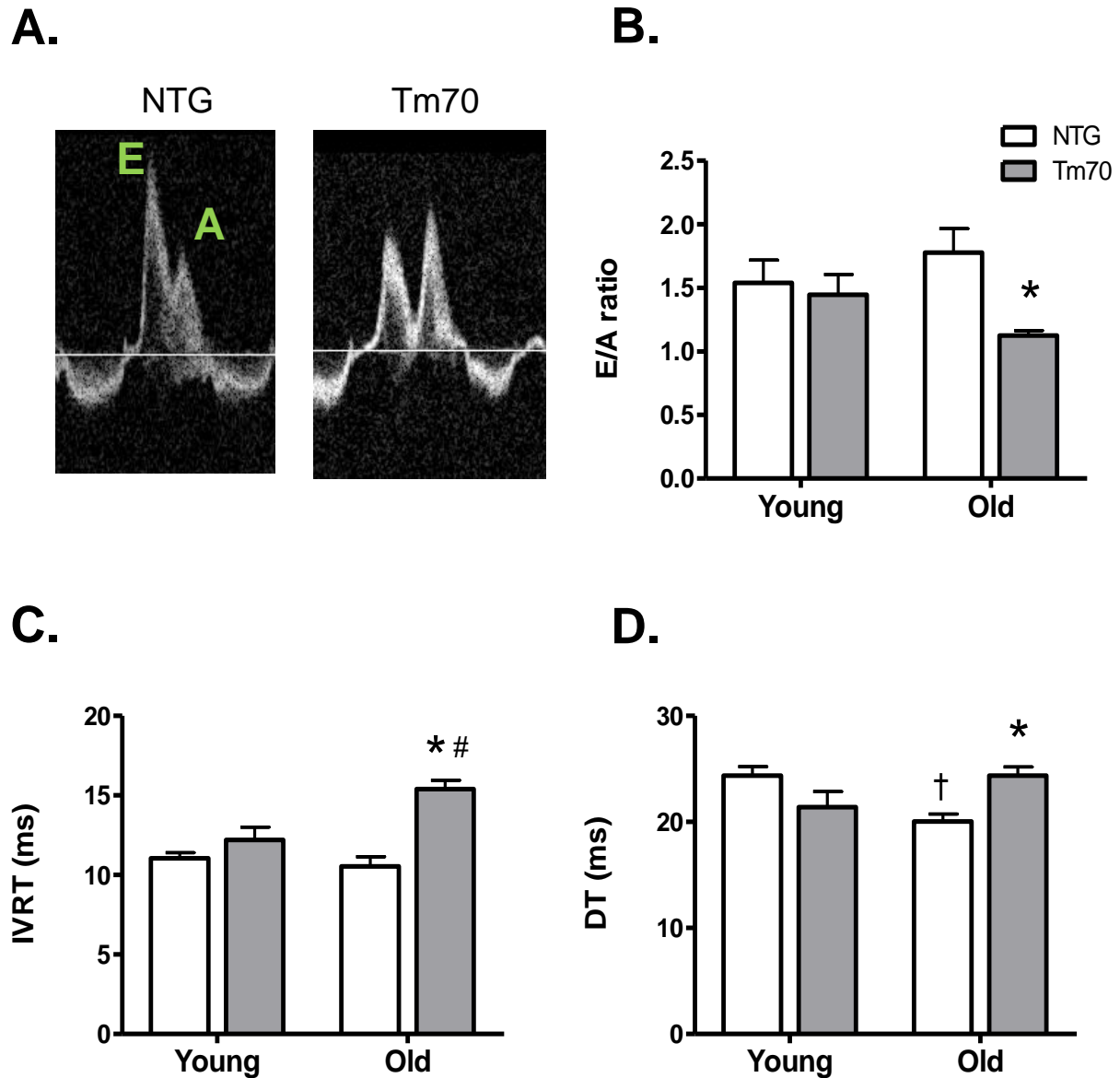


Figure 24: Diastolic parameters from echocardiography in NTG and Tm70 mice. A, Representative doppler image from echocardiography of 10 mo old mice depicting the maximal velocity of blood flow through the mitral valve in early LV filling (peak E) and maximal velocity of blood flow through the mitral valve after atrial contraction (peak A). B, Quantification of the E/A ratio C, the isovolumic relaxation time (IVRT) and D, the E- wave deceleration time (DT) as assessed by echocardiography in 4 mo and 10 mo old NTG and Tm70 mice. * $p > 0.05$ vs NTG 10 mo, # $p < 0.05$ vs Tm70 4 mo, † $p < 0.05$ vs NTG 4 mo.

3. Modifications in Excitation-Contraction Coupling with Persistent Increases in the Myofilament Calcium-Sensitivity

In vitro experiments by others have demonstrated an increased Ca^{2+} sensitivity in both virally-transfected adult cardiomyocytes and reconstituted fibers expressing the K70T mutant Tm (73, 124). We wanted to examine whether our Tm70 transgenic mice also displayed increased myofilament Ca^{2+} sensitivity. To do this, we measured Ca^{2+} -dependent tension generation in detergent-extracted fiber bundles from NTG and Tm70 mice at both 4 mo and 10 mo of age. Figure 25 and Table IV summarize the results from these experiments. Figure 25 shows the level of Ca^{2+} -dependent tension generation in young (Panel A) and old (Panel B) NTG and Tm70 fiber bundles. In both instances, the maximal Ca^{2+} -dependent tension generated in Tm70 fiber bundles was comparable to that of NTG fiber bundles. However, the concentration of Ca^{2+} required to produce half-maximal tension development (i.e. $-\log[\text{Ca}^{2+}]$ at 50% or pCa50) was decreased in both young and old Tm70 fiber bundles (decreased $[\text{Ca}^{2+}] = \text{increased pCa50}$). This increase in the pCa50 is apparent by the leftward shift in the force- Ca^{2+} relation curves shown in Figure 25 and occurs to a greater extent in older Tm70 animals (Panel B and ΔpCa in Table IV). There was also a significant reduction in the Hill coefficient, a measure of cooperativity, which occurred only in the older Tm70 fiber bundles. I would like to note here that the greater difference in the pCa50 and the significant reduction in the Hill coefficient of NTG and Tm70 fiber bundles from old mice was due solely to changes in the measurements of the NTG fiber bundles at 10 mo ($\Delta\text{pCa} = 0.08$ and $\Delta n_H = 1.35$) and not by significant changes in the absolute value of the pCa50 in

Tm70 fibers (see Table C). To my knowledge, there are only 2 previous reports examining the effects of aging on Ca^{2+} -dependent tension generation and in both instances the authors observed no change in the pCa_{50} or the Hill coefficient with age (4, 7). It should be noted, however, that both studies used male rats whereas this study examined the Ca^{2+} -dependent tension generation in mice with an equal distribution of males and females.

Using ventricular cardiomyocytes isolated from NTG or Tm70 hearts at both ages we were able to simultaneously record cell shortening and Ca^{2+} transients in the same cell to assess potential changes in cell shortening and $[\text{Ca}^{2+}]_i$ parameters. Measures of cell shortening showed no genotype-dependent or age-dependent differences in the percentage of cell shortening or in the kinetics of shortening or relengthening (data not shown). Figure 26A shows representative Ca^{2+} transient tracings from field stimulated cardiomyocytes isolated from NTG and Tm70 mice at both ages with the calculated parameters shown in Figure 26B. There were no differences in the end-diastolic $[\text{Ca}^{2+}]_i$, the peak amplitude of the Ca^{2+} transient or the time for decay of the transient (τ) between NTG and Tm70 cardiomyocytes isolated from 4 mo old animals. Conversely, comparison of Ca^{2+} transient parameters in older NTG and Tm70 cardiomyocytes showed an increase in the end-diastolic $[\text{Ca}^{2+}]_i$. Although the peak amplitude of the Ca^{2+} transient was not different, because of the increase in base-line $[\text{Ca}^{2+}]_i$, the maximal peak Ca^{2+} is increased (2.14 ± 0.13 vs 1.71 ± 0.12 for NTG) meaning that there is more Ca^{2+} in the cytosol overall in older Tm70 mice. After experiments were done, it was found that the concentration of BDM used during isolation of cardiomyocytes from 4 mo old

animals was 7.5 mM but the concentration used during isolation of 10 mo old cardiomyocytes was 10 mM. Based on this, comparisons between ages were not made, as altering the concentration of BDM itself can have significant effects on cardiomyocyte excitation-contraction coupling (104). Future studies are planned to assess isolated myocyte contractile and Ca^{2+} transient parameters using the same BDM concentration at both ages (10 mM). As depicted in Figure 27, we used immunoblotting to detect the expression level of SERCA2a, showing a significant reduction in SERCA2a protein levels in older Tm70 mice compared to NTG. It will be important to probe for the expression levels of phospholamban and the relative phosphorylation of phospholamban in the future to truly determine if Ca^{2+} re-uptake into the SR is altered however, the reduced SERCA2a expression coupled with the elevated end-diastolic $[\text{Ca}^{2+}]_i$ implies that this may be the case.

4. Arrhythmogenic Susceptibility in Tm70 Mice

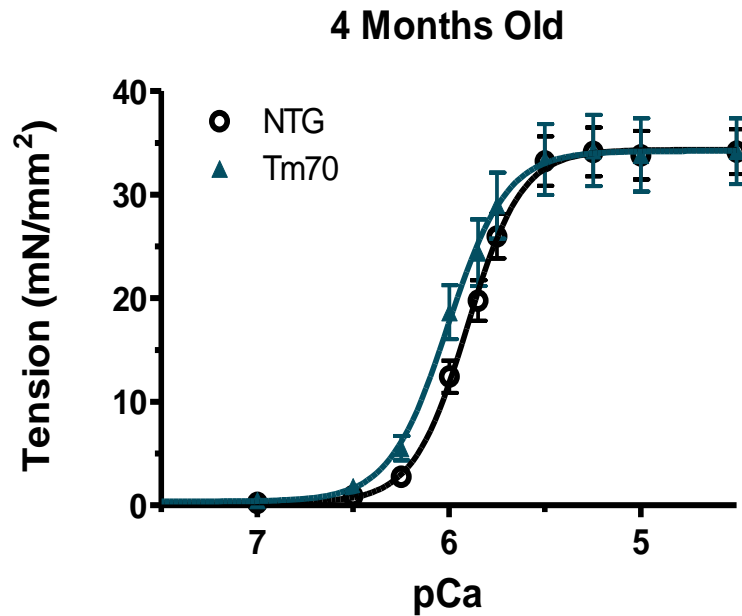
During isolated cardiomyocyte measurements, I noticed that the 10 mo old Tm70 myocytes had a tendency to contract between stimuli. While this is sometimes an indication of a dying myocyte, these instances happened in several cells from independent isolations and were always in healthy looking, nicely striated myocytes. On a single occasion, while recording I was able to capture one of these extra beats, which is shown in Figure 28A. The propensity for these older Tm70 myocytes to spontaneously depolarize, causing premature contractions, is highly suggestive of electrical abnormalities that may pave the way for reentrant arrhythmias. This prompted us to perform preliminary electrophysiological pacing in a 12 mo old Tm70

mouse that was available at the time to test our hypothesis that older Tm70 mice were more susceptible to arrhythmias. In this initial study, we captured a spontaneous premature ventricular contraction (PVC) while recording unpaced base-line EKGs and MAPs (shown in Figure 28B). We were also able to induce a non-sustained ventricular tachycardia (VT) using PES in this animal. Based on this pilot study, we carried out further electrophysiological studies on NTG and Tm70 mice at 4 mo and 10 mo of age.

Figure 29A shows induction of a sustained monomorphic VT (SMVT) in one of our 10 mo Tm70 mice following PES. We were not able to induce arrhythmias in any of the NTG mice at either age. However, we were able to induce arrhythmias in 2 out of the 5 young Tm70 mice we studied and in both instances they were males (difference not significant). A post-hoc statistical power analysis showed that the number of animals assess for arrhythmia inducibility at this age, with this difference was not sufficient to determine statistical difference (power = 0.1). In the older Tm70 animals, 6 of 7 mice were inducible and of these, males had a much more severe form of arrhythmia. Table V and Figure 29 summarize our findings from PES studies. Measurements of AP duration (APD) showed no significant differences between genotypes; however, although not significant with these numbers, the time it took to reach 70% and 90% of repolarization trended to be higher in 10 mo Tm70 mice compared to NTG mice (Figure 29C). This can be more easily visualized by overlaying the average AP's recorded from older NTG and Tm70 mice (Figure 29C). As of now, there is not a high enough number of animals to assess gender differences ($n = 2$ for NTG males and females), however determining if APDs differ

between sexes may provide further insights into the increased arrhythmogenic susceptibility in males.

A.



B.

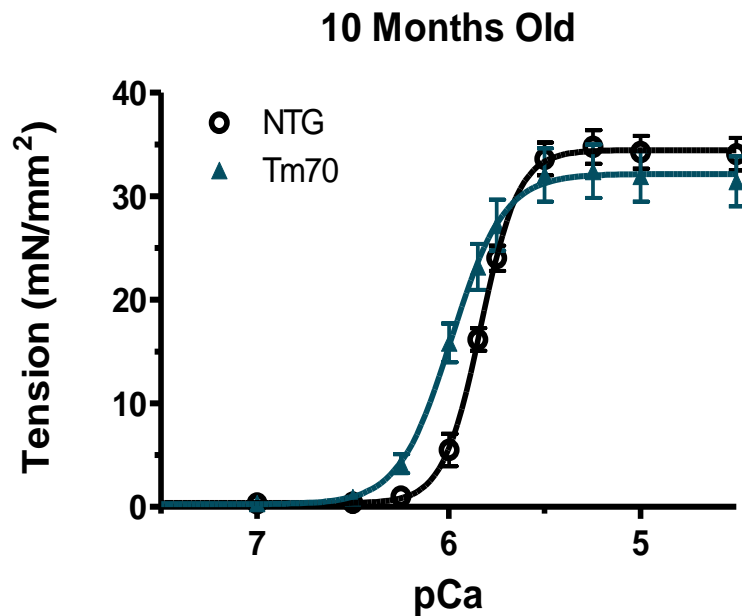


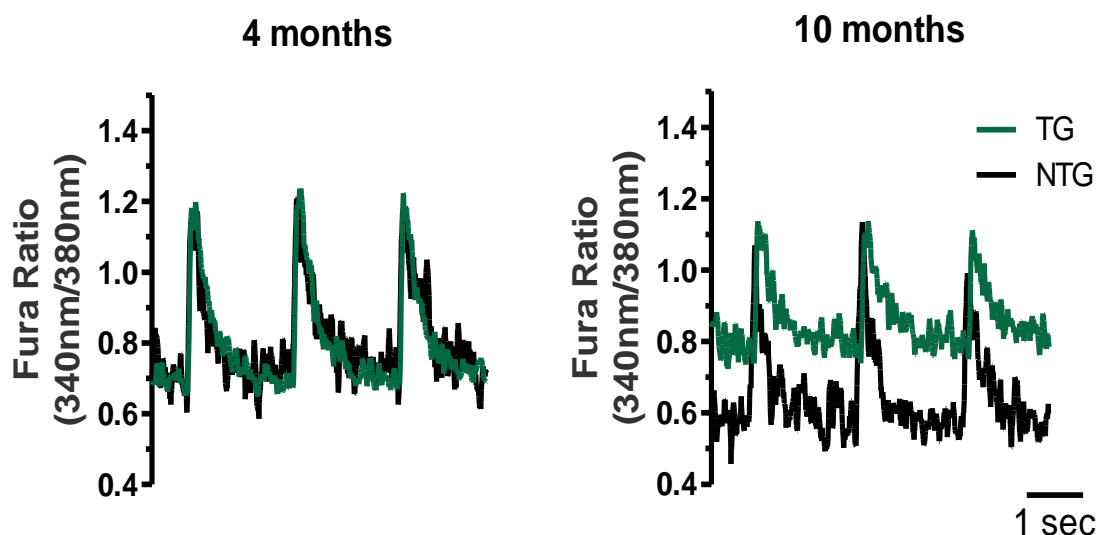
Figure 25: Force-Ca²⁺ relation in skinned fiber preparations from young and old Tm70 mice. A, Force-Ca²⁺ relation in 4 mo skinned fibers from NTG and Tm70 mice show an increase Ca²⁺-sensitivity of the myofilament in Tm70 fibers. B, Force-Ca²⁺ relation in 10 mo skinned fibers from NTG and Tm70 mice show an increase Ca²⁺-sensitivity and reduced Hill coefficient in Tm70 fibers. * $p < 0.05$ vs NTG 10 mo, † $p < 0.05$ vs NTG 4 mo.

Table IV: Force-pCa²⁺ relation in NTG and Tm70 skinned fiber preparations

	NTG at 4 mo (n = 9)	Tm70 at 4 mo (n = 8)	NTG at 10 mo (n = 9)	Tm70 at 10 mo (n = 9)
Max Tension (mN/mm ²)	34.35 ± 0.95	34.24 ± 1.38	34.46 ± 0.61	32.16 ± 0.99
Hill Coefficient (n _H)	3.08 ± 0.50	2.84 ± 0.65	4.43 ± 0.53†	3.18 ± 0.59*
pCa50	5.91 ± 0.02	6.01 ± 0.04†	5.83 ± 0.01†	5.99 ± 0.02*
ΔpCa	-	0.10 ± 0.06	-	0.15 ± 0.03

Results are means ± S.E.M. pCa50, -log [Ca²⁺] at 50% maximum developed tension; ΔpCa = pCa of Tm70 – pCa of NTG in each age group. *p<0.05 vs NTG 10 mo, † p<0.05 vs NTG 4 mo.

A.



B.

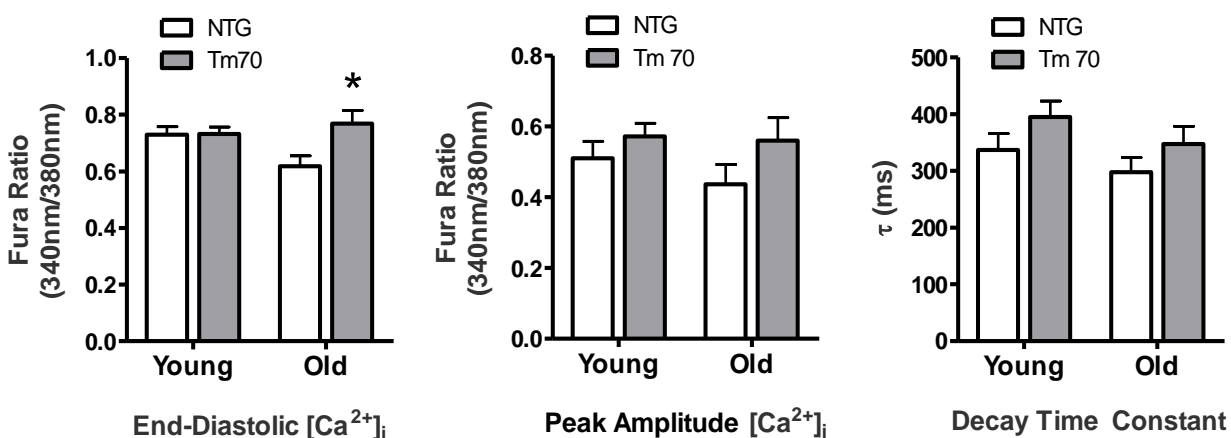


Figure 26: Measurement of $[Ca^{2+}]_i$ transient and kinetics in isolated cardiomyocytes from NTG and Tm70 mice. A, Overlay of Ca^{2+} transient recordings taken from 4 mo NTG (black) and Tm70 (green) cardiomyocytes, *left*, and 10 mo NTG and Tm70 cardiomyocytes, *right*, under field stimulation at 0.5 Hz B, Quantification of the base-line Fura 2 ratio as an indicator of end-diastolic $[Ca^{2+}]_i$, *left*, the peak amplitude of the Fura 2 ratio as an indicator of the peak amplitude of the Ca^{2+} transient, *center*, and the time constant for decay (τ) of the Ca^{2+} transient, *right*. * $p < 0.05$ vs NTG 10 mo, $n = 3$.

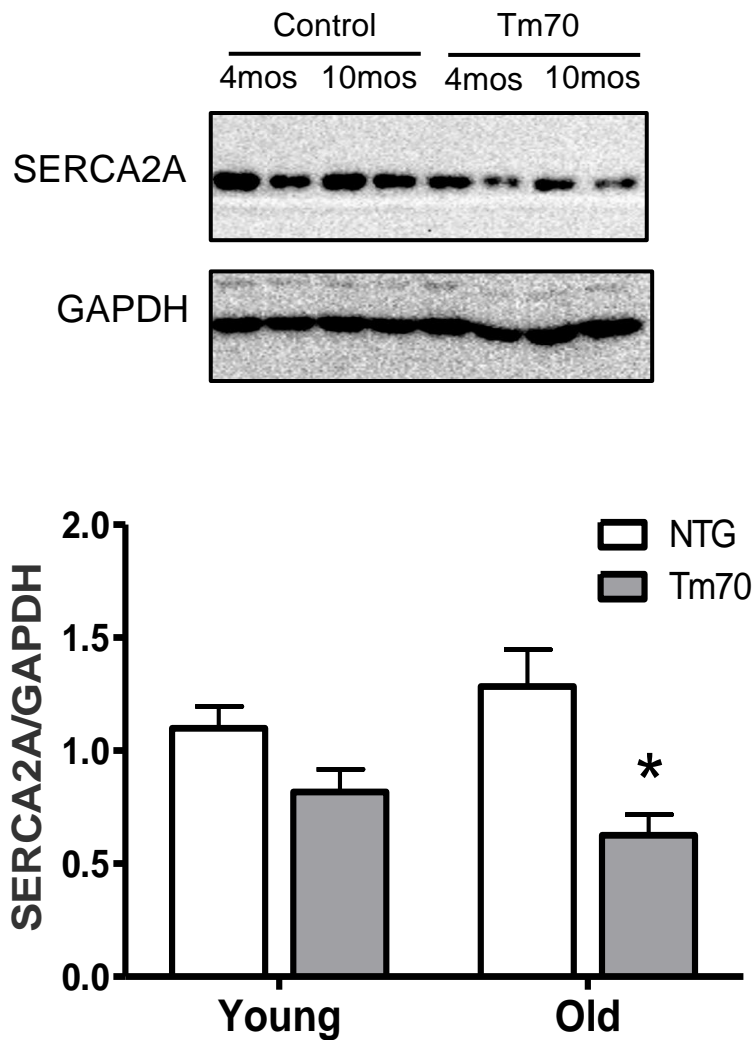
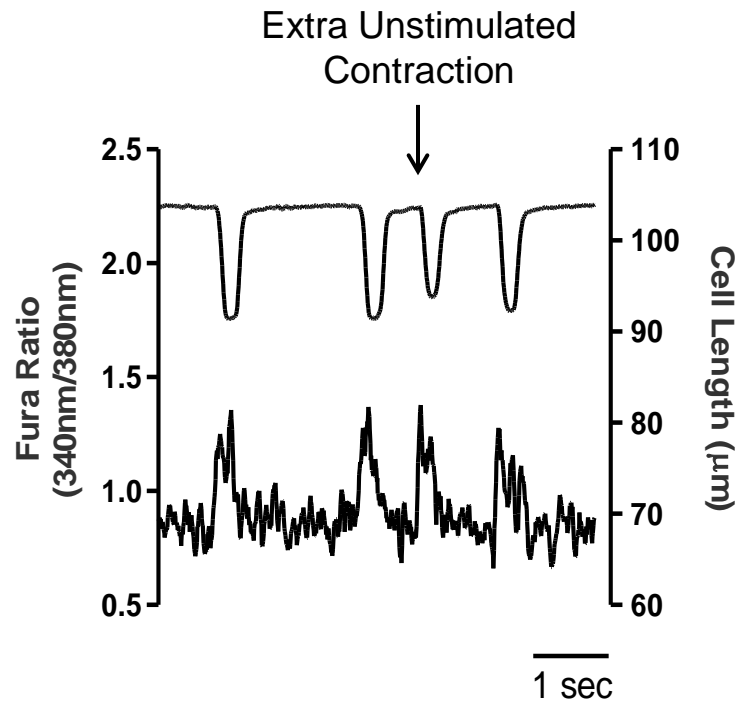


Figure 27: Expression level of SERCA2a protein. Representative Western blot showing relative SERCA2a protein levels in heart samples from 4 mo and 10 mo NTG and Tm70 mice with quantification of the ratio of total SERCA2a to GAPDH. * $p < 0.05$ vs 10mo NTG mice, $n = 6$.

A.



B.

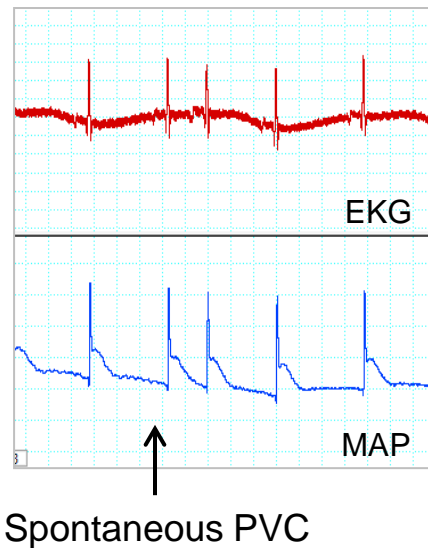


Figure 28: Spontaneous Premature Contractions in Older Tm70 Mice. A, Cardiomyocyte cell shortening and Ca^{2+} transient recordings taken from a 10 mo Tm70 mouse showing the presence of a premature extra contraction. B, Electrocardiogram (EKG) and monophasic action potential (MAP) recorded at baseline during preliminary studies conducted on a 12 mo Tm70 mouse showing a spontaneous premature ventricular contraction (PVC).

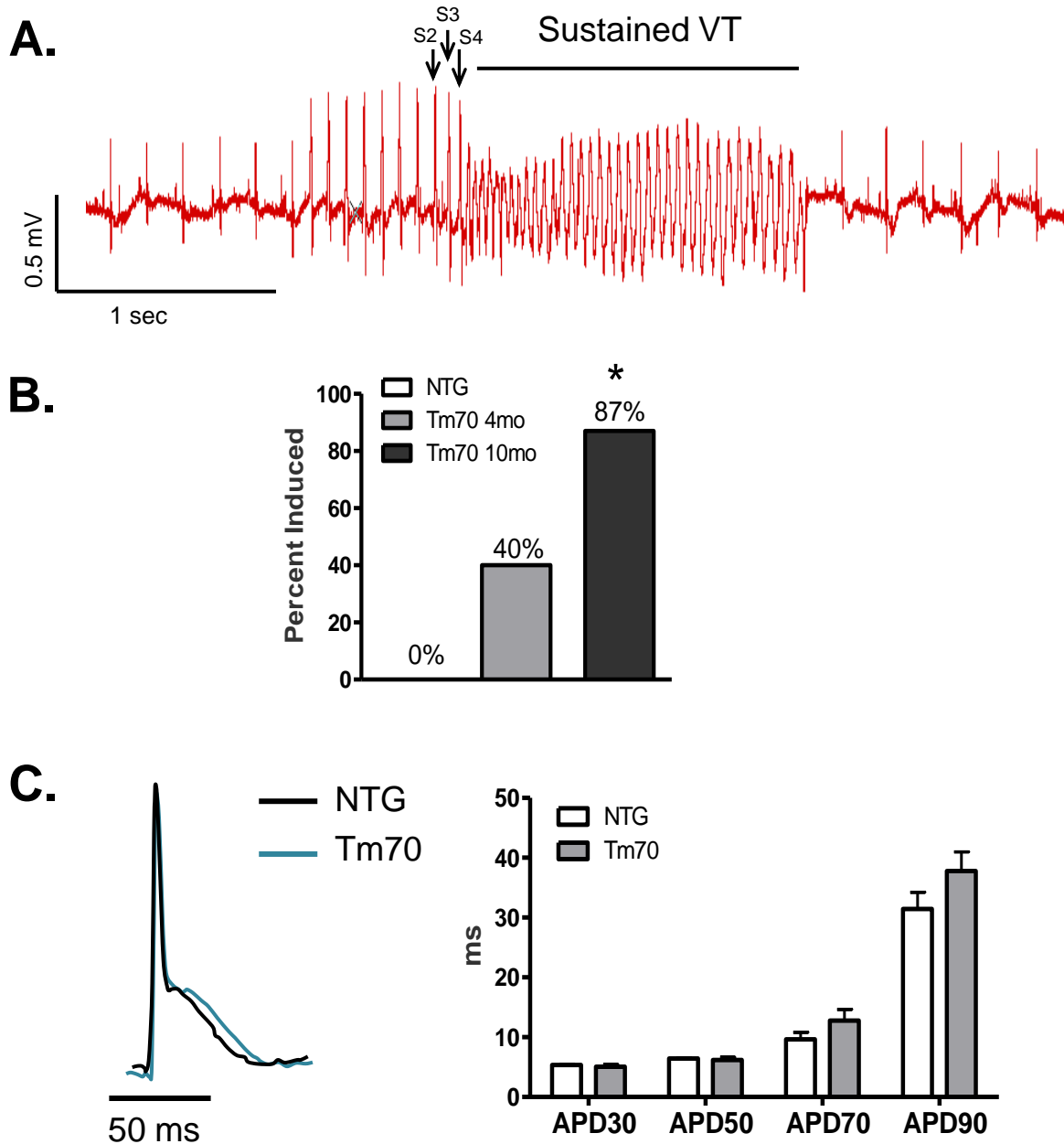


Figure 29: Arrhythmogenicity of Tm70 mice undergoing programmed electrical stimulation. A, Example of sustained ventricular tachycardia (VT) in a 10 mo old Tm70 mouse heart following a series of programmed stimulations. B, inducibility of arrhythmias in hearts for 4 mo and 10 mo NTG and Tm70 mice. Note that the single bar shown for NTG mice represents the percent of induction (0%) both at 4 mo and at 10 mo of age. C, *Left*, overlay of the average monophasic action potential (AP) taken at the base of the left ventricle from a 10 mo NTG (black) and Tm70 (blue) mouse prior to programmed stimulation. The two representative APs were matched by heart rate. *Right*, quantification of the AP duration (APD) at 30%, 50%, 70% and 90% of the total APD. * $p < 0.05$ vs NTG 10 mo.

Table V: Ventricular tachycardia during programmed electrical stimulation

	Total	Extra Beats	Sust. PVT	Sust MVT	Inducibility
<i>Young Mice</i>					
NTG	4	0	0	0	0%
Male	2	-	-	-	
Female	2	-		-	
Tm70	5	1	0	1	40%
Male	2	1	-	1	
Female	3	-		-	
<i>Old Mice</i>					
NTG	4	0	0	0	0%
Male	2	-	-	-	
Female	2				
Tm70	7	0	4	2	87%*
Male	2	-	-	2	
Female	4	-	4	-	

Sust PVT, sustained polymorphic ventricular tachycardia; Sust MVT, sustained monomorphic VT. * $p < 0.05$ vs NTG 10 mo.

D. Discussion

In data presented here we demonstrate that a single charge change on Tm within the thin filament structure is sufficient to induced alterations in cellular homeostasis leading to maladaptive remodeling and cardiac dysfunction. Moreover, the phenotypic and pathological findings from this Tm70 mouse model recapitulates the human disease and further provides critical insights into the mechanisms likely to be causal of SCD in patients bearing this mutation.

1. Alterations in Ca²⁺ Homeostasis Induce Contractile Dysfunction in Aging Tm70

Mice

One of the significant findings of the research presented in this chapter was that unrelenting Ca²⁺ sensitization of the myofilament, inherent to the mutation, induced age-dependent alterations in intracellular Ca²⁺ homeostasis, promoted hypertrophic induction and impaired relaxation. Our results from echocardiography showed that, despite increased myofilament Ca²⁺ sensitivity at both 4 and 10 mos, diastolic function was only depressed in older Tm70 mice. This would imply that the degree of myofilament Ca²⁺ sensitization associated with the Tm70 mutation is not sufficient to impair cardiac function alone. However, because there were no other apparent alterations in myofilament properties (i.e. cooperativity of activation, maximal tension generation) or changes in intracellular Ca²⁺ handling early on, the increased myofilament Ca²⁺ sensitivity must be central to cardiac remodeling and dysfunction that occurred later in life. We showed that with aging Tm70 mice developed increases in [Ca²⁺]_i, which is likely to play a significant role in impairing relaxation. Guinto et al (62) have also shown temporal alterations in Ca²⁺ homeostasis in transgenic mice with cTnT-related HCM. Similar to our observations, previous studies in cTnT HCM mice

have shown early increases in myofilament Ca^{2+} sensitivity without overt remodeling (68, 89). Elevations in the resting $[\text{Ca}^{2+}]_i$ in cTnT mutant myocytes was associated with reduced SR Ca^{2+} uptake owing to a reduction in the SERCA-to-PLB ratio. In experiments reported here, our observed increase in $[\text{Ca}^{2+}]_i$ in older Tm70 mice was associated with reduced SERCA2a expression, however, we have yet to probe for PLB expression or phosphorylation to fully determine changes in SR Ca^{2+} uptake.

Modulation of SR Ca^{2+} cycling is known to occur in mouse models of mutationally-induced HCM and with aging, and can be ascribed to reductions in SERCA2 expression (62, 82, 99). In HCM mouse model studies the decreased SERCA2 expression was associated with reduced SR Ca^{2+} loading and release resulting in systolic and diastolic dysfunction (62). Interestingly, previous work from our lab has shown that neonatal cardiac gene transfer of SERCA2a in Tm E180G-induced HCM delays hypertrophic remodeling and improves contractile performance (145), emphasizing the importance of altered Ca^{2+} homeostasis in HCM pathogenesis. It is likely that the reduced SERCA2 expression in older Tm70 mice observed here decreases SR Ca^{2+} uptake, accounting for our observed elevations in intracellular $[\text{Ca}^{2+}]_i$ and slightly longer Ca^{2+} transient. This in addition to the increased myofilament sensitivity to Ca^{2+} would explain the prolonged relaxation times and diastolic impairment. However, we did not observe any significant changes in the peak Ca^{2+} transient, indicating that Ca^{2+} release for the SR was not impaired. Likewise, there were no changes in systolic function in our mice. This suggests that there may be additional changes in excitation-contraction coupling occurring which could account for this observation. More studies will be needed to address this possibility.

2. Elevations in Intracellular Ca^{2+} Provide a Substrate for Reentrant Arrhythmias

Our results support the hypothesis that elevations in intracellular Ca^{2+} provide a substrate for reentry which is causal of the arrhythmias. A direct link between changes in intracellular Ca^{2+} and electrical excitability was first made by Tan et al (195), who showed that calmodulin (CaM) binds to the IQ domain of the Na channel in a Ca^{2+} -dependent manner enhancing slow inactivation of the channel. Ca^{2+} /calmodulin-dependent protein kinase II (CaMKII) has also been shown to modulate Na channel function by phosphorylation-dependent enhancement of the late I_{Na} (212). These effects would act to reduce the effective refractory period of the AP while concurrently prolonging the AP duration. Such heterogeneity in electrical conductance has been shown to be sufficient to induce extrasystoles capable of initiating ventricular tachycardia (VT) (175, 212).

Findings in isolated cells and data from electrical pacing experiments are suggestive of both reduced AP effective refractory periods and prolonged AP duration leading to our observed extrasystoles and arrhythmic inducibility. Moreover, although we have yet to examine Ca^{2+} -dependent changes in CaM or CaMKII, the correlation between increased $[\text{Ca}^{2+}]_i$ and arrhythmic inducibility warrants further examination for a link between the two. I'd like to digress for one moment to comment on an unexpected finding that I think has provided a valuable lesson in perseverance in the face of unexpected findings. In initial electrophysiological studies we chose to use a burst pacing protocol in which hearts are continually stimulated for 15 sec at a single PCL, beginning at 80 ms and

progressing to shorter and shorter PCL. The selection of our protocol was based on my initial hypothesis that the elevations in intracellular Ca^{2+} in older Tm70 mice were enough to induce Ca^{2+} -overload arrhythmias. Burst pacing has been shown to be the best suited to test for Ca^{2+} -overload arrhythmias (25) and therefore seemed like the appropriate choice. Despite this, we were not able to induce arrhythmias by burst pacing in any of our 12 mo old mice, even though at baseline we were already observing signs of arrhythmogenic potential (i.e. PVC). Reluctantly, we decided to test a PES protocol, which is designed to provoke reentrant arrhythmias (163), although we were not expecting to see anything. The fact then that using a PES protocol to induce arrhythmias was successful in inducing arrhythmias in our older Tm70 mice (and to some degree younger Tm70 mice) was a pleasant surprise and has served to be quite thought provoking. What I can conclude from this is that although we do see elevations in intracellular Ca^{2+} , the degree to which this occurs is not sufficient to “overload” the cells and cause spontaneous depolarization. However, the premise that a single charge change within the thin filament can lead to small, but significant, changes in $[\text{Ca}^{2+}]$, which may directly alter the electrical properties of the cell only emphasized the complex intricacies of the myocardium.

Although our predominating hypothesis is that elevations in intracellular Ca^{2+} provoke electrical heterogeneity and arrhythmogenicity, there appears to be other mechanisms at play. As mentioned previously, we observed a 40% inducibility of arrhythmias in younger Tm70 mice even though the only variance between these mice and age-matched NTGs was the increased myofilament Ca^{2+} sensitivity. This then implies that increasing the myofilament response to Ca^{2+} is adequate to

increase susceptibility to arrhythmias. In light of more recent studies (5, 47, 172) this is not entirely surprising; however, the mechanistic explanation is still somewhat unclear.

3. **The Onset and Severity of the Arrhythmias is Gender-dependent**

We have shown here that males develop both earlier onset and increased severity of arrhythmias, suggesting that there may be sex-dependent differences in HCM disease pathogenesis. Male Tm70 mice were the only ones to develop arrhythmias at 4 mo of age and at 10 mo of age, male mice all presented with sustained monomorphic VT whereas females showed sustained polymorphic VT. Furthermore, males were also more susceptible to hypertrophic remodeling. There is not a strong body of literature examining the differences in electrical properties or structural remodeling of the heart between genders. However, females have been shown to have longer AP durations compared to males (204) making them more susceptible to developing polymorphic VT (222). Likewise, males in general have a tendency to undergo a greater degree of hypertrophy than females (35). It is possible that this propensity for Tm70 males to undergo hypertrophic remodeling may be related to their altered electrical status as well, as hypertrophy has been shown to determine the type of arrhythmia induced after myocardial infarction (43). A recently published study has also shown that there are gender-dependent alterations in myofilament properties in a mouse model of HCM linked to the R403Q mutation in myosin heavy chain (MHC) (121). They found differences in myofilament Ca^{2+} -sensitive tension development which they ascribed to sex-dependent differences in β -MHC expression and cTnI phosphospecies. We have been careful during our

experimentation to include an equal proportion of male and female mice and have assessed the potential for gender differences in all our measures. We have not observed any difference in myofilament properties in Tm70 or NTG mice owing to gender. However, given our findings that gender plays a role in Tm70 disease phenotype, it will be critical to continue assessing for sexual dimorphism as we move forward.

In summary, we have extended *in vitro* studies, which have demonstrated that the Tm K70T mutation linked to HCM increases N-domain flexibility and alters myofilament Ca^{2+} sensitivity (73, 124), adding that these inherent changes in Tm are sufficient to disrupt intracellular homeostasis and promote disease progression. The mechanisms involved cause altered intracellular $[\text{Ca}^{2+}]$ and electrical remodeling over time and appear to differ between males and females. Further studies in Tm K70T mice may serve as a useful tool to unravel the molecular mechanisms underlying HCM pathogenesis and offers insights into the divergence in disease severity often seen.

CHAPTER V

GENERAL DISCUSSION

A. Conclusions of the Thesis

In this thesis I have reviewed evidence demonstrating the critical role for myofilament protein modifications in the regulation of cardiac function. The mechanisms discovered here exemplify the cross-talk that occurs within the cardiomyocyte to aid in this regulatory process and how, when persistent, such mechanisms can contribute to cardiac dysfunction. The scientific contributions this work has provided are as follows:

1. We show that acute ceramide treatment initiates a novel signaling mechanism by which alterations in metabolism can augment cardiac function through PKC-mediated phosphorylation of the myofilament proteins. These findings suggest that ceramide's ability to directly regulate contractile function should be considered as a significant contributor to the depressed cardiac function associated with diseases in which ceramide accumulates.
2. We provide the first evidence of increased susceptibility of arrhythmias in a mouse model of HCM caused by a mutation in Tm. Furthermore, our findings demonstrate gender-dependent differences in disease onset and severity, which are consistent with epidemiologic findings in humans.
3. We demonstrate that increased arrhythmogenic susceptibility, independent of gender, is not due to increased myofilament Ca^{2+} -sensitivity alone, as shown for

other thin-filament mutations, but depends on alterations in overall Ca^{2+} homeostasis. This may suggest a divergence in disease mechanism initiated by thin-filament HCM mutations or imply that a greater degree of Ca^{2+} sensitivity than observed here is required to provoke arrhythmias.

4. We consider that the novelty of the Tm K70T mouse model may, perhaps, lay in the potential insights which could be gained from future studies in these mice. Given the slower time course for disease development and gender differences in etiology, future studies in these mice could be uniquely designed to identify the earliest cellular events which trigger disease and further elucidate how these mechanisms differ in males versus females.

B. Speculations

1. Communication to the Sarcomere

Communication to the sarcomere from the intracellular space is nothing new, in the sense that over 50 years ago it was established that changes in intracellular Ca^{2+} could proportionally change force development (215). Our understanding of how this occurred was advanced when cTnC binding to Ca^{2+} (39) provided a direct link between the intracellular environment and the sarcomere. However, regulation of cardiac function goes beyond alterations in binding kinetics and one requires little imagination to see that a more complex regulatory network is necessary for beat-to-beat tuning of contractile function in the face of ever-fluctuating hemodynamic demands. The presence of multiple modification sites on the myofilament proteins, targeted by a multitude of signaling molecules, emphasizes the central role of the sarcomere in this

regulatory process. Traditionally, the focus of much of the literature has been on phosphorylation of the myofilament by kinases, such as PKA, PKC and PKD, which are activated by extracellular ligands coupled to receptors. However, recent endeavors are just beginning to expand our knowledge of contractile regulation to include signaling molecules activated by intracellular “stress gauges”.

Recent studies have linked changes in energy state, oxidative state and ionic state to regulation of cardiac function directly through the sarcomere. The activated form of AMP-activated protein kinase (AMPK), which occurs following energy reduction (as sensed by the AMP/ATP ratio), has been shown to phosphorylate cTnI at Ser150 (168) resulting in increased myofilament Ca^{2+} sensitivity (132, 138). These effects were proposed to enhance contractility without altering energetic cost. In states of elevated intracellular Ca^{2+} , such as in the stunned myocardium following ischemia-reperfusion (I/R) injury, activation of CaMKII has also been shown to result in direct modification of the myofilament, specifically on Ser-282 of cMyBP-C (53, 70, 171). Ser-282 of cMyBP-C has also been shown to be targeted by p90 ribosomal S6 kinase (RSK) in response to endothelin treatment (32). As mentioned in Chapter III, modification of this site appears to be critical for enhancing contractility by cMyBP-C. Given the large number of modification sites on cMyBP-C (see Figure 15 in Chapter III) it would not be surprising if, in the near future, other kinases not traditionally thought to associate with the sarcomere will prove to be sarcomeric modifiers. In fact, a study published earlier this year found glycogen synthase kinase 3 β (GSK3 β)

phosphorylates a novel, previously unidentified site on human cMyBP-C (Ser301).

More recognized and appreciated is the link between oxidative state and the sarcomere. I've already mentioned in my earlier discussions (Chapter III) the numerous direct oxidative modifications that have been shown to occur within the sarcomere. However, beyond these, oxidation has been also been shown to activate signaling molecules which target the myofilament for phosphorylation. In particular, both c-Src and mammalian sterile 20-like kinase 1 (Mst1) induce phosphorylation of the cTn (191, 223). Phosphorylation of cTnI and cTnT by Mst1 caused a conformational change within the cTn structure, effectively reducing the Ca^{2+} binding affinity for cTnC (223). This effect was suggested to be protective in cases of ischemic injury where, as just mentioned, intracellular Ca^{2+} levels are elevated. However, over-expression of Mst1 in the heart lead to the development of contractile impairment and dilated cardiomyopathy (220), implying that while Mst1-mediated phosphorylation of cTn might be beneficial acutely, long-term activation is deleterious. The activation of c-Src by oxidative stress is coupled to PKC δ activation through c-Src-specific tyrosine phosphorylation (Tyr-311) (164-165, 191). Phosphorylation of PKC δ at Tyr-311 induces auto-phosphorylation of Thr-505 and further leads to targeting of cTnI and preferential phosphorylation at Thr-144 (191). This same group has also shown that Raf-1 can phosphorylate of cTnT at Thr-206 (147).

Such communication to the sarcomere is certainly not limited to modifications of the myofilament proteins. Indeed, the Z-disk is well-known to act as both a

mechanosensor of the heart, as well as an anchor for signaling molecules, such as calcineurin, p-21 activated kinase (Pak1), muscle LIM protein (MLP) and, PKC ϵ (for review see (50)). Future studies are likely to add to this list of Z-disk associated signaling molecules and provide a greater understanding of how intracellular cross-talk is localized.

2. **Communication from the Sarcomere**

It has become apparent that there is also reciprocity in regulation of cardiac homeostasis through communication from the sarcomere to the intracellular environment. Transgenic mouse models have contributed significantly to this understanding, shedding light on how single modifications at the level of the myofilament can disrupt intracellular homeostasis resulting in disease. As a whole, HCM mutations increase myofilament Ca²⁺ sensitivity, which has been shown to greatly enhance the myofilament's ability to buffer Ca²⁺ (90, 161, 201). Consequently, this altered Ca²⁺ buffering may underlie the observed alterations in intracellular Ca²⁺ concentration, as shown here (Chapter IV, Figure 26) and by others (62, 89, 172). The implications for this include the likely activation of Ca²⁺-sensitive kinases, such as CaMKII and altered function of the NCX, which is allosterically regulated by the intracellular Na⁺ and Ca²⁺ concentrations. This, in turn, can disrupt electrical homeostasis and increase the risk for arrhythmias and sudden cardiac death (89).

Some of these same HCM mutations used to study alterations in cTn Ca²⁺ buffering have also been examined for changes in myocardial energetic (71),

demonstrating an overall reduction in energetic efficiency of HCM hearts (30, 71, 156, 193). The consensus is that cardiac inefficiency is due to the greater cost of force production inherent to the structural changes induced by the HCM mutations. Moreover, it appears that these early changes in energetics are a primary defect and not a consequence of hypertrophic induction (30). One might speculate that the higher tension cost of contraction would result in enough energy depletion to effect proper functioning of ATP-dependent pumps, such as the SERCA2a pump, possibly leading to disruptions in ion homeostasis. Interestingly, studies using the cTnT R92 mutations (R92L and R92W) showed that the degree of inefficiency was dictated by the amino acid substituted, with the R92W mutation causing the more severe energetic phenotype (71). It is interesting to note that patients with the R92W mutation have a much higher frequency of sudden cardiac death compared to R92L carriers (49, 160). This would imply a role for altered energetic in arrhythmogenic susceptibility. It is also likely that alterations in energetics caused by sarcomeric modifications can, in turn promote further modifications of the sarcomere. Activation of AMPK as a consequence of energy depletion from inefficient ATP utilization may modify the myofilament response to Ca^{2+} through phosphorylation of cTnI, as mentioned above.

This 'sarcomere-kinase-sarcomere' activation axis is not unique to the energy sensor AMPK. c-Src activation has also been shown to occur through changes in the biophysical properties of the sarcomere (170), with the potential for activated c-Src to activate PKC δ and, in turn, alter cTnI phosphorylation.

Furthermore, the sarcomeric protein titin has intrinsic kinase abilities which are thought to play a role in myofibrillogenesis through phosphorylation of telothonin (117). The complexity does not stop there and our general understanding of signaling *from* the sarcomere appears to only have scratched the surface.

In essence, the intricacies of cardiac regulation go far beyond our reductionist models. And while we are limited by these, forward thinkers will always be finding new ways to exploit technology so that we may continue to strive toward integrating these complex signaling networks and feedback mechanisms which dictate function. It has been my honor and privilege to work alongside some of these very people; individuals who have been given the gifts of curiosity, passion and creativity to explore science and make a significant contribution to our world.

“When we cast our bread upon the waters, we can presume that someone downstream whose face we will never know will benefit from our action, as we who are downstream from another will profit from that grantor's gift.”

- Maya Angelou

CHAPTER VI

CITED LITERATURE

1. Avner BS, Shioura, KM, Scruggs, SB, Grachoff, M, Geenen, DL, Helseth, DL, Jr., Farjah, M, Goldspink, PH, and John Solaro, R. (2012) Myocardial infarction in mice alters sarcomeric function via post-translational protein modification. *Mol Cell Biochem* 363: 203-215.
2. Ayaz-Guner S, Zhang, J, Li, L, Walker, JW, and Ge, Y. (2009) In vivo phosphorylation site mapping in mouse cardiac troponin I by high resolution top-down electron capture dissociation mass spectrometry: Ser22/23 are the only sites basally phosphorylated. *Biochemistry* 48: 8161-8170.
3. Bai F, Weis, A, Takeda, AK, Chase, PB, and Kawai, M. (2011) Enhanced active cross-bridges during diastole: molecular pathogenesis of tropomyosin's HCM mutations. *Biophys J* 100: 1014-1023.
4. Ball KL, and Solaro, RJ. (1994) Discoordinate regulation of contractile protein gene expression in the senescent rat myocardium. *J Mol Cell Cardiol* 26: 519-525.
5. Baudenbacher F, Schober, T, Pinto, JR, Sidorov, VY, Hilliard, F, Solaro, RJ, Potter, JD, and Knollmann, BC. (2008) Myofilament Ca²⁺ sensitization causes susceptibility to cardiac arrhythmia in mice. *J Clin Invest* 118: 3893-3903.
6. Belin RJ, Sumandea, MP, Allen, EJ, Schoenfelt, K, Wang, H, Solaro, RJ, and de Tombe, PP. (2007) Augmented protein kinase C- α -induced myofilament protein phosphorylation contributes to myofilament dysfunction in experimental congestive heart failure. *Circ Res* 101: 195-204.
7. Bhatnagar GM, Walford, GD, Beard, ES, Humphreys, S, and Lakatta, EG. (1984) ATPase activity and force production in myofibrils and twitch characteristics in intact muscle from neonatal, adult, and senescent rat myocardium. *J Mol Cell Cardiol* 16: 203-218.
8. Bielawska A, Crane, HM, Liotta, D, Obeid, LM, and Hannun, YA. (1993) Selectivity of ceramide-mediated biology. Lack of activity of erythro-dihydroceramide. *J Biol Chem* 268: 26226-26232.
9. Bielawska A, Linardic, CM, and Hannun, YA. (1992) Modulation of cell growth and differentiation by ceramide. *FEBS Lett* 307: 211-214.

10. Blaustein MP, and Lederer, WJ. (1999) Sodium/calcium exchange: its physiological implications. *Physiol Rev* 79: 763-854.
11. Bowling N, Walsh, RA, Song, G, Estridge, T, Sandusky, GE, Fouts, RL, Mintze, K, Pickard, T, Roden, R, Bristow, MR, Sabbah, HN, Mizrahi, JL, Gromo, G, King, GL, and Vlahos, CJ. (1999) Increased protein kinase C activity and expression of Ca²⁺-sensitive isoforms in the failing human heart. *Circulation* 99: 384-391.
12. Bowman JC, Steinberg, SF, Jiang, T, Geenen, DL, Fishman, GI, and Buttrick, PM. (1997) Expression of protein kinase C beta in the heart causes hypertrophy in adult mice and sudden death in neonates. *J Clin Invest* 100: 2189-2195.
13. Brandes R, and Bers, DM. (1997) Intracellular Ca²⁺ increases the mitochondrial NADH concentration during elevated work in intact cardiac muscle. *Circ Res* 80: 82-87.
14. Brenner B. (1988) Effect of Ca²⁺ on cross-bridge turnover kinetics in skinned single rabbit psoas fibers: implications for regulation of muscle contraction. *Proc Natl Acad Sci U S A* 85: 3265-3269.
15. Brown JH, Zhou, Z, Reshetnikova, L, Robinson, H, Yammani, RD, Tobacman, LS, and Cohen, C. (2005) Structure of the mid-region of tropomyosin: bending and binding sites for actin. *Proc Natl Acad Sci U S A* 102: 18878-18883.
16. Brutsaert DL, and Sys, SU. (1989) Relaxation and diastole of the heart. *Physiol Rev* 69: 1228-1315.
17. Burkart EM, Sumandea, MP, Kobayashi, T, Nili, M, Martin, AF, Homsher, E, and Solaro, RJ. (2003) Phosphorylation or glutamic acid substitution at protein kinase C sites on cardiac troponin I differentially depress myofilament tension and shortening velocity. *J Biol Chem* 278: 11265-11272.
18. Canton M, Menazza, S, Sheeran, FL, Polverino de Laureto, P, Di Lisa, F, and Pepe, S. (2011) Oxidation of myofibrillar proteins in human heart failure. *J Am Coll Cardiol* 57: 300-309.
19. Canton M, Neverova, I, Menabo, R, Van Eyk, J, and Di Lisa, F. (2004) Evidence of myofibrillar protein oxidation induced by postischemic reperfusion in isolated rat hearts. *Am J Physiol Heart Circ Physiol* 286: H870-877.
20. Canton M, Skyschally, A, Menabo, R, Boengler, K, Gres, P, Schulz, R, Haude, M, Erbel, R, Di Lisa, F, and Heusch, G. (2006) Oxidative modification of

- tropomyosin and myocardial dysfunction following coronary microembolization. *Eur Heart J* 27: 875-881.
21. Challoner DR. (1968) Respiration in myocardium. *Nature* 217: 78-79.
 22. Chiu HC, Kovacs, A, Blanton, RM, Han, X, Courtois, M, Weinheimer, CJ, Yamada, KA, Brunet, S, Xu, H, Nerbonne, JM, Welch, MJ, Fettig, NM, Sharp, TL, Sambandam, N, Olson, KM, Ory, DS, and Schaffer, JE. (2005) Transgenic expression of fatty acid transport protein 1 in the heart causes lipotoxic cardiomyopathy. *Circ Res* 96: 225-233.
 23. Chiu HC, Kovacs, A, Ford, DA, Hsu, FF, Garcia, R, Herrero, P, Saffitz, JE, and Schaffer, JE. (2001) A novel mouse model of lipotoxic cardiomyopathy. *J Clin Invest* 107: 813-822.
 24. Chokshi A, Drosatos, K, Cheema, FH, Ji, R, Khawaja, T, Yu, S, Kato, T, Khan, R, Takayama, H, Knoll, R, Milting, H, Chung, CS, Jorde, U, Naka, Y, Mancini, DM, Goldberg, IJ, and Schulze, PC. (2012) Ventricular assist device implantation corrects myocardial lipotoxicity, reverses insulin resistance, and normalizes cardiac metabolism in patients with advanced heart failure. *Circulation* 125: 2844-2853.
 25. Coetzee WA, and Opie, LH. (1987) Effects of components of ischemia and metabolic inhibition on delayed afterdepolarizations in guinea pig papillary muscle. *Circ Res* 61: 157-165.
 26. Cortassa S, Aon, MA, O'Rourke, B, Jacques, R, Tseng, HJ, Marban, E, and Winslow, RL. (2006) A computational model integrating electrophysiology, contraction, and mitochondrial bioenergetics in the ventricular myocyte. *Biophys J* 91: 1564-1589.
 27. Coulton AT, and Stelzer, JE. (2012) Cardiac myosin binding protein C and its phosphorylation regulate multiple steps in the cross-bridge cycle of muscle contraction. *Biochemistry* 51: 3292-3301.
 28. Coviello DA, Maron, BJ, Spirito, P, Watkins, H, Vosberg, HP, Thierfelder, L, Schoen, FJ, Seidman, JG, and Seidman, CE. (1997) Clinical features of hypertrophic cardiomyopathy caused by mutation of a "hot spot" in the alpha-tropomyosin gene. *J Am Coll Cardiol* 29: 635-640.
 29. Craig R, and Lehman, W. (2001) Crossbridge and tropomyosin positions observed in native, interacting thick and thin filaments. *J Mol Biol* 311: 1027-1036.

30. Crilley JG, Boehm, EA, Blair, E, Rajagopalan, B, Blamire, AM, Styles, P, McKenna, WJ, Ostman-Smith, I, Clarke, K, and Watkins, H. (2003) Hypertrophic cardiomyopathy due to sarcomeric gene mutations is characterized by impaired energy metabolism irrespective of the degree of hypertrophy. *J Am Coll Cardiol* 41: 1776-1782.
31. Crosbie RH, Miller, C, Cheung, P, Goodnight, T, Muhlrads, A, and Reisler, E. (1994) Structural connectivity in actin: effect of C-terminal modifications on the properties of actin. *Biophys J* 67: 1957-1964.
32. Cuello F, Bardswell, SC, Haworth, RS, Ehler, E, Sadayappan, S, Kentish, JC, and Avkiran, M. (2011) Novel role for p90 ribosomal S6 kinase in the regulation of cardiac myofilament phosphorylation. *J Biol Chem* 286: 5300-5310.
33. Cui J, Engelman, RM, Maulik, N, and Das, DK. (2004) Role of ceramide in ischemic preconditioning. *J Am Coll Surg* 198: 770-777.
34. D'Alessandro ME, Chicco, A, and Lombardo, YB. (2008) Dietary fish oil reverses lipotoxicity, altered glucose metabolism, and nPKCepsilon translocation in the heart of dyslipemic insulin-resistant rats. *Metabolism* 57: 911-919.
35. de Simone G, Devereux, RB, Daniels, SR, and Meyer, RA. (1995) Gender differences in left ventricular growth. *Hypertension* 26: 979-983.
36. de Tombe PP, Belus, A, Piroddi, N, Scellini, B, Walker, JS, Martin, AF, Tesi, C, and Poggesi, C. (2007) Myofilament calcium sensitivity does not affect cross-bridge activation-relaxation kinetics. *Am J Physiol Regul Integr Comp Physiol* 292: R1129-1136.
37. de Tombe PP, and Solaro, RJ. (2000) Integration of cardiac myofilament activity and regulation with pathways signaling hypertrophy and failure. *Ann Biomed Eng* 28: 991-1001.
38. Drosatos K, Bharadwaj, KG, Lympieropoulos, A, Ikeda, S, Khan, R, Hu, Y, Agarwal, R, Yu, S, Jiang, H, Steinberg, SF, Blaner, WS, Koch, WJ, and Goldberg, IJ. (2011) Cardiomyocyte lipids impair beta-adrenergic receptor function via PKC activation. *Am J Physiol Endocrinol Metab* 300: E489-499.
39. Ebashi S, and Endo, M. (1968) Calcium ion and muscle contraction. *Prog Biophys Mol Biol* 18: 123-183.

40. Edman KA, and Mattiazzi, AR. (1981) Effects of fatigue and altered pH on isometric force and velocity of shortening at zero load in frog muscle fibres. *J Muscle Res Cell Motil* 2: 321-334.
41. Eisenberg B, and Eisenberg, RS. (1968) Transverse tubular system in glycerol-treated skeletal muscle. *Science* 160: 1243-1244.
42. Fabiato A. (1983) Calcium-induced release of calcium from the cardiac sarcoplasmic reticulum. *Am J Physiol* 245: C1-14.
43. Fauconnier J, Pasquie, JL, Bideaux, P, Lacampagne, A, and Richard, S. (2010) Cardiomyocytes hypertrophic status after myocardial infarction determines distinct types of arrhythmia: role of the ryanodine receptor. *Prog Biophys Mol Biol* 103: 71-80.
44. Ferreira LF, Moylan, JS, Gilliam, LA, Smith, JD, Nikolova-Karakashian, M, and Reid, MB. (2010) Sphingomyelinase stimulates oxidant signaling to weaken skeletal muscle and promote fatigue. *Am J Physiol Cell Physiol* 299: C552-560.
45. Ferreira LF, Moylan, JS, Stasko, S, Smith, JD, Campbell, KS, and Reid, MB. (2012) Sphingomyelinase depresses force and calcium sensitivity of the contractile apparatus in mouse diaphragm muscle fibers. *J Appl Physiol* 112: 1538-1545.
46. Finck BN, Han, X, Courtois, M, Aimond, F, Nerbonne, JM, Kovacs, A, Gross, RW, and Kelly, DP. (2003) A critical role for PPARalpha-mediated lipotoxicity in the pathogenesis of diabetic cardiomyopathy: modulation by dietary fat content. *Proc Natl Acad Sci U S A* 100: 1226-1231.
47. Flevari P, Parissis, JT, Leftheriotis, D, Panou, F, Kourea, K, and Kremastinos, DT. (2006) Effect of levosimendan on ventricular arrhythmias and prognostic autonomic indexes in patients with decompensated advanced heart failure secondary to ischemic or dilated cardiomyopathy. *Am J Cardiol* 98: 1641-1645.
48. Florea S, Anjak, A, Cai, WF, Qian, J, Vafiadaki, E, Figueria, S, Haghghi, K, Rubinstein, J, Lorenz, J, and Kranias, EG. (2012) Constitutive phosphorylation of inhibitor-1 at Ser67 and Thr75 depresses calcium cycling in cardiomyocytes and leads to remodeling upon aging. *Basic Res Cardiol* 107: 279.
49. Forissier JF, Carrier, L, Farza, H, Bonne, G, Bercovici, J, Richard, P, Hainque, B, Townsend, PJ, Yacoub, MH, Faure, S, Dubourg, O, Millaire, A, Hagege, AA, Desnos, M, Komajda, M, and Schwartz, K. (1996) Codon 102 of the cardiac troponin T gene is a putative hot spot for mutations in familial hypertrophic cardiomyopathy. *Circulation* 94: 3069-3073.

50. Frank D, and Frey, N. (2011) Cardiac Z-disc signaling network. *J Biol Chem* 286: 9897-9904.
51. Franzini-Armstrong C, Protasi, F, and Ramesh, V. (1999) Shape, size, and distribution of Ca(2+) release units and couplons in skeletal and cardiac muscles. *Biophys J* 77: 1528-1539.
52. Garcia-Ruiz C, Colell, A, Mari, M, Morales, A, and Fernandez-Checa, JC. (1997) Direct effect of ceramide on the mitochondrial electron transport chain leads to generation of reactive oxygen species. Role of mitochondrial glutathione. *J Biol Chem* 272: 11369-11377.
53. Gautel M, Zuffardi, O, Freiburg, A, and Labeit, S. (1995) Phosphorylation switches specific for the cardiac isoform of myosin binding protein-C: a modulator of cardiac contraction? *EMBO J* 14: 1952-1960.
54. Geisterfer-Lowrance AA, Kass, S, Tanigawa, G, Vosberg, HP, McKenna, W, Seidman, CE, and Seidman, JG. (1990) A molecular basis for familial hypertrophic cardiomyopathy: a beta cardiac myosin heavy chain gene missense mutation. *Cell* 62: 999-1006.
55. Goldspink PH, Montgomery, DE, Walker, LA, Urboniene, D, McKinney, RD, Geenen, DL, Solaro, RJ, and Buttrick, PM. (2004) Protein kinase Cepsilon overexpression alters myofilament properties and composition during the progression of heart failure. *Circ Res* 95: 424-432.
56. Golitsina N, An, Y, Greenfield, NJ, Thierfelder, L, Iizuka, K, Seidman, JG, Seidman, CE, Lehrer, SS, and Hitchcock-DeGregori, SE. (1999) Effects of two familial hypertrophic cardiomyopathy-causing mutations on alpha-tropomyosin structure and function. *Biochemistry* 38: 3850.
57. Gordon AM, Huxley, AF, and Julian, FJ. (1966) The variation in isometric tension with sarcomere length in vertebrate muscle fibres. *J Physiol* 184: 170-192.
58. Granzier H, and Labeit, S. (2002) Cardiac titin: an adjustable multi-functional spring. *J Physiol* 541: 335-342.
59. Granzier HL, and Labeit, S. (2004) The giant protein titin: a major player in myocardial mechanics, signaling, and disease. *Circulation Research* 94: 284-295.
60. Gregorio CC, Granzier, H, Sorimachi, H, and Labeit, S. (1999) Muscle assembly: a titanic achievement? *Current opinion in cell biology* 11: 18-25.

61. Grutzner A, Garcia-Manyes, S, Kotter, S, Badilla, CL, Fernandez, JM, and Linke, WA. (2009) Modulation of titin-based stiffness by disulfide bonding in the cardiac titin N2-B unique sequence. *Biophys J* 97: 825-834.
62. Guinto PJ, Haim, TE, Dowell-Martino, CC, Sibinga, N, and Tardiff, JC. (2009) Temporal and mutation-specific alterations in Ca²⁺ homeostasis differentially determine the progression of cTnT-related cardiomyopathies in murine models. *Am J Physiol Heart Circ Physiol* 297: H614-626.
63. Hajjar RJ, and Gwathmey, JK. (1992) Cross-bridge dynamics in human ventricular myocardium. Regulation of contractility in the failing heart. *Circulation* 86: 1819-1826.
64. Hajri T, and Abumrad, NA. (2002) Fatty acid transport across membranes: relevance to nutrition and metabolic pathology. *Annu Rev Nutr* 22: 383-415.
65. Hannun YA. (1996) Functions of ceramide in coordinating cellular responses to stress. *Science* 274: 1855-1859.
66. Hannun YA, and Luberto, C. (2000) Ceramide in the eukaryotic stress response. *Trends Cell Biol* 10: 73-80.
67. Hannun YA, and Obeid, LM. (2008) Principles of bioactive lipid signalling: lessons from sphingolipids. *Nat Rev Mol Cell Biol* 9: 139-150.
68. Harada K, and Potter, JD. (2004) Familial hypertrophic cardiomyopathy mutations from different functional regions of troponin T result in different effects on the pH and Ca²⁺ sensitivity of cardiac muscle contraction. *J Biol Chem* 279: 14488-14495.
69. Hartman TJ, Martin, JL, Solaro, RJ, Samarel, AM, and Russell, B. (2009) CapZ dynamics are altered by endothelin-1 and phenylephrine via PIP₂- and PKC-dependent mechanisms. *Am J Physiol Cell Physiol* 296: C1034-1039.
70. Hartzell HC, and Glass, DB. (1984) Phosphorylation of purified cardiac muscle C-protein by purified cAMP-dependent and endogenous Ca²⁺-calmodulin-dependent protein kinases. *J Biol Chem* 259: 15587-15596.
71. He H, Javadpour, MM, Latif, F, Tardiff, JC, and Ingwall, JS. (2007) R-92L and R-92W mutations in cardiac troponin T lead to distinct energetic phenotypes in intact mouse hearts. *Biophys J* 93: 1834-1844.

72. Head JG, Ritchie, MD, and Geeves, MA. (1995) Characterization of the equilibrium between blocked and closed states of muscle thin filaments. *Eur J Biochem* 227: 694-699.
73. Heller MJ, Nili, M, Homsher, E, and Tobacman, LS. (2003) Cardiomyopathic tropomyosin mutations that increase thin filament Ca²⁺ sensitivity and tropomyosin N-domain flexibility. *J Biol Chem* 278: 41742-41748.
74. Heusch P, Canton, M, Aker, S, van de Sand, A, Konietzka, I, Rassaf, T, Menazza, S, Brodde, OE, Di Lisa, F, Heusch, G, and Schulz, R. (2010) The contribution of reactive oxygen species and p38 mitogen-activated protein kinase to myofilament oxidation and progression of heart failure in rabbits. *Br J Pharmacol* 160: 1408-1416.
75. Hilario E, da Silva, SL, Ramos, CH, and Bertolini, MC. (2004) Effects of cardiomyopathic mutations on the biochemical and biophysical properties of the human alpha-tropomyosin. *Eur J Biochem* 271: 4132-4140.
76. Hill AV. (1949) The abrupt transition from rest to activity in muscle. *Proc R Soc Lond B Biol Sci* 136: 399-420.
77. Hinken AC, Hanft, LM, Scruggs, SB, Sadayappan, S, Robbins, J, Solaro, RJ, and McDonald, KS. (2012) Protein kinase C depresses cardiac myocyte power output and attenuates myofilament responses induced by protein kinase A. *J Muscle Res Cell Motil*
78. Holland WL, Brozinick, JT, Wang, LP, Hawkins, ED, Sargent, KM, Liu, Y, Narra, K, Hoehn, KL, Knotts, TA, Siesky, A, Nelson, DH, Karathanasis, SK, Fontenot, GK, Birnbaum, MJ, and Summers, SA. (2007) Inhibition of ceramide synthesis ameliorates glucocorticoid-, saturated-fat-, and obesity-induced insulin resistance. *Cell Metab* 5: 167-179.
79. Hug H, and Sarre, TF. (1993) Protein kinase C isoenzymes: divergence in signal transduction? *Biochem J* 291 (Pt 2): 329-343.
80. Huxley AF. (1957) Muscle structure and theories of contraction. *Prog Biophys Biophys Chem* 7: 255-318.
81. Jaaskelainen P, Soranta, M, Miettinen, R, Saarinen, L, Pihlajamaki, J, Silvennoinen, K, Tikanoja, T, Laakso, M, and Kuusisto, J. (1998) The cardiac beta-myosin heavy chain gene is not the predominant gene for hypertrophic cardiomyopathy in the Finnish population. *J Am Coll Cardiol* 32: 1709-1716.

82. Janczewski AM, and Lakatta, EG. (2010) Modulation of sarcoplasmic reticulum Ca(2+) cycling in systolic and diastolic heart failure associated with aging. *Heart Fail Rev* 15: 431-445.
83. Jideama NM, Noland, TA, Jr., Raynor, RL, Blobe, GC, Fabbro, D, Kazanietz, MG, Blumberg, PM, Hannun, YA, and Kuo, JF. (1996) Phosphorylation specificities of protein kinase C isozymes for bovine cardiac troponin I and troponin T and sites within these proteins and regulation of myofilament properties. *J Biol Chem* 271: 23277-23283.
84. Jongbloed RJ, Marcelis, CL, Doevendans, PA, Schmeitz-Mulkens, JM, Van Dockum, WG, Geraedts, JP, and Smeets, HJ. (2003) Variable clinical manifestation of a novel missense mutation in the alpha-tropomyosin (TPM1) gene in familial hypertrophic cardiomyopathy. *J Am Coll Cardiol* 41: 981-986.
85. Karibe A, Tobacman, LS, Strand, J, Butters, C, Back, N, Bachinski, LL, Arai, AE, Ortiz, A, Roberts, R, Homsher, E, and Fananapazir, L. (2001) Hypertrophic cardiomyopathy caused by a novel alpha-tropomyosin mutation (V95A) is associated with mild cardiac phenotype, abnormal calcium binding to troponin, abnormal myosin cycling, and poor prognosis. *Circulation* 103: 65-71.
86. Kawamura S, Yoshida, K, Miura, T, Mizukami, Y, and Matsuzaki, M. (1998) Ischemic preconditioning translocates PKC-delta and -epsilon, which mediate functional protection in isolated rat heart. *Am J Physiol* 275: H2266-2271.
87. Keren A, Syrris, P, and McKenna, WJ. (2008) Hypertrophic cardiomyopathy: the genetic determinants of clinical disease expression. *Nat Clin Pract Cardiovasc Med* 5: 158-168.
88. Kirk JA, MacGowan, GA, Evans, C, Smith, SH, Warren, CM, Mamidi, R, Chandra, M, Stewart, AF, Solaro, RJ, and Shroff, SG. (2009) Left ventricular and myocardial function in mice expressing constitutively pseudophosphorylated cardiac troponin I. *Circ Res* 105: 1232-1239.
89. Knollmann BC, Kirchhof, P, Sirenko, SG, Degen, H, Greene, AE, Schober, T, Mackow, JC, Fabritz, L, Potter, JD, and Morad, M. (2003) Familial hypertrophic cardiomyopathy-linked mutant troponin T causes stress-induced ventricular tachycardia and Ca2+-dependent action potential remodeling. *Circ Res* 92: 428-436.
90. Kobayashi T, and Solaro, RJ. (2006) Increased Ca2+ affinity of cardiac thin filaments reconstituted with cardiomyopathy-related mutant cardiac troponin I. *J Biol Chem* 281: 13471-13477.

91. Kooij V, Boontje, N, Zaremba, R, Jaquet, K, dos Remedios, C, Stienen, GJ, and van der Velden, J. (2010) Protein kinase C alpha and epsilon phosphorylation of troponin and myosin binding protein C reduce Ca²⁺ sensitivity in human myocardium. *Basic Res Cardiol* 105: 289-300.
92. Korte FS, McDonald, KS, Harris, SP, and Moss, RL. (2003) Loaded shortening, power output, and rate of force redevelopment are increased with knockout of cardiac myosin binding protein-C. *Circ Res* 93: 752-758.
93. Kremneva E, Boussouf, S, Nikolaeva, O, Maytum, R, Geeves, MA, and Levitsky, DI. (2004) Effects of two familial hypertrophic cardiomyopathy mutations in alpha-tropomyosin, Asp175Asn and Glu180Gly, on the thermal unfolding of actin-bound tropomyosin. *Biophys J* 87: 3922-3933.
94. Lang RM, Bierig, M, Devereux, RB, Flachskampf, FA, Foster, E, Pellikka, PA, Picard, MH, Roman, MJ, Seward, J, Shanewise, JS, Solomon, SD, Spencer, KT, Sutton, MS, and Stewart, WJ. (2005) Recommendations for chamber quantification: a report from the American Society of Echocardiography's Guidelines and Standards Committee and the Chamber Quantification Writing Group, developed in conjunction with the European Association of Echocardiography, a branch of the European Society of Cardiology. *J Am Soc Echocardiogr* 18: 1440-1463.
95. Layland J, Grieve, DJ, Cave, AC, Sparks, E, Solaro, RJ, and Shah, AM. (2004) Essential role of troponin I in the positive inotropic response to isoprenaline in mouse hearts contracting auxotonically. *J Physiol* 556: 835-847.
96. Leavis PC, and Gergely, J. (1984) Thin filament proteins and thin filament-linked regulation of vertebrate muscle contraction. *CRC Crit Rev Biochem* 16: 235-305.
97. Lehman W, Rosol, M, Tobacman, LS, and Craig, R. (2001) Troponin organization on relaxed and activated thin filaments revealed by electron microscopy and three-dimensional reconstruction. *J Mol Biol* 307: 739-744.
98. Lester JW, and Hofmann, PA. (2000) Role for PKC in the adenosine-induced decrease in shortening velocity of rat ventricular myocytes. *Am J Physiol Heart Circ Physiol* 279: H2685-2693.
99. Li Q, Wu, S, Li, SY, Lopez, FL, Du, M, Kajstura, J, Anversa, P, and Ren, J. (2007) Cardiac-specific overexpression of insulin-like growth factor 1 attenuates aging-associated cardiac diastolic contractile dysfunction and protein damage. *Am J Physiol Heart Circ Physiol* 292: H1398-1403.

100. Li XE, Suphamungmee, W, Janco, M, Geeves, MA, Marston, SB, Fischer, S, and Lehman, W. (2012) The flexibility of two tropomyosin mutants, D175N and E180G, that cause hypertrophic cardiomyopathy. *Biochem Biophys Res Commun* 424: 493-496.
101. Liu SJ, and Kennedy, RH. (2003) Positive inotropic effect of ceramide in adult ventricular myocytes: mechanisms dissociated from its reduction in Ca²⁺ influx. *Am J Physiol Heart Circ Physiol* 285: H735-744.
102. Loong CK, Zhou, HX, and Chase, PB. (2012) Familial hypertrophic cardiomyopathy related E180G mutation increases flexibility of human cardiac alpha-tropomyosin. *FEBS Lett* 586: 3503-3507.
103. Lopaschuk GD, Ussher, JR, Folmes, CD, Jaswal, JS, and Stanley, WC. (2010) Myocardial fatty acid metabolism in health and disease. *Physiol Rev* 90: 207-258.
104. Louch WE, Sheehan, KA, and Wolska, BM. (2011) Methods in cardiomyocyte isolation, culture, and gene transfer. *J Mol Cell Cardiol* 51: 288-298.
105. Lovelock JD, Monasky, MM, Jeong, EM, Lardin, HA, Liu, H, Patel, BG, Taglieri, DM, Gu, L, Kumar, P, Pokhrel, N, Zeng, D, Belardinelli, L, Sorescu, D, Solaro, RJ, and Dudley, SC, Jr. (2012) Ranolazine improves cardiac diastolic dysfunction through modulation of myofilament calcium sensitivity. *Circ Res* 110: 841-850.
106. Luptak I, Balschi, JA, Xing, Y, Leone, TC, Kelly, DP, and Tian, R. (2005) Decreased contractile and metabolic reserve in peroxisome proliferator-activated receptor-alpha-null hearts can be rescued by increasing glucose transport and utilization. *Circulation* 112: 2339-2346.
107. Makhoul M, Ackerman, MJ, Atkins, DL, and Law, IH. (2011) Clinical spectrum in a family with tropomyosin-mediated hypertrophic cardiomyopathy and sudden death in childhood. *Pediatr Cardiol* 32: 215-220.
108. Marfella R, Di Filippo, C, Portoghese, M, Barbieri, M, Ferraraccio, F, Siniscalchi, M, Cacciapuoti, F, Rossi, F, D'Amico, M, and Paolisso, G. (2009) Myocardial lipid accumulation in patients with pressure-overloaded heart and metabolic syndrome. *J Lipid Res* 50: 2314-2323.
109. Maron BJ, Gardin, JM, Flack, JM, Gidding, SS, Kurosaki, TT, and Bild, DE. (1995) Prevalence of hypertrophic cardiomyopathy in a general population of young adults. Echocardiographic analysis of 4111 subjects in the CARDIA Study. Coronary Artery Risk Development in (Young) Adults. *Circulation* 92: 785-789.

110. Maron BJ, Maron, MS, and Semsarian, C. (2012) Genetics of hypertrophic cardiomyopathy after 20 years: clinical perspectives. *J Am Coll Cardiol* 60: 705-715.
111. Maron BJ, Pelliccia, A, and Spirito, P. (1995) Cardiac disease in young trained athletes. Insights into methods for distinguishing athlete's heart from structural heart disease, with particular emphasis on hypertrophic cardiomyopathy. *Circulation* 91: 1596-1601.
112. Maron BJ, Shirani, J, Poliac, LC, Mathenge, R, Roberts, WC, and Mueller, FO. (1996) Sudden death in young competitive athletes. Clinical, demographic, and pathological profiles. *JAMA* 276: 199-204.
113. Marston S, Copeland, O, Jacques, A, Livesey, K, Tsang, V, McKenna, WJ, Jalilzadeh, S, Carballo, S, Redwood, C, and Watkins, H. (2009) Evidence from human myectomy samples that MYBPC3 mutations cause hypertrophic cardiomyopathy through haploinsufficiency. *Circ Res* 105: 219-222.
114. Mathias S, Pena, LA, and Kolesnick, RN. (1998) Signal transduction of stress via ceramide. *Biochem J* 335 (Pt 3): 465-480.
115. Matsunaga T, Kotamraju, S, Kalivendi, SV, Dhanasekaran, A, Joseph, J, and Kalyanaraman, B. (2004) Ceramide-induced intracellular oxidant formation, iron signaling, and apoptosis in endothelial cells: protective role of endogenous nitric oxide. *J Biol Chem* 279: 28614-28624.
116. Maughan DW. (2005) Kinetics and energetics of the crossbridge cycle. *Heart failure reviews* 10: 175-185.
117. Mayans O, van der Ven, PF, Wilm, M, Mues, A, Young, P, Furst, DO, Wilmanns, M, and Gautel, M. (1998) Structural basis for activation of the titin kinase domain during myofibrillogenesis. *Nature* 395: 863-869.
118. Maytum R, Lehrer, SS, and Geeves, MA. (1999) Cooperativity and switching within the three-state model of muscle regulation. *Biochemistry* 38: 1102-1110.
119. McClellan G, Kulikovskaya, I, Flavigny, J, Carrier, L, and Winegrad, S. (2004) Effect of cardiac myosin-binding protein C on stability of the thick filament. *J Mol Cell Cardiol* 37: 823-835.
120. McGavock JM, Lingvay, I, Zib, I, Tillery, T, Salas, N, Unger, R, Levine, BD, Raskin, P, Victor, RG, and Szczepaniak, LS. (2007) Cardiac steatosis in diabetes

- mellitus: a ¹H-magnetic resonance spectroscopy study. *Circulation* 116: 1170-1175.
121. McKee LA, Chen, H, Regan, JA, Behunin, SM, Walker, JW, Walker, JS, and Konhilas, JP. (2013) Sexually dimorphic myofilament function and cardiac troponin I phosphospecies distribution in hypertrophic cardiomyopathy mice. *Arch Biochem Biophys*
 122. McKillop DF, and Geeves, MA. (1991) Regulation of the acto.myosin subfragment 1 interaction by troponin/tropomyosin. Evidence for control of a specific isomerization between two acto.myosin subfragment 1 states. *Biochem J* 279 (Pt 3): 711-718.
 123. McKillop DF, and Geeves, MA. (1993) Regulation of the interaction between actin and myosin subfragment 1: evidence for three states of the thin filament. *Biophys J* 65: 693-701.
 124. Michele DE, Albayya, FP, and Metzger, JM. (1999) Direct, convergent hypersensitivity of calcium-activated force generation produced by hypertrophic cardiomyopathy mutant alpha-tropomyosins in adult cardiac myocytes. *Nat Med* 5: 1413-1417.
 125. Montes LR, Ruiz-Arguello, MB, Goni, FM, and Alonso, A. (2002) Membrane restructuring via ceramide results in enhanced solute efflux. *J Biol Chem* 277: 11788-11794.
 126. Montgomery DE, Chandra, M, Huang, Q, Jin, J, and Solaro, RJ. (2001) Transgenic incorporation of skeletal TnT into cardiac myofilaments blunts PKC-mediated depression of force. *Am J Physiol Heart Circ Physiol* 280: H1011-1018.
 127. Muthuchamy M, Pieples, K, Rethinasamy, P, Hoit, B, Grupp, IL, Boivin, GP, Wolska, B, Evans, C, Solaro, RJ, and Wieczorek, DF. (1999) Mouse model of a familial hypertrophic cardiomyopathy mutation in alpha-tropomyosin manifests cardiac dysfunction. *Circ Res* 85: 47-56.
 128. Nagueh SF, Appleton, CP, Gillebert, TC, Marino, PN, Oh, JK, Smiseth, OA, Waggoner, AD, Flachskampf, FA, Pellikka, PA, and Evangelista, A. (2009) Recommendations for the evaluation of left ventricular diastolic function by echocardiography. *J Am Soc Echocardiogr* 22: 107-133.
 129. Nakajima-Taniguchi C, Matsui, H, Nagata, S, Kishimoto, T, and Yamauchi-Takahara, K. (1995) Novel missense mutation in alpha-tropomyosin gene found in Japanese patients with hypertrophic cardiomyopathy. *J Mol Cell Cardiol* 27: 2053-2058.

130. Nielsen LB, Bartels, ED, and Bollano, E. (2002) Overexpression of apolipoprotein B in the heart impedes cardiac triglyceride accumulation and development of cardiac dysfunction in diabetic mice. *J Biol Chem* 277: 27014-27020.
131. Nitanaï Y, Minakata, S, Maeda, K, Oda, N, and Maeda, Y. (2007) Crystal structures of tropomyosin: flexible coiled-coil. *Adv Exp Med Biol* 592: 137-151.
132. Nixon BR, Thawornkaiwong, A, Jin, J, Brundage, EA, Little, SC, Davis, JP, Solaro, RJ, and Biesiadecki, BJ. (2012) AMP-activated protein kinase phosphorylates cardiac troponin I at Ser-150 to increase myofilament calcium sensitivity and blunt PKA-dependent function. *J Biol Chem* 287: 19136-19147.
133. Noland TA, Jr., Guo, X, Raynor, RL, Jideama, NM, Averyhart-Fullard, V, Solaro, RJ, and Kuo, JF. (1995) Cardiac troponin I mutants. Phosphorylation by protein kinases C and A and regulation of Ca²⁺-stimulated MgATPase of reconstituted actomyosin S-1. *J Biol Chem* 270: 25445-25454.
134. Noland TA, Jr., and Kuo, JF. (1991) Protein kinase C phosphorylation of cardiac troponin I or troponin T inhibits Ca²⁺-stimulated actomyosin MgATPase activity. *J Biol Chem* 266: 4974-4978.
135. Noland TA, Jr., and Kuo, JF. (1992) Protein kinase C phosphorylation of cardiac troponin T decreases Ca²⁺-dependent actomyosin MgATPase activity and troponin T binding to tropomyosin-F-actin complex. *Biochem J* 288 (Pt 1): 123-129.
136. Noland TA, Jr., Raynor, RL, Jideama, NM, Guo, X, Kazanietz, MG, Blumberg, PM, Solaro, RJ, and Kuo, JF. (1996) Differential regulation of cardiac actomyosin S-1 MgATPase by protein kinase C isozyme-specific phosphorylation of specific sites in cardiac troponin I and its phosphorylation site mutants. *Biochemistry* 35: 14923-14931.
137. Noureddine L, Azzam, R, Nemer, G, Bielawski, J, Nasser, M, Bitar, F, and Dbaibo, GS. (2008) Modulation of total ceramide and constituent ceramide species in the acutely and chronically hypoxic mouse heart at different ages. *Prostaglandins Other Lipid Mediat* 86: 49-55.
138. Oliveira SM, Zhang, YH, Solis, RS, Isackson, H, Bellahcene, M, Yavari, A, Pinter, K, Davies, JK, Ge, Y, Ashrafian, H, Walker, JW, Carling, D, Watkins, H, Casadei, B, and Redwood, C. (2012) AMP-activated protein kinase phosphorylates cardiac troponin I and alters contractility of murine ventricular myocytes. *Circ Res* 110: 1192-1201.

139. Otsuka H, Arimura, T, Abe, T, Kawai, H, Aizawa, Y, Kubo, T, Kitaoka, H, Nakamura, H, Nakamura, K, Okamoto, H, Ichida, F, Ayusawa, M, Nunoda, S, Isobe, M, Matsuzaki, M, Doi, YL, Fukuda, K, Sasaoka, T, Izumi, T, Ashizawa, N, and Kimura, A. (2012) Prevalence and distribution of sarcomeric gene mutations in Japanese patients with familial hypertrophic cardiomyopathy. *Circ J* 76: 453-461.
140. Page E. (1978) Quantitative ultrastructural analysis in cardiac membrane physiology. *Am J Physiol* 235: C147-158.
141. Pan BS, and Solaro, RJ. (1987) Calcium-binding properties of troponin C in detergent-skinned heart muscle fibers. *J Biol Chem* 262: 7839-7849.
142. Park TS, Hu, Y, Noh, HL, Drosatos, K, Okajima, K, Buchanan, J, Tuinei, J, Homma, S, Jiang, XC, Abel, ED, and Goldberg, IJ. (2008) Ceramide is a cardiotoxin in lipotoxic cardiomyopathy. *J Lipid Res* 49: 2101-2112.
143. Passarelli C, Petrini, S, Pastore, A, Bonetto, V, Sale, P, Gaeta, LM, Tozzi, G, Bertini, E, Canepari, M, Rossi, R, and Piemonte, F. (2008) Myosin as a potential redox-sensor: an in vitro study. *J Muscle Res Cell Motil* 29: 119-126.
144. Pellieux C, Montessuit, C, Papageorgiou, I, Pedrazzini, T, and Lerch, R. (2012) Differential effects of high-fat diet on myocardial lipid metabolism in failing and nonfailing hearts with angiotensin II-mediated cardiac remodeling in mice. *Am J Physiol Heart Circ Physiol* 302: H1795-1805.
145. Pena JR, Szkudlarek, AC, Warren, CM, Heinrich, LS, Gaffin, RD, Jagatheesan, G, del Monte, F, Hajjar, RJ, Goldspink, PH, Solaro, RJ, Wieczorek, DF, and Wolska, BM. (2010) Neonatal gene transfer of Serca2a delays onset of hypertrophic remodeling and improves function in familial hypertrophic cardiomyopathy. *J Mol Cell Cardiol* 49: 993-1002.
146. Petrache I, Medler, TR, Richter, AT, Kamocki, K, Chukwueke, U, Zhen, L, Gu, Y, Adamowicz, J, Schweitzer, KS, Hubbard, WC, Berdyshev, EV, Lungarella, G, and Tudor, RM. (2008) Superoxide dismutase protects against apoptosis and alveolar enlargement induced by ceramide. *Am J Physiol Lung Cell Mol Physiol* 295: L44-53.
147. Pfeleiderer P, Sumandea, MP, Rybin, VO, Wang, C, and Steinberg, SF. (2009) Raf-1: a novel cardiac troponin T kinase. *J Muscle Res Cell Motil* 30: 67-72.
148. Pi Y, and Walker, JW. (2000) Diacylglycerol and fatty acids synergistically increase cardiomyocyte contraction via activation of PKC. *Am J Physiol Heart Circ Physiol* 279: H26-34.

149. Prabhakar R, Boivin, GP, Grupp, IL, Hoit, B, Arteaga, G, Solaro, RJ, and Wieczorek, DF. (2001) A familial hypertrophic cardiomyopathy alpha-tropomyosin mutation causes severe cardiac hypertrophy and death in mice. *J Mol Cell Cardiol* 33: 1815-1828.
150. Probst S, Oechslin, E, Schuler, P, Greutmann, M, Boye, P, Knirsch, W, Berger, F, Thierfelder, L, Jenni, R, and Klaassen, S. (2011) Sarcomere gene mutations in isolated left ventricular noncompaction cardiomyopathy do not predict clinical phenotype. *Circ Cardiovasc Genet* 4: 367-374.
151. Prockop DJ, and Udenfriend, S. (1960) A specific method for the analysis of hydroxyproline in tissues and urine. *Anal Biochem* 1: 228-239.
152. Pyle WG, Chen, Y, and Hofmann, PA. (2003) Cardioprotection through a PKC-dependent decrease in myofilament ATPase. *Am J Physiol Heart Circ Physiol* 285: H1220-1228.
153. Pyle WG, Sumandea, MP, Solaro, RJ, and De Tombe, PP. (2002) Troponin I serines 43/45 and regulation of cardiac myofilament function. *Am J Physiol Heart Circ Physiol* 283: H1215-1224.
154. Rao VS, La Bonte, LR, Xu, Y, Yang, Z, French, BA, and Guilford, WH. (2007) Alterations to myofibrillar protein function in nonischemic regions of the heart early after myocardial infarction. *Am J Physiol Heart Circ Physiol* 293: H654-659.
155. Rayment I, Rypniewski, WR, Schmidt-Base, K, Smith, R, Tomchick, DR, Benning, MM, Winkelmann, DA, Wesenberg, G, and Holden, HM. (1993) Three-dimensional structure of myosin subfragment-1: a molecular motor. *Science* 261: 50-58.
156. Redwood CS, Moolman-Smook, JC, and Watkins, H. (1999) Properties of mutant contractile proteins that cause hypertrophic cardiomyopathy. *Cardiovasc Res* 44: 20-36.
157. Regitz-Zagrosek V, Erdmann, J, Wellnhofer, E, Raible, J, and Fleck, E. (2000) Novel mutation in the alpha-tropomyosin gene and transition from hypertrophic to hypocontractile dilated cardiomyopathy. *Circulation* 102: E112-116.
158. Relling DP, Hintz, KK, and Ren, J. (2003) Acute exposure of ceramide enhances cardiac contractile function in isolated ventricular myocytes. *Br J Pharmacol* 140: 1163-1168.

159. Reuter H, Seuthe, K, Korkmaz, Y, Gronke, S, Hoyer, DP, Rottlaender, D, Zobel, C, Addicks, K, Hoyer, J, Grimminger, P, Brabender, J, Wilkie, TM, and Erdmann, E. (2012) The G protein Galpha11 is essential for hypertrophic signalling in diabetic myocardium. *Int J Cardiol*
160. Revera M, Van der Merwe, L, Heradien, M, Goosen, A, Corfield, VA, Brink, PA, and Moolman-Smook, JC. (2007) Long-term follow-up of R403WMYH7 and R92WTNNT2 HCM families: mutations determine left ventricular dimensions but not wall thickness during disease progression. *Cardiovasc J Afr* 18: 146-153.
161. Robinson P, Griffiths, PJ, Watkins, H, and Redwood, CS. (2007) Dilated and hypertrophic cardiomyopathy mutations in troponin and alpha-tropomyosin have opposing effects on the calcium affinity of cardiac thin filaments. *Circ Res* 101: 1266-1273.
162. Roman BB, Goldspink, PH, Spaite, E, Urboniene, D, McKinney, R, Geenen, DL, Solaro, RJ, and Buttrick, PM. (2004) Inhibition of PKC phosphorylation of cTnl improves cardiac performance in vivo. *Am J Physiol Heart Circ Physiol* 286: H2089-2095.
163. Rosen MR. (1986) Is the response to programmed electrical stimulation diagnostic of mechanisms for arrhythmias? *Circulation* 73: II18-27.
164. Rybin VO, Guo, J, Gertsberg, Z, Elouardighi, H, and Steinberg, SF. (2007) Protein kinase Cepsilon (PKCepsilon) and Src control PKCdelta activation loop phosphorylation in cardiomyocytes. *J Biol Chem* 282: 23631-23638.
165. Rybin VO, Guo, J, Sabri, A, Elouardighi, H, Schaefer, E, and Steinberg, SF. (2004) Stimulus-specific differences in protein kinase C delta localization and activation mechanisms in cardiomyocytes. *J Biol Chem* 279: 19350-19361.
166. Sadayappan S, Gulick, J, Osinska, H, Barefield, D, Cuello, F, Avkiran, M, Lasko, VM, Lorenz, JN, Maillet, M, Martin, JL, Brown, JH, Bers, DM, Molkentin, JD, James, J, and Robbins, J. (2011) A critical function for Ser-282 in cardiac Myosin binding protein-C phosphorylation and cardiac function. *Circ Res* 109: 141-150.
167. Sadayappan S, Gulick, J, Osinska, H, Martin, LA, Hahn, HS, Dorn, GW, 2nd, Klevitsky, R, Seidman, CE, Seidman, JG, and Robbins, J. (2005) Cardiac myosin-binding protein-C phosphorylation and cardiac function. *Circ Res* 97: 1156-1163.
168. Sancho Solis R, Ge, Y, and Walker, JW. (2011) A preferred AMPK phosphorylation site adjacent to the inhibitory loop of cardiac and skeletal troponin I. *Protein Sci* 20: 894-907.

169. Sancho Solis R, Ge, Y, and Walker, JW. (2008) Single amino acid sequence polymorphisms in rat cardiac troponin revealed by top-down tandem mass spectrometry. *J Muscle Res Cell Motil* 29: 203-212.
170. Sawada Y, Tamada, M, Dubin-Thaler, BJ, Cherniavskaya, O, Sakai, R, Tanaka, S, and Sheetz, MP. (2006) Force sensing by mechanical extension of the Src family kinase substrate p130Cas. *Cell* 127: 1015-1026.
171. Schlender KK, and Bean, LJ. (1991) Phosphorylation of chicken cardiac C-protein by calcium/calmodulin-dependent protein kinase II. *J Biol Chem* 266: 2811-2817.
172. Schober T, Huke, S, Venkataraman, R, Gryshchenko, O, Kryshtal, D, Hwang, HS, Baudenbacher, FJ, and Knollmann, BC. (2012) Myofilament Ca sensitization increases cytosolic Ca binding affinity, alters intracellular Ca homeostasis, and causes pause-dependent Ca-triggered arrhythmia. *Circ Res* 111: 170-179.
173. Scruggs SB, Reisdorph, R, Armstrong, ML, Warren, CM, Reisdorph, N, Solaro, RJ, and Buttrick, PM. (2010) A novel, in-solution separation of endogenous cardiac sarcomeric proteins and identification of distinct charged variants of regulatory light chain. *Mol Cell Proteomics* 9: 1804-1818.
174. Scruggs SB, Walker, LA, Lyu, T, Geenen, DL, Solaro, RJ, Buttrick, PM, and Goldspink, PH. (2006) Partial replacement of cardiac troponin I with a non-phosphorylatable mutant at serines 43/45 attenuates the contractile dysfunction associated with PKCepsilon phosphorylation. *J Mol Cell Cardiol* 40: 465-473.
175. Shimizu W, and Antzelevitch, C. (1997) Sodium channel block with mexiletine is effective in reducing dispersion of repolarization and preventing torsade des pointes in LQT2 and LQT3 models of the long-QT syndrome. *Circulation* 96: 2038-2047.
176. Smith GA, Dixon, HB, Kirschenlohr, HL, Grace, AA, Metcalfe, JC, and Vandenberg, JI. (2000) Ca²⁺ buffering in the heart: Ca²⁺ binding to and activation of cardiac myofibrils. *Biochem J* 346 Pt 2: 393-402.
177. Solaro RJ, and de Tombe, PP. (2008) Review focus series: sarcomeric proteins as key elements in integrated control of cardiac function. *Cardiovasc Res* 77: 616-618.
178. Solaro RJ, and Rarick, HM. (1998) Troponin and tropomyosin: proteins that switch on and tune in the activity of cardiac myofilaments. *Circ Res* 83: 471-480.

179. Solaro RJ, and van der Velden, J. (2010) Why does troponin I have so many phosphorylation sites? Fact and fancy. *J Mol Cell Cardiol* 48: 810-816.
180. Son NH, Park, TS, Yamashita, H, Yokoyama, M, Huggins, LA, Okajima, K, Homma, S, Szabolcs, MJ, Huang, LS, and Goldberg, IJ. (2007) Cardiomyocyte expression of PPARgamma leads to cardiac dysfunction in mice. *J Clin Invest* 117: 2791-2801.
181. Spiegelman BM, and Flier, JS. (2001) Obesity and the regulation of energy balance. *Cell* 104: 531-543.
182. Stamm C, Friehs, I, Cowan, DB, Cao-Danh, H, Noria, S, Munakata, M, McGowan, FX, Jr., and del Nido, PJ. (2001) Post-ischemic PKC inhibition impairs myocardial calcium handling and increases contractile protein calcium sensitivity. *Cardiovasc Res* 51: 108-121.
183. Stelzer JE, Dunning, SB, and Moss, RL. (2006) Ablation of cardiac myosin-binding protein-C accelerates stretch activation in murine skinned myocardium. *Circ Res* 98: 1212-1218.
184. Stelzer JE, Fitzsimons, DP, and Moss, RL. (2006) Ablation of myosin-binding protein-C accelerates force development in mouse myocardium. *Biophys J* 90: 4119-4127.
185. Stern MD, Song, LS, Cheng, H, Sham, JS, Yang, HT, Boheler, KR, and Rios, E. (1999) Local control models of cardiac excitation-contraction coupling. A possible role for allosteric interactions between ryanodine receptors. *J Gen Physiol* 113: 469-489.
186. Stewart M. (2001) Structural basis for bending tropomyosin around actin in muscle thin filaments. *Proc Natl Acad Sci U S A* 98: 8165-8166.
187. Strang KT, and Moss, RL. (1995) Alpha 1-adrenergic receptor stimulation decreases maximum shortening velocity of skinned single ventricular myocytes from rats. *Circ Res* 77: 114-120.
188. Subramaniam A, Jones, WK, Gulick, J, Wert, S, Neumann, J, and Robbins, J. (1991) Tissue-specific regulation of the alpha-myosin heavy chain gene promoter in transgenic mice. *J Biol Chem* 266: 24613-24620.
189. Suematsu N, Tsutsui, H, Wen, J, Kang, D, Ikeuchi, M, Ide, T, Hayashidani, S, Shiomi, T, Kubota, T, Hamasaki, N, and Takeshita, A. (2003) Oxidative stress

- mediates tumor necrosis factor-alpha-induced mitochondrial DNA damage and dysfunction in cardiac myocytes. *Circulation* 107: 1418-1423.
190. Sumandea MP, Pyle, WG, Kobayashi, T, de Tombe, PP, and Solaro, RJ. (2003) Identification of a functionally critical protein kinase C phosphorylation residue of cardiac troponin T. *J Biol Chem* 278: 35135-35144.
 191. Sumandea MP, Rybin, VO, Hinken, AC, Wang, C, Kobayashi, T, Harleton, E, Sievert, G, Balke, CW, Feinmark, SJ, Solaro, RJ, and Steinberg, SF. (2008) Tyrosine phosphorylation modifies protein kinase C delta-dependent phosphorylation of cardiac troponin I. *J Biol Chem* 283: 22680-22689.
 192. Sumida JP, Wu, E, and Lehrer, SS. (2008) Conserved Asp-137 imparts flexibility to tropomyosin and affects function. *J Biol Chem* 283: 6728-6734.
 193. Sweeney HL, Feng, HS, Yang, Z, and Watkins, H. (1998) Functional analyses of troponin T mutations that cause hypertrophic cardiomyopathy: insights into disease pathogenesis and troponin function. *Proc Natl Acad Sci U S A* 95: 14406-14410.
 194. Takeishi Y, Ping, P, Bolli, R, Kirkpatrick, DL, Hoit, BD, and Walsh, RA. (2000) Transgenic overexpression of constitutively active protein kinase C epsilon causes concentric cardiac hypertrophy. *Circ Res* 86: 1218-1223.
 195. Tan HL, Kupersmidt, S, Zhang, R, Stepanovic, S, Roden, DM, Wilde, AA, Anderson, ME, and Balsler, JR. (2002) A calcium sensor in the sodium channel modulates cardiac excitability. *Nature* 415: 442-447.
 196. Tardiff JC. (2005) Sarcomeric proteins and familial hypertrophic cardiomyopathy: linking mutations in structural proteins to complex cardiovascular phenotypes. *Heart failure reviews* 10: 237-248.
 197. Tardiff JC. (2011) Thin filament mutations: developing an integrative approach to a complex disorder. *Circ Res* 108: 765-782.
 198. Teare D. (1958) Asymmetrical hypertrophy of the heart in young adults. *Br Heart J* 20: 1-8.
 199. Thierfelder L, MacRae, C, Watkins, H, Tomfohrde, J, Williams, M, McKenna, W, Bohm, K, Noeske, G, Schlepper, M, Bowcock, A, and et al. (1993) A familial hypertrophic cardiomyopathy locus maps to chromosome 15q2. *Proc Natl Acad Sci U S A* 90: 6270-6274.

200. Thierfelder L, Watkins, H, MacRae, C, Lamas, R, McKenna, W, Vosberg, HP, Seidman, JG, and Seidman, CE. (1994) Alpha-tropomyosin and cardiac troponin T mutations cause familial hypertrophic cardiomyopathy: a disease of the sarcomere. *Cell* 77: 701-712.
201. Tobacman LS, Lin, D, Butters, C, Landis, C, Back, N, Pavlov, D, and Homsher, E. (1999) Functional consequences of troponin T mutations found in hypertrophic cardiomyopathy. *J Biol Chem* 274: 28363-28370.
202. Tobacman LS, Nihli, M, Butters, C, Heller, M, Hatch, V, Craig, R, Lehman, W, and Homsher, E. (2002) The troponin tail domain promotes a conformational state of the thin filament that suppresses myosin activity. *J Biol Chem* 277: 27636-27642.
203. Tong CW, Stelzer, JE, Greaser, ML, Powers, PA, and Moss, RL. (2008) Acceleration of crossbridge kinetics by protein kinase A phosphorylation of cardiac myosin binding protein C modulates cardiac function. *Circ Res* 103: 974-982.
204. Trepanier-Boulay V, St-Michel, C, Tremblay, A, and Fiset, C. (2001) Gender-based differences in cardiac repolarization in mouse ventricle. *Circ Res* 89: 437-444.
205. Tyska MJ, and Warshaw, DM. (2002) The myosin power stroke. *Cell motility and the cytoskeleton* 51: 1-15.
206. Unger RH. (2002) Lipotoxic diseases. *Annu Rev Med* 53: 319-336.
207. Urboniene D, Dias, FA, Pena, JR, Walker, LA, Solaro, RJ, and Wolska, BM. (2005) Expression of slow skeletal troponin I in adult mouse heart helps to maintain the left ventricular systolic function during respiratory hypercapnia. *Circ Res* 97: 70-77.
208. van der Velden J, Klein, LJ, van der Bijl, M, Huybregts, MA, Stoker, W, Witkop, J, Eijnsman, L, Visser, CA, Visser, FC, and Stienen, GJ. (1999) Isometric tension development and its calcium sensitivity in skinned myocyte-sized preparations from different regions of the human heart. *Cardiovasc Res* 42: 706-719.
209. Van Driest SL, Ellsworth, EG, Ommen, SR, Tajik, AJ, Gersh, BJ, and Ackerman, MJ. (2003) Prevalence and spectrum of thin filament mutations in an outpatient referral population with hypertrophic cardiomyopathy. *Circulation* 108: 445-451.

210. Van Driest SL, Will, ML, Atkins, DL, and Ackerman, MJ. (2002) A novel TPM1 mutation in a family with hypertrophic cardiomyopathy and sudden cardiac death in childhood. *Am J Cardiol* 90: 1123-1127.
211. Ventura-Clapier R, Garnier, A, and Veksler, V. (2004) Energy metabolism in heart failure. *J Physiol* 555: 1-13.
212. Wagner S, Dybkova, N, Rasenack, EC, Jacobshagen, C, Fabritz, L, Kirchhof, P, Maier, SK, Zhang, T, Hasenfuss, G, Brown, JH, Bers, DM, and Maier, LS. (2006) Ca²⁺/calmodulin-dependent protein kinase II regulates cardiac Na⁺ channels. *J Clin Invest* 116: 3127-3138.
213. Warren CM, Arteaga, GM, Rajan, S, Ahmed, RP, Wieczorek, DF, and Solaro, RJ. (2008) Use of 2-D DIGE analysis reveals altered phosphorylation in a tropomyosin mutant (Glu54Lys) linked to dilated cardiomyopathy. *Proteomics* 8: 100-105.
214. Watts JD, Gu, M, Patterson, SD, Aebersold, R, and Polverino, AJ. (1999) On the complexities of ceramide changes in cells undergoing apoptosis: lack of evidence for a second messenger function in apoptotic induction. *Cell Death Differ* 6: 105-114.
215. Weber A, and Winicur, S. (1961) The role of calcium in the superprecipitation of actomyosin. *J Biol Chem* 236: 3198-3202.
216. Weith A, Sadayappan, S, Gulick, J, Previs, MJ, Vanburen, P, Robbins, J, and Warshaw, DM. (2012) Unique single molecule binding of cardiac myosin binding protein-C to actin and phosphorylation-dependent inhibition of actomyosin motility requires 17 amino acids of the motif domain. *J Mol Cell Cardiol* 52: 219-227.
217. Wende AR, and Abel, ED. (2010) Lipotoxicity in the heart. *Biochim Biophys Acta* 1801: 311-319.
218. Wu G, Toyokawa, T, Hahn, H, and Dorn, GW, 2nd. (2000) Epsilon protein kinase C in pathological myocardial hypertrophy. Analysis by combined transgenic expression of translocation modifiers and Galphaq. *J Biol Chem* 275: 29927-29930.
219. Xiao L, Zhao, Q, Du, Y, Yuan, C, Solaro, RJ, and Buttrick, PM. (2007) PKCepsilon increases phosphorylation of the cardiac myosin binding protein C at serine 302 both in vitro and in vivo. *Biochemistry* 46: 7054-7061.

220. Yamamoto S, Yang, G, Zablocki, D, Liu, J, Hong, C, Kim, SJ, Soler, S, Odashima, M, Thaisz, J, Yehia, G, Molina, CA, Yatani, A, Vatner, DE, Vatner, SF, and Sadoshima, J. (2003) Activation of Mst1 causes dilated cardiomyopathy by stimulating apoptosis without compensatory ventricular myocyte hypertrophy. *J Clin Invest* 111: 1463-1474.
221. Yamauchi-Takahara K, Nakajima-Taniguchi, C, Matsui, H, Fujio, Y, Kunisada, K, Nagata, S, and Kishimoto, T. (1996) Clinical implications of hypertrophic cardiomyopathy associated with mutations in the alpha-tropomyosin gene. *Heart* 76: 63-65.
222. Yang PC, and Clancy, CE. (2012) In silico Prediction of Sex-Based Differences in Human Susceptibility to Cardiac Ventricular Tachyarrhythmias. *Front Physiol* 3: 360.
223. You B, Yan, G, Zhang, Z, Yan, L, Li, J, Ge, Q, Jin, JP, and Sun, J. (2009) Phosphorylation of cardiac troponin I by mammalian sterile 20-like kinase 1. *Biochem J* 418: 93-101.
224. Young ME, Guthrie, PH, Razeghi, P, Leighton, B, Abbasi, S, Patil, S, Youker, KA, and Taegtmeyer, H. (2002) Impaired long-chain fatty acid oxidation and contractile dysfunction in the obese Zucker rat heart. *Diabetes* 51: 2587-2595.
225. Zhang J, Dong, X, Hacker, TA, and Ge, Y. (2010) Deciphering modifications in swine cardiac troponin I by top-down high-resolution tandem mass spectrometry. *J Am Soc Mass Spectrom* 21: 940-948.
226. Zhang J, Guy, MJ, Norman, HS, Chen, YC, Xu, Q, Dong, X, Guner, H, Wang, S, Kohmoto, T, Young, KH, Moss, RL, and Ge, Y. (2011) Top-down quantitative proteomics identified phosphorylation of cardiac troponin I as a candidate biomarker for chronic heart failure. *J Proteome Res* 10: 4054-4065.
227. Zhang P, Kirk, JA, Ji, W, dos Remedios, CG, Kass, DA, Van Eyk, JE, and Murphy, AM. (2012) Multiple reaction monitoring to identify site-specific troponin I phosphorylated residues in the failing human heart. *Circulation* 126: 1828-1837.
228. Zhou YT, Grayburn, P, Karim, A, Shimabukuro, M, Higa, M, Baetens, D, Orci, L, and Unger, RH. (2000) Lipotoxic heart disease in obese rats: implications for human obesity. *Proc Natl Acad Sci U S A* 97: 1784-1789.

CHAPTER VII

APPENDIX A



February 16, 2011

Jillian Simon
Physiology & Biophysics
M/C 901

Office of Animal Care and
Institutional Biosafety Committees (MC 672)
Office of the Vice Chancellor for Research
206 Administrative Office Building
1737 West Polk Street
Chicago, Illinois 60612-7227

Dear Dr. Simon:

The protocol indicated below was reviewed at a convened ACC meeting in accordance with the Animal Care Policies of the University of Illinois at Chicago on 2/15/2011. *The protocol is approved for a period of 2 years with annual continuation.*

Title of Application: Role of Ceramide in PTMs of Cardiac Proteins in I/R Injury

ACC Number: 11-013

Initial Approval Period: 2/15/2011 to 2/15/2012

Current Funding: *Portions of this protocol are supported by the funding sources indicated in the table below.*

Number of funding sources: 1

Funding Agency	Funding Title			Portion of Proposal Matched
AHA- American Heart Association	Role of Ceramide in PTMs of Cardiac Proteins in I/R Injury			Matched
Funding Number	Current Status	UIC PAF NO.	Performance Site	Funding PI
11PRE5560021	Funded	2011-00417	UIC	Jillian Simon

This institution has Animal Welfare Assurance Number A3460.01 on file with the Office of Laboratory Animal Welfare (OLAW), NIH. **This letter may only be provided as proof of IACUC approval for those specific funding sources listed above in which all portions of the funding proposal are matched to this ACC protocol.**

In addition, all investigators are responsible for ensuring compliance with all federal and institutional policies and regulations related to use of animals under this protocol and the funding sources listed on this protocol. Please use OLAW's "What Investigators Need to Know about the Use of Animals" (<http://grants.nih.gov/grants/olaw/InvestigatorsNeed2Know.pdf>) as a reference guide. Thank you for complying with the Animal Care Policies and Procedures of UIC.

Sincerely yours,

Richard D. Minshall, PhD
Chair, Animal Care Committee
RDM/ss

cc: BRL, ACC File, Beata M. Wolska, PAF # 2011-00417

CHAPTER VII

APPENDIX B



Office of Animal Care and
Institutional Biosafety Committees (MC 672)
Office of the Vice Chancellor for Research
206 Administrative Office Building
1737 West Polk Street
Chicago, Illinois 60612-7227

February 15, 2012

R. John Solaro
Physiology & Biophysics
M/C 901

Dear Dr. Solaro:

The protocol indicated below was reviewed at a convened ACC meeting in accordance with the Animal Care Policies of the University of Illinois at Chicago on 1/17/2012. *The protocol was not initiated until final clarifications were reviewed and approved on 2/10/2012. The protocol is approved for a period of 3 years with annual continuation.*

Title of Application: Molecular Signaling in Cardiac Myocytes

ACC Number: 11-229

Initial Approval Period: 2/10/2012 to 1/17/2013

Current Funding: *Portions of this protocol are supported by the funding sources indicated in the table below.*

Number of funding sources: 2

Funding Agency	Funding Title			Portion of Proposal Matched
NHLI	<i>Troponin Modulation In Heart Failure (linked to Form G 09-049)</i>			<i>Matched to portion of the grant</i>
Funding Number	Current Status	UIC PAF NO.	Performance Site	Funding PI
<i>ROI HL64035 (years 11-15)</i>	<i>Funded</i>	<i>209901189</i>	<i>PS1</i>	<i>R. John Solaro</i>
Funding Agency	Funding Title			Portion of Proposal Matched
NHLI	<i>Modulation of Calcium Control in Cardiac Myofibrils (linked to 11-229)</i>			<i>Matched to portion of the grant</i>
Funding Number	Current Status	UIC PAF NO.	Performance Site	Funding PI
<i>ROI HL022231 (years 33-37) Original</i>	<i>Pending</i>	<i>201101862</i>	<i>PS2</i>	<i>R. John Solaro</i>

This institution has Animal Welfare Assurance Number A3460.01 on file with the Office of Laboratory Animal Welfare (OLAW), NIH. **This letter may only be provided as proof of IACUC approval for those specific funding sources listed above in which all portions of the funding proposal are matched to this ACC protocol.**

In addition, all investigators are responsible for ensuring compliance with all federal and institutional policies and regulations related to use of animals under this protocol and the funding sources listed on this protocol. Please use OLAW's "*What Investigators Need to Know about the Use of Animals*" (<http://grants.nih.gov/grants/olaw/InvestigatorsNeed2Know.pdf>) as a reference guide. Thank you for complying with the Animal Care Policies and Procedures of UIC.

Sincerely yours,



Bradley Merrill, PhD
Chair, Animal Care Committee

BM/mbb

cc: BRL, ACC File, Beata M. Wolska, Madhu Gupta, Lindsey Duncan

CHAPTER VII

APPENDIX C



Office of Animal Care and
Institutional Biosafety Committees (MC 672)
Office of the Vice Chancellor for Research
206 Administrative Office Building
1737 West Polk Street
Chicago, Illinois 60612-7227

May 18, 2012

Beata M. Wolska
Medicine/Cardiology
M/C 715

Dear Dr. Wolska:

The protocol indicated below was reviewed at a convened ACC meeting in accordance with the Animal Care Policies of the University of Illinois at Chicago on **4/17/2012**. *The protocol was not initiated until final clarifications were reviewed and approved on 5/17/2012. The protocol is approved for a period of 3 years with annual continuation.*

Title of Application: Control of Cardiac Function By Calcium and Myofilaments

ACC Number: 12-063

Initial Approval Period: 5/17/2012 to 4/17/2013

Current Funding: *Portions of this protocol are supported by the funding sources indicated in the table below.*

Number of funding sources: 2

Funding Agency	Funding Title			Portion of Proposal Matched
NIH	Troponin Modulation In Heart Failure			Linked to 12-054
Funding Number	Current Status	UIC PAF NO.	Performance Site	Funding PI
ROI HL064035	Funded	2009-01189	UIC	John Solaro (CO-PI Dr. Wolska)
Funding Agency	Funding Title			Portion of Proposal Matched
NIH	Tropomyosin - Critical Regulator Of Normal And Diseased Cardiac Muscle Function			Matched
Funding Number	Current Status	UIC PAF NO.	Performance Site	Funding PI
PO1 116252	Pending	2012-03585	UIC	Beata Wolska

This institution has Animal Welfare Assurance Number A3460.01 on file with the Office of Laboratory Animal Welfare (OLAW), NIH. This letter may only be provided as proof of IACUC approval for those specific funding sources listed above in which all portions of the funding proposal are matched to this ACC protocol.

In addition, all investigators are responsible for ensuring compliance with all federal and institutional policies and regulations related to use of animals under this protocol and the funding sources listed on this protocol. Please use OLAW's "*What Investigators Need to Know about the Use of Animals*" (<http://grants.nih.gov/grants/olaw/InvestigatorsNeed2Know.pdf>) as a reference guide. Thank you for complying with the Animal Care Policies and Procedures of UIC.

Sincerely yours,



Bradley Merrill, PhD
Chair, Animal Care Committee

BM/ss

cc: BRL, ACC File, R. John Solaro, Lindsey Duncan, Shamim Chowdhury, **PAF # 2012-03585**

CHAPTER VIII
CIRRICULUM VITAE

EDUCATION

- 2002-2006 Alma College, Alma, Michigan, USA
B.S. in Exercise and Health Science, Chemistry minor
- 2007-Present University of Illinois at Chicago, Chicago, Illinois, USA
Ph.D. in Physiology and Biophysics, College of Medicine
Thesis Advisor: Beata M. Wolska, Ph.D. (bwolska@uic.edu)

RESEARCH EXPERIENCE

- 2003-2006 Undergraduate Research
Alma College, Department of Exercise and Health Science
Alma, Michigan, United States
Advisor: Karen L. Ball, Ph.D.
Project Title: "Supplementation with Myostatin Negatively
Regulates Myogenesis"
- 2007-Present Graduate Research Assistant
University of Illinois at Chicago, Department of Physiology &
Biophysics
Chicago, Illinois, United States
Advisor: Beata M. Wolska, Ph.D.
Project Title: "The Importance of the Cardiac
Myofilament in Regulating Acute and Chronic
Responses to Stress"

TEACHING EXPERIENCE

- 2006-2007 Laboratory Coordinator
Alma College
Department of Exercise and Health Science
Responsible for teaching course laboratories and assisting with
departmental research focused on exercise and performance
physiology at both the molecular and human studies level

- 2010-2011 Guest Lecturer – HPE201: Human Pathophysiology
North Central College
Department of Health and Physical Education
 Invited to teach 3 lectures on basic cardiovascular physiology
 and pathophysiology to undergraduate students
- 2009-Present Course Instructor – PHYB310: M1 Pre-matriculation Program
University of Illinois at Chicago
College of Medicine, University of Illinois at Chicago
- Cell Physiology Section, 2012
 - Renal Physiology Section, 2009 & 2011
 - Muscle Physiology Section, 2010
- 2009-Present Course Instructor – PHYB301: Physiology & Pathophys for Pharm.D
University of Illinois at Chicago
College of Pharmacy, University of Illinois at Chicago
- Renal Physiology Section, 2011 & 2012
 - Muscle Physiology Review Session, 2010
 - Cardiovascular Review Session, 2009

PROFESSIONAL SOCIETIES

- 2008-Present Biophysical Society, Member
- 2008-Present Physiology and Biophysics Graduate Student Association, Member
President, 2/2010 to 2/2012
- 2009-Present American Heart Association, Member
- 2013 International Society for Heart Research, Member

HONORS AND AWARDS

- 8/2010 Abstract Selected for Oral Presentation, *Center for Cardiovascular Research (CCVR) Research Day*, University of Illinois at Chicago
Title of Talk: “The Role of Ceramide in Cardiac Excitation-
Contraction Coupling”
- 8/2008-8/2010 National Institutes of Health Training Fellowship
Program Title: “Cellular Signaling in the Cardiovascular System”
P.I., R. John Solaro

- 1/2011-12/2012 American Heart Association Pre-doctoral Fellowship
Program Title: "The Role of Ceramide in Post-translational Modifications of Cardiac Proteins in Ischemia-Reperfusion Injury"
P.I., Jillian N. Simon
- 11/2011 Mark R. Lambrecht Award for Scholarship and Commitment
University Of Illinois at Chicago, Department of Physiology and Biophysics (annual award presented to one graduate student who demonstrates a high degree of scholastic achievement and service to the department)

PUBLICATIONS

1. **Simon, J.N.**, Tardiff, J.C., Wolska, B.M. The sarcomere and the biophysics of heart failure. In: *The Biophysics of Heart Failure*, eds. R.J. Solaro and J.C. Tardiff. (*In press*)
2. Alves, M.L., Dias, F.A.L., Gaffin, R.D., **Simon, J.N.**, Montminy, E.M., Biesiadecki, B.J., Hinken, A.C., Sadayappan, S., Robbins, J., Wieczorek, D.F., Solaro, R.J., Wolska, B.M. Desensitization of the myofilament to Ca²⁺ as a therapeutic target for hypertrophic cardiomyopathy with mutations in thin filament proteins. *Circulation (In Revision)*
3. **Simon, J.N.**, Chowdury, S.A.K., Warren, C.M., Sadayappan, S., Wieczorek, D.F., Solaro, R.J., Wolska, B.M. Ceramide-mediated depression in cardiomyocyte contractility through PKC activation and modulation of myofilament protein phosphorylation. *Basic Res Cardiol (In Revision)*

PUBLICATIONS (*In Preparation*)

1. **Simon, J.N.**, Chowdhury, S.A.K., Jagatheesan, G., Wieczorek, D.F., Solaro, R.J., Wolska, B.M. Age-dependent cardiac dysfunction and increased susceptibility to arrhythmias in transgenic mice bearing the K70T tropomyosin mutation.
2. Alves, M.L., Gaffin, R.D., Chowdury, S.A.K., **Simon, J.N.**, Montminy, E.M., Wieczorek, D.F., Solaro, R.J., Wolska, B.M. Rescue of a dilated cardiomyopathy mouse model caused by a mutation in tropomyosin (E54K) by expression of slow skeletal troponin I.
3. Chowdhury, S.A.K., **Simon, J.N.**, Davis, R.T., Solaro, R.J., Kranias, E.G., Tardiff, J.C., Wolska, B.M. Long-term rescue of cTnT-related hypertrophic cardiomyopathy by reducing expression of phospholamban.

PROFESSIONAL ABSTRACTS

1. Warren, C.M., Alves, M.S.L., Montminy, E.M., **Simon, J.N.**, Gaffin, R.D., Rajan, S., Wieczorek, D.F., Solaro, R.J., Wolska, B.M. Rescue of a dilated cardiomyopathy mouse model caused by a mutation in tropomyosin (E54K) by expression of slow skeletal troponin I. *Biophys J* 102(3): 560a, 2012
2. **Simon, J.N.**, Chowdhury, S.A.K., Jagatheesan, G., Wieczorek, D.F., Solaro, R.J., Wolska, B.M. A new model of familial hypertrophic cardiomyopathy with a mutation in tropomyosin at position 70: insights into the development of cardiac dysfunction and increased risk for sudden cardiac death. *Biophysical Society 2012 Annual Meeting*, San Diego, California. 2012 (Poster presentation)
3. **Simon, J.N.**, Warren, C.M., Chowdhury, S.A.K., Gupta, M., Sadayappan, S., Solaro, R.J., Wolska, B.M. The role of ceramide in cardiac excitation-contraction coupling. *University of Illinois Center for Cardiovascular Research: Research Day*, Chicago, Illinois. 2011 (Poster presentation)
4. **Simon, J.N.**, Chowdhury, S.A.K., Jagatheesan, G., Wieczorek, D.F., Solaro, R.J., Wolska, B.M. A new model of familial hypertrophic cardiomyopathy with a mutation in tropomyosin at position 70: insights into the development of cardiac dysfunction and increased risk for sudden cardiac death. *University of Illinois College of Medicine Research Day*, Chicago, Illinois. 2011 (Poster presentation)
5. **Simon, J.N.**, Warren, C.M., Chowdhury, S.A.K., Sadayappan, S., Solaro, R.J., Wolska, B.M. The role of ceramide in cardiac excitation-contraction coupling. *Myofilament Meeting*, Madison, Wisconsin. 2010 (Poster presentation)
6. **Simon, J.N.**, Warren, C.M., Chowdhury, S.A.K., Sadayappan, S., Solaro, R.J., Wolska, B.M. The role of ceramide in cardiac excitation-contraction coupling. *University of Illinois Center for Cardiovascular Research: Research Day*, Chicago, Illinois. 2010 (Oral presentation)